A Residential Energy Control Algorithm Assessment Tool for Smart Grid: Multi-Criteria Decision Making Using the Analytical Hierarchy Process

---

A Dissertation

Presented to

the faculty of the School of Engineering and Applied Science

Department of Electrical and Computer Engineering

University of Virginia

In partial fulfillment
of the requirements for the Degree

Doctor of Philosophy (Electrical Engineering)

by

Farhad Omar

May, 2019

APPROVAL SHEET

This dissertation is submitted in partial fulfillment of the
requirements of the degree of
Doctor of Philosophy (Electrical Engineering)

Farhad Omar

This dissertation has been read and approved by the Examining Committee:

Ronald D. Williams, Dissertation Advisor

Joanne Bechta Dugan, Committee Chair

Harry Powell, Committee Member

Zongli Lin, Committee Member

Phoebe Crisman, Committee Member

Accepted for the School of Engineering and Applied Science:

Dean, School of Engineering
and Applied Science

May, 2019

Abstract

For homes to become active participants in a smart grid, intelligent control algorithms are needed to facilitate autonomous interactions that take homeowner preferences into consideration. Many control algorithms for demand response have been proposed in the literature. Comparing the performance of these algorithms has been difficult because each algorithm makes different assumptions or considers different scenarios, e.g., reducing the peak load, minimizing cost in response to the variable price of electricity, minimizing energy, or achieving a balance between overall energy savings, ensuring comfort, and minimizing cost. A comprehensive framework for assessing the performance of these algorithms that considering simultaneously considers multiple objectives and users' subjective preferences has not previously been studied and it is necessary to be able to compare their performances. To overcome these limitations, a flexible assessment framework using the Analytical Hierarchy Process was developed to compare and rank residential energy management control algorithms. The framework is a hybrid mechanism that derives a ranking from a combination of subjective user inputs, representing preferences, and objective data from the algorithm performance related to energy consumption, cost and comfort. The Analytical Hierarchy Process results in a single overall score used to rank the alternatives. Testing and validation of the assessment framework is illustrated by applying the assessment process to six residential energy management control algorithms. The control algorithms were developed and tested using a simulation model of the Net-Zero Energy Residential Test Facility located on the campus of the National Institute of Standards and Technology in Gaithersburg, MD. The Net-Zero Energy Residential Test Facility is a research house that is comparable in size and aesthetics to the houses in the greater Washington DC metro area. One algorithm was designed to match a real heat pump controller used in the house model. A second was the same as the first with relaxed comfort deadbands. Four others used linear integer optimization with varying optimization objectives to generate forecasted heat pump control actions. The algorithms were compared by analyzing their performance over a year based on energy consumption, cost, and comfort as measured by predicted mean vote and predicted percentage of dissatisfied. Successful implementation of the assessment framework produces a figure of merit that enables policy makers, control algorithm engineers, and other stakeholders to compare the performance of residential energy management control algorithms.

Preface

In August of 2001, my family and I immigrated to the United States and resettled in Charlottesville, VA. From the very early days, the University of Virginia has had a profound impact on my thoughts. I visited Clemons library on a daily basis; interacting with staff and students. The future was uncertain, though my imagination was not. I imagined that one day I will study and graduate from this great institution. The task was monumental; I could barely speak or understand English. After many years of perseverance, I am ready to write the final chapters of my academic career at Mr. Jefferson's University. I believe that it is time to graduate and call myself a triple Hoo! Throughout this journey, I have been fortunate to have met, learned from, and worked with so many kind, and supportive teachers, friends, and colleagues. They have challenged me, intellectually tortured me (joking of course), and most of all guided me in my research. For this, I am grateful and indebted to:

Prof. Ronald D. Williams, for advising and guiding me throughout this research;

Members of my dissertation committee, for their insightful feedback and support: Prof. Joanne Bechta Dugan, Prof. Harry Powell, Prof. Zongli Lin, and Prof. Phoebe Crisman who I had the pleasure of working with on the Learning Barge;

I am especially grateful to Prof. Dugan for her continued counseling and support. Without her help, I would have not succeeded in this endeavor;

My colleagues at NIST, Steve Bushby, Andrew Persily, David Holmberg, Mark Kedzierski, Vance Payne, Harrison Skye, David Yashar, Natascha Milesi Ferretti, Mike Galler, Glen Glaeser, Piotr Domanski, Bill Heally, and the rest of the Net-Zero house team members;

My AI Glee Club colleagues at NIST, Dan Veronica, Amanda Pertzborn, and Parastou Delgoshaei for being there when I needed it the most;

Steve Bushy, for being a wonderful mentor; his guidance and support has helped me become a better researcher and a writer, in large part, due to his continued constructive criticism;

Mark Kedzierski, for being a great mentor; his guidance and support has helped me become a better researcher even though we disagree about politics and of course he is wrong;

Elizabeth Balke, for developing and tuning the transient simulation model of the Net-Zero house;

Prof. Paxton Marshall, for guiding me through my undergraduate and master's degree; he had an invaluable influence in my academic success;

Dabney T. Waring (deceased), for teaching me English in preparation for my academic life;

My friends at UVa, for sharing memories and for helping me to become a good friend: Tejas Shah, Hamid Hashime, Angad Sachdeva, Suchit Ligade, Jorge Chevas, Kosta Popovic, Christian Rothenbach, Benjamin Kidd, and many more;

I am grateful for the incredible administrative staff at SEAS, Beth Eastwood-Beatty, Dan Fetko, David Durocher, Susan Malone, Iva Gillet, Barbra Graves, Jennifer Mauller, and many more;

My family, Nadira, Marina, Tariq, Melody, Ahmad Farid, grandparents (deceased), and many more for unconditionally loving me and supporting me throughout my life; and finally

My wife Weezha, for loving me and helping me stay the course when I had doubted myself.

Lastly, I would like to end this by quoting my lovely little niece Melody “All done!”

Table of Contents

List of Figures

List of Tables

Chapter 1

1. Introduction and Motivation

The current electric grid is under stress from increasing demand and aging infrastructure. A significant component of the demand is residential heating and cooling. In 2016, residential buildings consumed 38 % of all electricity sold in the U.S. [1] with space heating and cooling accounting for 24 % of the electricity consumption [2]. The Energy Independence and Security Act of 2007 (EISA) established a national policy to support the modernization of the national electric grid to maintain a reliable and secure electricity infrastructure that can meet future growth [3]. The vision of a modern electric grid, a smart electric grid, is “a modernized grid that enables bidirectional flows of energy and uses two-way communication and control capabilities that will lead to an array of new functionalities and applications” [4].

According to Title XIII of EISA [3] a few key characteristics of a smart grid include:

1. “Increased use of digital information and controls technology to improve reliability, security, and efficiency of the electric grid;
2. Development and incorporation of demand response, demand-side resources, and energy-efficiency resources;
3. Deployment of “smart” technologies (real-time, automated, interactive technologies that optimize the physical operation of appliances and consumer devices) for metering, communications concerning grid operations and status, and distribution automation; and
4. Integration of “smart” appliances and consumer devices.”

The new smart electric grid paradigm creates a complex environment that requires decision making, developing and deploying advanced technologies, and facilitating the exchange of energy and information between interested parties. A conceptual model of the interaction between different smart electric grid domains, which was developed by the National Institute of Standards and Technology (NIST) is shown in Figure 1[4].

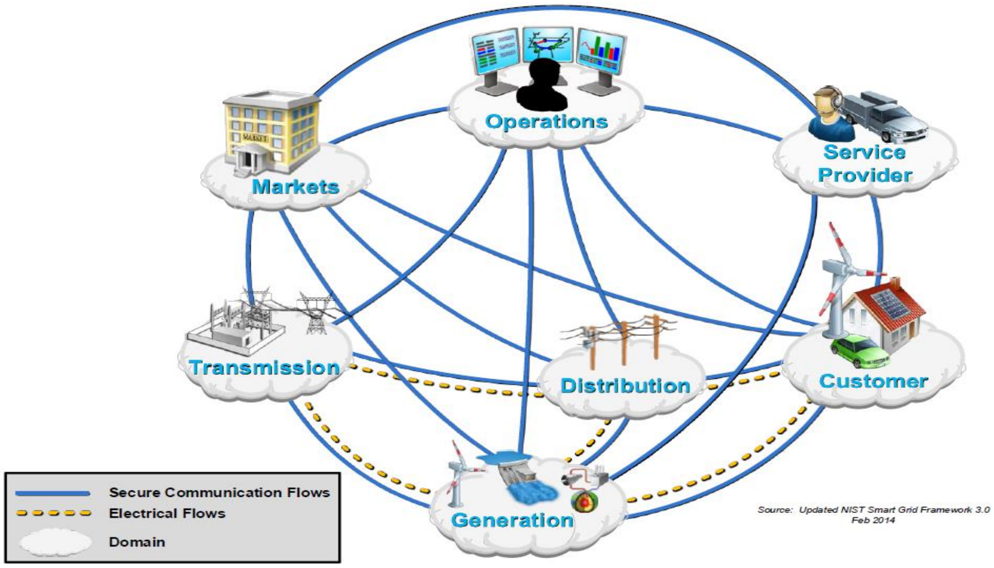

Figure 1. The NIST conceptual model representing the interaction of different smart electric grid domains

The conceptual model divides the smart electric grid into seven major domains, each consisting of many applications and roles. A brief description of each domain is provided in Table 1 and further details are given in [4].

Table 1. A description of various domains of a smart electric grid

Domain	**Description**
Customer	The end users of electricity. May also generate, store, and manage the use of energy. Traditionally, three customer types are discussed, each with its own sub-domain: home, commercial/building, and industrial.
Markets	The operators and participants in electricity markets.
Service Provider	The organization providing services to electricity customers and utilities.
Operations	The managers of the movement of electricity.
Generation	The generators of electricity. May also store energy for later distribution.
Transmission	The carriers of bulk electricity over long distances. May also store and generate electricity.
Distribution	The distributors of electricity to and from customers. May also store and generate electricity.

The focus of the research in this dissertation is the home (residential) subcategory of the Customer domain. According to the U.S. Department of Energy (DOE), consumers can play a significant role in the operation of the electric grid by shifting or reducing their electricity use to off-peak times in response to time-based electric rates or other financial incentives [5]. One of the ways that users (customers) could interact with a smart electric grid is through demand response (DR), a process by which electric power consumption (demand) is moderated to support grid needs. DR is commonly used to reduce peaks, but can also be used to increase consumption when the total demand on the grid is low, to support voltage regulation, or for other grid needs. DR can be implemented using dynamic prices or other signals from the grid. Some methods for implementing DR and the possible benefits are described in [6].

Realizing a smart electric grid requires intelligent control algorithms to facilitate autonomous interaction between homeowners and the grid. Many optimization models and control algorithms for DR have been proposed in the literature to achieve this goal. Comprehensive reviews of utility DR programs, approaches, and optimization techniques are presented in [7]–[9]. Common optimization objectives include cutting cost, reducing energy consumption, or both, while trying to maintain thermal comfort. The actions resulting from the optimization include controlling appliances, performing temperature setbacks, and preheating or precooling. However, it has been difficult to compare these approaches because they rely on different assumptions and consider different objectives. Furthermore, they may consider the perspective of the utility (cost, profit, peak load shaving, capacity, etc.), but often fail to consider that the perspective of the homeowner whose needs or interests (energy, cost, comfort, etc.) may differ. A user may also have conflicting goals such as reducing cost and maintaining comfort. Therefore, an assessment framework is needed that can evaluate the impact of control actions on multiple and potentially conflicting objectives such as minimizing cost or energy, while maintaining thermal comfort or other user preferences.

1.1. Thesis Statement

This thesis statement summarizes the main objective of this dissertation research that:

> It is possible to rank (using key performance criteria such as energy consumption, cost, and comfort) the performance of control algorithms managing residential energy use in a smart electric grid.

Until now, it was not known if an effective comparison (ranking) between the control algorithms can be performed.

1.2. Research Contributions

Realizing this research objective requires an assessment framework that can handle multiple performance criteria, capture user's subjective preferences and realistic objective performance data for testing the validation. Considering these objectives, the assessment framework must also enable a direct comparison of the performance of residential energy management control algorithms (EMCA) and effectively rank them. Figure 2 shows a schematic representation of this assessment framework that was developed for to meet the objectives of this dissertation research outlined above. This assessment framework is titled the Residential Energy Control Algorithm Assessment Tool (reCAAT).

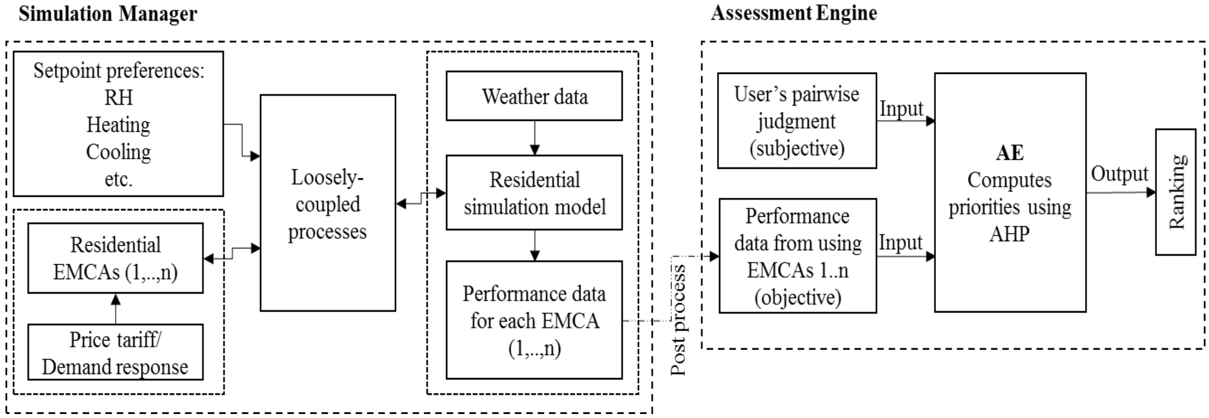

Figure 2. The reCAAT architecture showing the interaction of the components and the assessment engine (AE)

The reCAAT architecture describes the interaction of user preferences, residential EMCAs, a residential simulation model, and the assessment engine (AE). The reCAAT architecture is separated into two distinct implementations: The Simulation Manager (SM) and the AE. The AE is responsible for ranking the performance of residential EMCAs using subjective judgments for pairwise comparisons of energy consumption, cost, and comfort criteria; and objective performance data for pairwise comparisons of residential EMCAs. This is a multi-criteria decision-making problem that requires both qualitative and quantitative analyses. A widely used multi-criteria decision-making framework, the Analytical Hierarchy Process (AHP), was used to solve this problem. The AE uses a hybrid mechanism that derives a ranking from a combination of subjective user inputs, representing preferences, and objective data from the algorithm performance related to energy consumption, cost and comfort. The SM facilitates the loosely-coupled integration of residential EMCAs with a residential simulation model while capturing user preferences such as heating and cooling setpoints. A residential simulation model is used because it is impractical to conduct reproducible experiments in a real house. This provides the ability to substitute a simulation model for any house, which can also be tested in different climate zones by only changing the weather file. This loosely-coupled architecture provides an efficient mechanism for evaluating different types of residential EMCAs and simulation models without changing the core functionality of the SM for exchanging data.

The implementation of the architecture shown in Figure 2 meets the following requirements:

1. Supports a wide range of tariff structures and DR signals;
2. Accommodates customer preferences and constraints;
3. Accommodates different climate zones;
4. Accommodates simulation models for different types of residences;
5. Accommodates different residential energy management control algorithms;

6. Provides interfaces that loosely-couple components to accommodate a wide range of user input, residential EMCAs, and residential simulation model without impacting the core functionality of the AE; and
7. Allows bi-directional flow of information between an EMCA and residential simulation model.

Testing and validation of the AE is illustrated by applying the assessment process to six residential EMCAs. One algorithm was designed to match a real heat pump controller used in the house model. A second was the same as the first with relaxed comfort deadbands. Four others used linear integer optimization with varying optimization objectives to generate forecasted control actions. The algorithms were compared by analyzing their performance over a year based on energy consumption, cost, and comfort as measured by predicted mean vote (PMV) and predicted percentage of dissatisfied (PPD). The control algorithms were developed and tested using a simulation model of the Net-Zero Energy Residential Test Facility (NZERTF) located on the campus of the National Institute of Standards and Technology (NIST) in Gaithersburg, MD. A simulation model of this house was developed in Transient System Simulation Tool (TRNSYS) [10] and adopted for this study. The model was verified using measurement data from the NZERTF. The NZERTF is a research house that is comparable in size and aesthetics to the houses in the greater Washington DC metro area. Successful implementation of the AE produces a figure of merit that enables policy makers, customers, and other stakeholders to compare the performance of residential energy management control algorithms.

A summary of the research contributions is listed below:

1. Implementation of the SM;
2. Development of the AE;
3. Development of a mapping algorithm;
4. Development of a new TRNSYS component (Type277);
5. Development of six residential EMCAs; and
6. Development of a learning algorithm.

Chapter 2

2. Simulation Manager

This chapter describes the development of a co-simulation environment that enables a model of a residential home to exchange data with residential EMCAs while otherwise operating autonomously. Ideally, the EMCAs would interact with a real house to generate realistic operating conditions such as energy consumption and thermal comfort. However, it is impractical to conduct reproducible experiments in a real house and; therefore, a basic requirement for this study was to use a simulation model of a residential home. This provides the ability to substitute a simulation model for any house. Therefore, a TRNSYS based model is used to simulate the behavior of a residential home. TRNSYS is a FORTRAN-based whole building transient system simulation tool [11].

The methodology for coupling the residential model with a Java server (Server) using socket communication is also discussed. The Server enables the residential model to be loosely-coupled with residential EMCAs developed in Matrix Laboratory (MATLAB). An implementation of the co-simulation environment needs to support the following requirements:

1. Accommodate user preferences and constraints;
2. Accommodate loosely-coupling of residential EMCAs with simulation models for different types of residences;
3. Enable bi-directional flow of information between residential EMCAs and the simulation model; and
4. Accommodate different software environments for developing residential EMCAs.

To satisfy these requirements, Figure 3 shows the schematic representation of the co-simulation environment, describing the interaction of the user preferences, residential EMCAs and the simulation model.

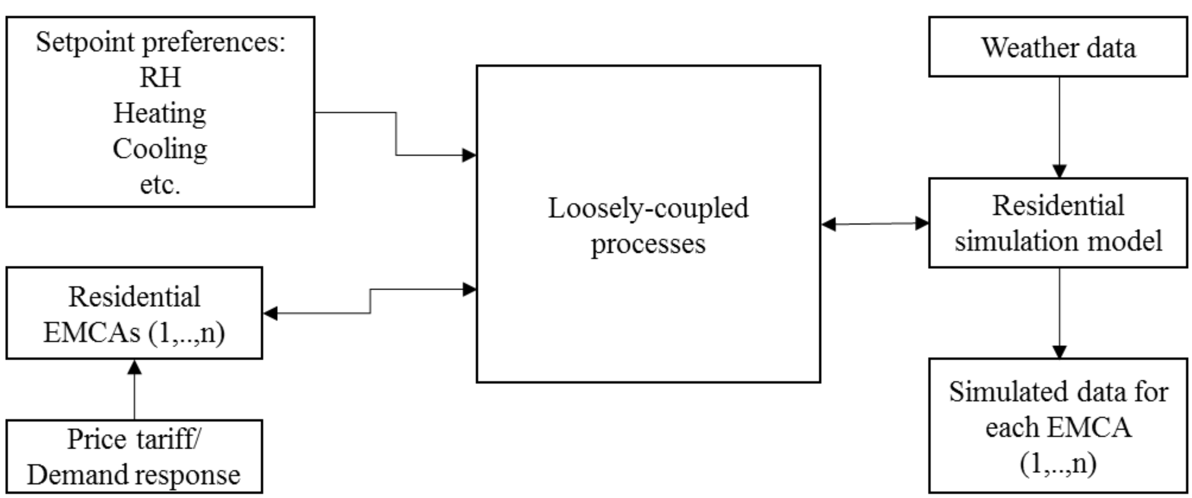

Figure 3. Schematic representation of the co-simulation environment

The implementation of the co-simulation environment captures user preferences, launches MATLAB, executes the TRNSYS model, and enables bi-directional flow of data between residential EMCAs and the simulation model. A user interface, the SM, was developed to provide the necessary foundation for implementing the co-simulation environment.

The SM facilitates the loosely-coupled integration of residential EMCAs and the residential model. The key idea behind this approach is to enable TRNSYS based simulation models to interact with components that are likely to be written in other software languages. For example, the SM is developed in Java, while residential EMCAs are written in MATLAB, and the residential model is developed in TRNSYS. The loosely-coupled architecture provides an efficient mechanism for evaluating different types of residential EMCAs and simulation models without changing its core functionality for exchanging data. A schematic representation of the SM architecture that facilitates these interactions is given in Figure 4. The TRNSYS simulation model, as a Client, sends and receives serialized data to the Server using socket communication. The Server and Client communicate over an arbitrary port (1345). The MATLAB environment exchanges data with the Server through a proxy, using the matlabcontrol Java application programming interface [12].

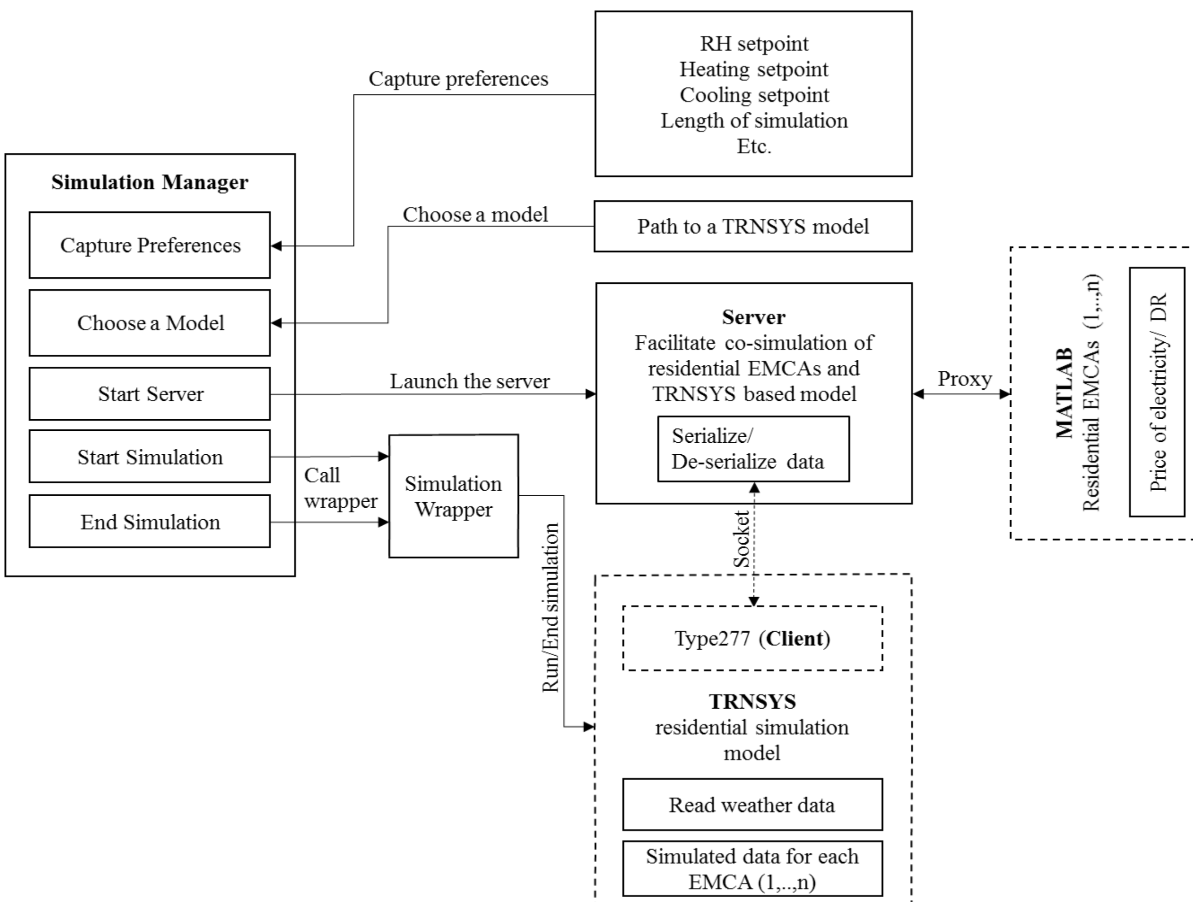

Figure 4. A schematic representation of the SM, facilitating loosely-coupled integration of TRNSYS and MATLAB

2.1. Net-Zero Energy Residential Test Facility

The residential simulation model used in this study is a model of the Net-Zero Energy Residential Test Facility (NZERTF) [10]. The detailed model of the NZERTF was developed in TRNSYS and validated using measurement data [10]. The NZERTF is a research house that is comparable in size and aesthetics to the houses in the greater Washington DC metro area [13]. NZERTF is located on the campus of the National Institute of Standards and Technology (NIST) in Gaithersburg, Maryland [2, 3]. The NZERTF is a 251 m^2 (2700 ft^2) four-bedroom house with a detached garage built entirely with commercially available products. It was designed to demonstrate the feasibility of achieving net-zero energy operation (energy generated using photovoltaic modules and solar hot water heaters equals the total energy consumed) over the course of one year, and test existing and new energy efficient technologies. The exterior of the NZERTF is shown in Figure 5.

Figure 5. The NZERTF house exterior

2.2. The User Interface

Realizing the SM involved developing a user interface (UI), shown in Figure 6, that encapsulates the requirements of the co-simulation environment described in Sec. 2. The UI is implemented in Java. It captures a user's preferences such as heating and cooling setpoints as well as the length of time, in minutes, for running the simulation. It also enables users to choose a desired TRNSYS model. A TRNSYS model is stored in a text file commonly known as the deck file, which contains all the information on the simulation model. The SM enables a user to choose a TRNSYS model by selecting the corresponding deck file. As schematically represented in Figure 4, the UI stores the path to the deck file, which is then used by the Simulation Wrapper to launch TRNSYS and simulate the model. The UI also creates the Server which launches MATLAB and listens for a client request on a socket. A socket is bound to a port and it is an endpoint for linking two programs that are sending and receiving data over a network or within the same computer. The client, in this case, is the TRNSYS model.

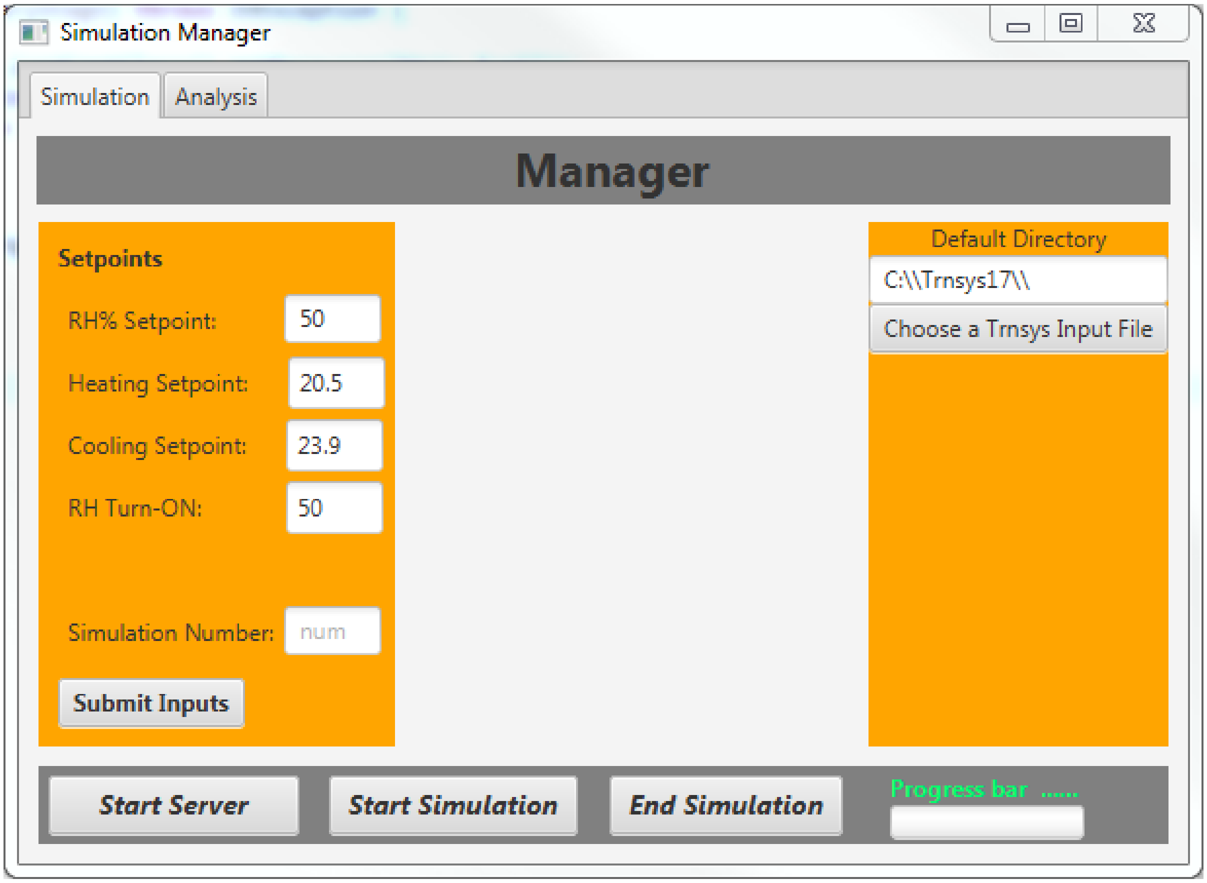

Figure 6. The simulation manager user interface

2.3. Simulation Wrapper

The Simulation Wrapper uses a FORTRAN subroutine compiled into a Dynamic Link Library (DLL) to cause the TRNSYS model to run. The Simulation Wrapper handles data exchange between Java and FORTRAN and runs the TRNSYS model. Figure 7 shows a schematic representation of the Simulation Wrapper.

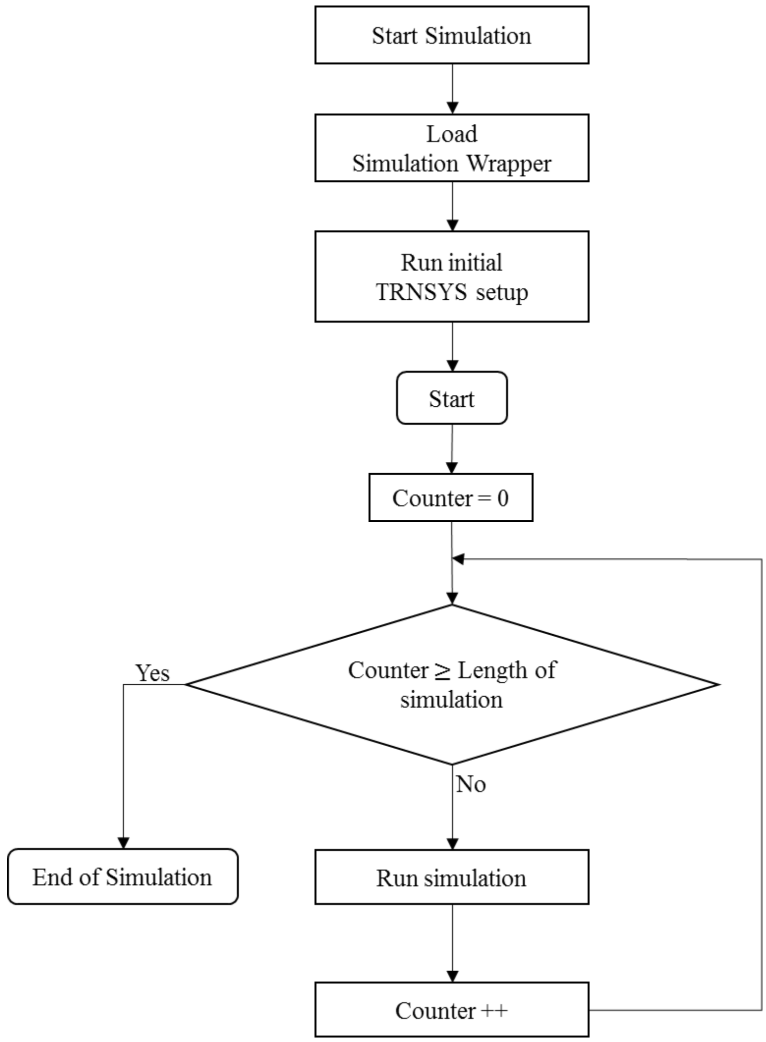

Figure 7. The Simulation Wrapper flowchart

The Start Simulation button utilizes the Java Native Access (JNA) library [15] to load the Simulation Wrapper. JNA is developed and maintained by a community of developers to provide easy access to the native libraries. Immediately after being loaded, the Simulation Wrapper makes special calls to TRNSYS, directing its main subroutine to find all other DLLs and load the deck file selected by the user. Next, the Simulation Wrapper starts the main simulation routine, which is implemented in a control flow (for-loop) to iteratively execute each time step of the TRNSYS model. The simulation terminates upon receipt of a special call to TRNSYS's main subroutine, which occurs when the loop counter exceeds the length of the simulation run specified by the user.

2.4. Type277

TRNSYS is a modular and extendable simulation environment that consists of a suite of software tools designed to accommodate transient simulation of multi-zone buildings and other thermal systems. The main user interface is Simulation Studio, in which users can setup projects by graphically connecting model components. Each component is mathematically described in the TRNSYS simulation engine and has a corresponding graphical representation (proforma) in the Simulation Studio. A proforma is a black-box description of inputs, outputs, and parameters. TRNSYS components are commonly referred to as Types and are identified by a number which relates a component to the model of that component written as a subroutine.

An advantage of TRNSYS's modular architecture is its ability to support the integration of user-defined types. In this study, a new type (Type277) was developed to enable a TRNSYS model to exchange data with the Server. The type number 277 was arbitrarily selected from a range of 200 – 299 which are reserved for user written components. Type277 is written in C++ and compiled as a 32-bit Windows DLL. It is compiled in 32-bit because the NZERTF model was developed and tuned using the 32-bit version of the TRNSYS simulation software. Type277 is responsible for exchanging data between a TRNSYS model and the Server. Like all standard types in TRNSYS, Type277 has a proforma that defines its inputs and outputs. The inputs of Type277 are sent to the Server and its outputs, the returned values from the Server, are connected to other TRNSYS types. Figure 8 shows Type277's proforma and a few of its connections with other types.

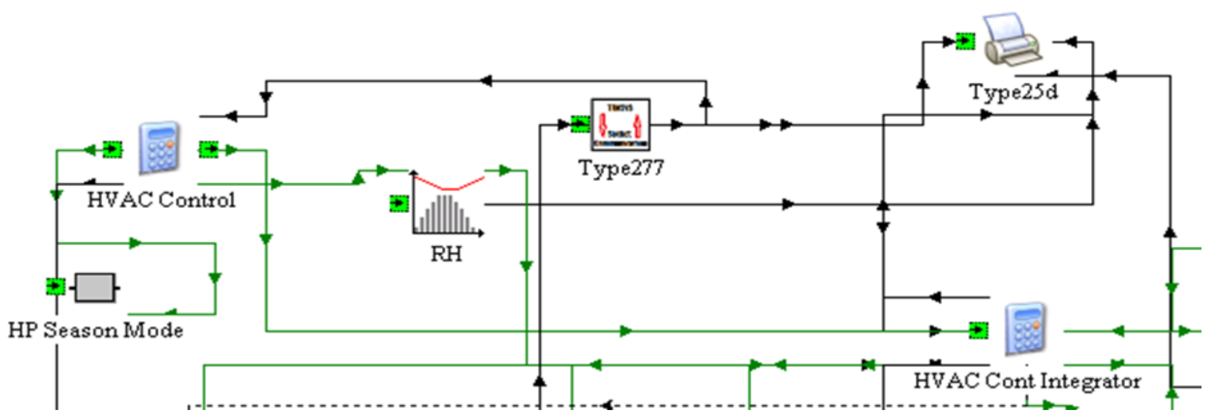

Figure 8. Type277's proforma

Using Type277 effectively turns a TRNSYS model into a Client. To ensure a reliable exchange of information between the Server and the Client, the data is serialized on both ends using Google's protocol buffers [16]. Protocol buffers are efficient, language and platform neutral, and expandable mechanism for serializing structured data. The current implementation of Type277 supports the exchange of double precision data type in a 1xn dimensional vector form, where n is the number of inputs or outputs.

Chapter 3

Disclaimer: The material presented in this chapter has previously been published in:

1. F. Omar and S. T. Bushby, "A Self-Learning Algorithm for Temperature Prediction in a Single Family Residence," NIST Tech. Note 1891, 2015.
2. F. Omar, S. T. Bushby, and R. D. Williams, "A self-learning algorithm for estimating solar heat gain and temperature changes in a single-Family residence," Energy Build., vol. 150, 2017.

Credit to my co-authors:

1. Steven T. Bushby, National Institute of Standards and Technology, steve.bushy@nist.gov
2. Ronald D. Williams, University of Virginia, rdw@virginia.edu

3. Learning Algorithm

Developing effective control strategies to manage residential electricity consumption in a smart grid environment requires predictive algorithms for all significant electrical loads that are simple to implement, minimize custom configuration, and provide enough accuracy to enable meaningful control decisions. In a smart grid environment, time-varying prices, demand response agreements, or possibly market-based transactions to buy or sell electricity, may significantly influence the cost of electricity consumption. Other key inputs to control decisions include weather and occupant choices.

Heating, ventilating, and air-conditioning (HVAC) is one of the largest electrical loads in a typical house. To evaluate control strategies that might involve preheating or precooling, temperature setbacks, or letting the temperature drift during peak price periods, it is important to be able to predict the resulting indoor air temperature changes. Many tools to simulate building energy use and comfort conditions have been developed that have this capability [17]. Although details vary, these tools require information about the location, orientation, windows, and other construction details of the house. They also require expertise in crafting a simulation. A simpler approach is needed to develop control strategies that might be used in a typical home.

In this chapter, a self-learning algorithm for temperature prediction in a single-family residence was developed. The approach taken was to define a simple lumped capacitance model where key parameters for the model can be learned through observation instead of derived from in depth knowledge of the construction details. The algorithm was validated using performance measurements from the NZERTF [13], [14].

3.1. Lumped Capacitance Model

In order to predict the interior air temperature of a house, a first order lumped capacitance model described in [18] is utilized. The house is assumed to be a single control volume with a uniform interior temperature. Figure 9 shows a schematic of the overall energy balance on a house.

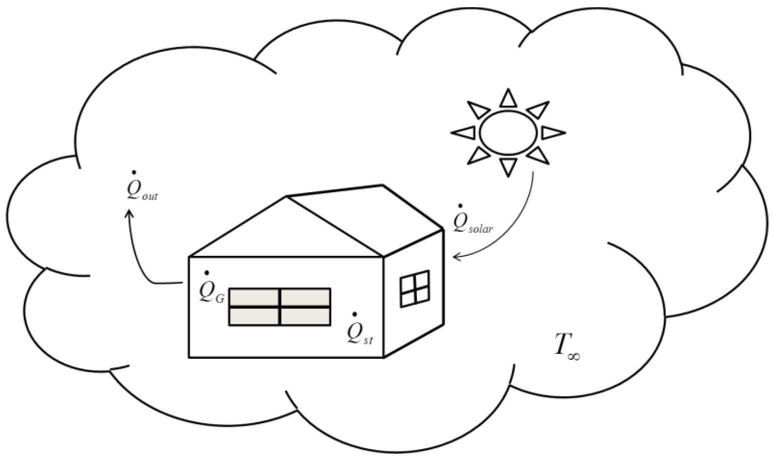

Figure 9. A house thermal energy balance

The energy balance equation as a rate of change of energy is given by:

$$\dot{Q}_{st} = \dot{Q}_{solar} + \dot{Q}_G - \dot{Q}_{out}\,, \tag{1.1}$$

where:

$\dot{Q}_{st} = \frac{dQ_{st}}{dt} = \frac{dT}{dt}\rho V c_p$ is the rate of the thermal energy stored in the house;
ρ is the density;
c_p is the specific heat;
V is the volume;
$\dot{Q}_{Solar} = (q_{sol})$ is the total solar heat gain added to the house;
$\dot{Q}_G = (q_{hp} + q_l)$ is the internal heat generated inside the house by the heat pump (q_{hp}), and plug-loads (q_l) including sensible heat generated by the occupants; and
$\dot{Q}_{Out} = UA(T - T_\infty)$ is the heat loss to the environment due to the temperature difference between the inside and the outside. UA is the overall heat transfer coefficient, T is the indoor dry-bulb and T_∞ is the outside ambient dry-bulb temperatures, respectively. Note that radiation heat losses are neglected.

Applying these definitions, Eq. (1.1) can be rewritten as follows:

$$\rho V c_p \frac{dT}{dt} = q_{sol} + q_{hp} + q_l - UA(T - T_\infty)\,. \tag{1.2}$$

If we let $\psi = \left(T - T_\infty\right)$, then $\dfrac{dT}{dt} = \dfrac{d\psi}{dt}$ and Eq. (1.2) becomes:

$$\rho V c_p \frac{d\psi}{dt} = q_{sol} + q_{hp} + q_l - UA\psi \ . \tag{1.3}$$

Dividing both side of Eq. (1.3) by $\rho V c_p$ we obtain the following first-order differential equation:

$$\frac{d\psi}{dt} = \frac{q_{sol} + q_{hp} + q_l}{\rho V c_p} - \frac{UA\psi}{\rho V c_p} \ . \tag{1.4}$$

Re-writing Eq. (1.4):

$$\frac{d\psi}{dt} = b - a\psi \ , \tag{1.5}$$

where:

$a = \dfrac{UA}{\rho V c_p}$, and $b = \dfrac{q_{sol} + q_{hp} + q_l}{\rho V c_p}$.

Multiplying both sides of Eq. (1.5) by an integrating factor e^{at} and rearranging gives:

$$e^{at} \frac{d\psi(t)}{dt} + e^{at} a\psi(t) = e^{at} b \ . \tag{1.6}$$

Using the product rule, the left hand side of Eq. (1.6) can be written as:

$$\frac{d}{dt}\left(e^{at}\psi(t)\right) = e^{at} b \ . \tag{1.7}$$

Integrating both sides of Eq. (1.7) with respect to t gives:

$$\begin{aligned} \int d\left(e^{at}\psi(t)\right) &= \int e^{at} b\,dt \\ e^{at}\psi(t) &= b\frac{1}{a}e^{at} + C. \end{aligned} \tag{1.8}$$

Dividing both sides of Eq. (1.8) by e^{at} gives:

$$\psi(t) = \frac{b}{a} + Ce^{-at} \ , \tag{1.9}$$

when $t = 0$, $C = \psi(0) - \dfrac{b}{a}$ then Eq. (1.9) becomes:

$$\psi(t) = \frac{b}{a} + \left[\psi(0) - \frac{b}{a}\right] e^{-at}. \tag{1.10}$$

Substituting the values for *a, b, ψ* back into the Eq. (1.10) results in the first order lumped capacitance model. If we let $\psi(0) = T_i - T_\infty$ where T_i is the initial temperature of the house and T_∞ is the ambient temperature then Eq. (1.10) becomes

$$T - T_\infty = \frac{q_{sol} + q_{hp} + q_l}{UA} + \left(T_i - T_\infty - \frac{q_{sol} + q_{hp} + q_l}{UA}\right) \exp\left(-\frac{UA}{\rho V c_p} t\right). \tag{1.11}$$

Defining the thermal time constant τ such that:

$$\tau = \left(\frac{1}{UA}\right)\left(\rho V c_p\right),$$

where:

$\left(\frac{1}{UA}\right)$ is the overall-lumped thermal resistance; and

$\left(\rho V c_p\right)$ is the lumped thermal capacitance.

Re-writing and re-arranging Eq. (1.11) gives the first order model to predict the interior temperature:

$$T = T_\infty + \frac{q_{sol} + q_{hp} + q_l}{UA} + \left(T_i - T_\infty - \frac{q_{sol} + q_{hp} + q_l}{UA}\right) \exp\left(-\frac{t}{\tau}\right), \tag{1.12}$$

where:

T_∞ is the outside ambient dry-bulb temperatures, °C;
q_{sol} is the total solar heat gain added to the house, W;
q_{hp} is the rate of heat generated inside the house by the heat pump, W;
q_l is the rate of heat generated inside the house by the internal loads, W;
T_i is the initial indoor temperature, °C;
UA is Overall heat transfer coefficient, W/K; and
τ is the building time constant, h.

The value of (q_{sol}) can be estimated from measurements of solar irradiance using methods discussed later in this document. The value of (q_l) is also known through a fixed occupancy schedule described in [14]. However, the values of *UA* and τ are not known a priori. A learning algorithm is used to estimate these values from measured data. In this paper they are denoted as effective quantities (UA_e, τ_e) to acknowledge the fact that the values are not the true *UA* and τ of the NZERTF but an approximation that will enable us to predict the indoor temperature.

A discrete form of Eq. (1.12) is developed by defining *t* as $\Delta t = t_{k+1} - t_k$ where $k = 1, 2, \ldots, n$ are the discrete time steps and *n* is the number of data points. Let ($Q_h = q_{sol} + q_{hp} + q_l$) represent the total heat gain inside the NZERTF in every time step. Let T_i represent the indoor temperature. Applying these concepts to Eq. (1.12) gives the one-step learning/prediction model:

$$T_{i,k+1} = T_{\infty,k} + \frac{Q_{h,k}}{UA_e} + \left(T_{i,k} - T_{\infty,k} - \frac{Q_{h,k}}{UA_e} \right) \exp\left(-\frac{\Delta t}{\tau_e} \right). \tag{1.13}$$

3.2. Learning the Overall Heat Transfer Coefficient and Thermal Time Constant

Estimates for the UA_e and τ_e are needed to use Eq. (1.13) to predict the indoor temperature. Since both UA_e and τ_e are mainly driven by the temperature difference between the inside and outside, a single test was conducted in the NZERTF on a cold winter night. Testing at night eliminated the impact of direct solar heat gain into the interior space. During the test, the house's main thermostat setpoint was lowered to approximately 15.6 °C (60 °F), and the heat recovery ventilation unit was turned off. The first floor and outdoor dry-bulb temperatures were measured throughout the night. The first-floor temperature is an average of measurements made in all the rooms on the first floor. Figure 10 shows the results of the test. The uncertainty in measuring the indoor and outdoor dry-bulb temperature described in [19], with a confidence level of 95 %, is ± 0.2 °C (0.4 °F) and ± 0.6 °C (1.0 °F), respectively.

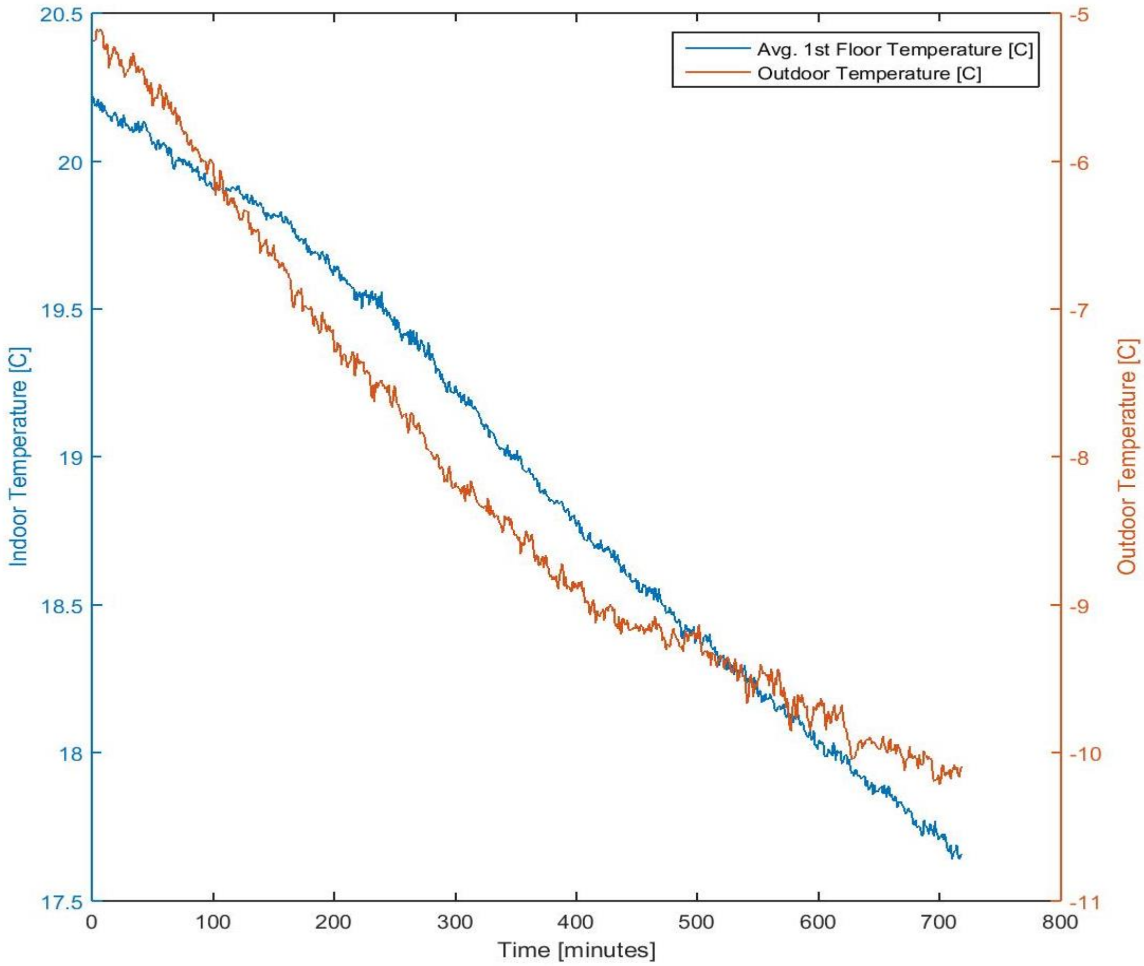

Figure 10. Results from a night temperature decay test

Because the heat pump energy and solar heat gain to the house are equal to zero in this test, Eq. (1.13) is reduced to the following:

$$T_{i,k+1} = T_{\infty,k} + \frac{q_{l,k}}{UA_e} + \left(T_{i,k} - T_{\infty,k} - \frac{q_{l,k}}{UA_e} \right) \exp\left(-\frac{\Delta t}{\tau_e} \right). \tag{1.14}$$

In order to estimate UA_e and τ_e using an optimization technique, an objective function is defined as the sum of squared error (SSE) between the measured average first floor temperature (T_m) and the predicted temperature (T_p) obtained from Eq. (1.14). The objective function is

$$f\left(UA_e, \tau_e\right) = \left\| T_m - T_p \right\|_2^2, \tag{1.15}$$

and, the optimization problem is:

$$\begin{aligned} \min_{UA_e,\tau_e} \quad & f\left(UA_e,\tau_e\right) \\ & 1 \le UA_e \le \infty \\ & 60 \le \tau_e \le \infty, \end{aligned} \tag{1.16}$$

where, the units for upper and lower bounds of the UA_e are in W/K and τ_e are in minutes. For numerical stability, the lower bound of UA_e was set to 1; however, the upper bound was allowed to float because it was not known a priori. Similarly, the lower bound of τ_e was set to 1 hour and the upper bound was allowed float as well. A Matlab non-linear optimization function (*fmincon*) with its default interior-point algorithm was used to minimize Eq. (1.16) subject to the upper and lower bound constraints. The result of the optimization is shown in Figure 11.

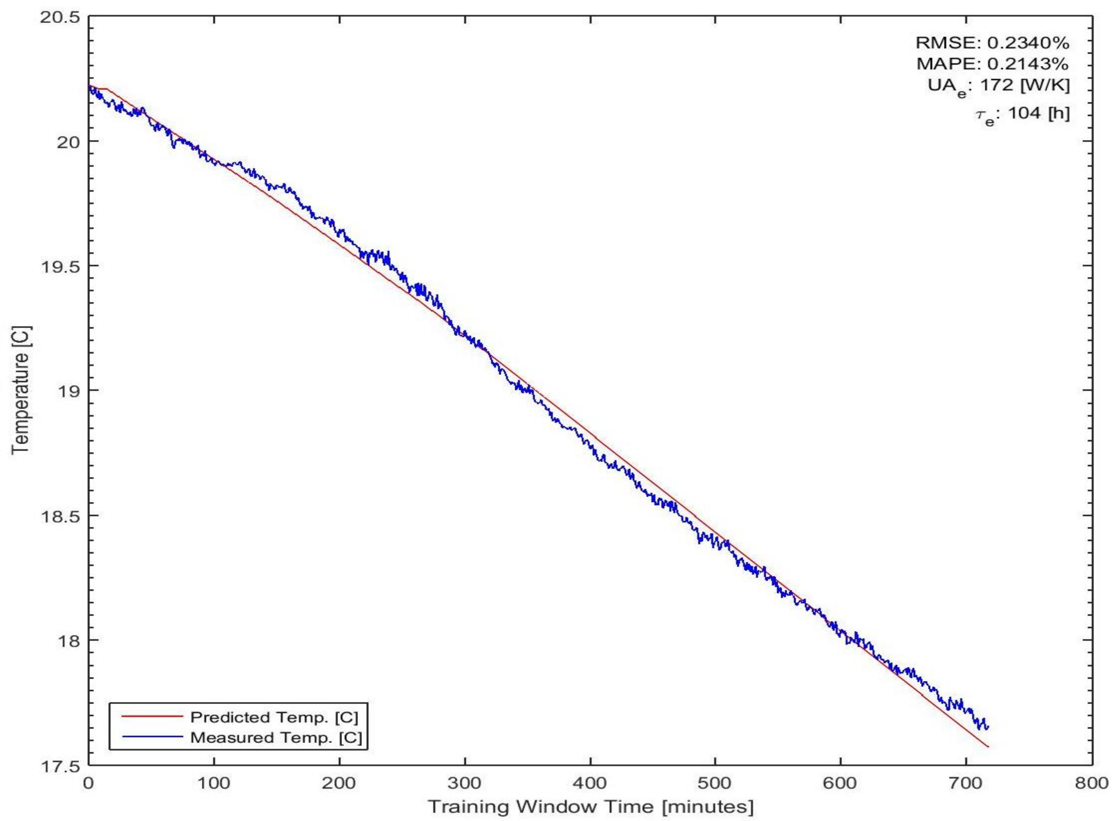

Figure 11. Comparison of predicted and measured first floor temperatures during a night test

Figure 11 shows the predicted and measured first floor temperature, for the test period, and statistics describing the goodness of fit. The resulting learned parameters are, UAe = 172 W/K and τe = 104 h.

To verify the value of UA_e an alternative method was used to provide a comparison estimate. Daily heat pump thermal energy output for the period of October 2014 – May 2015 were plotted with respect to the indoor/outdoor temperature difference as shown in Figure 12. The uncertainty in measuring $T_{outdoor}$ and *Thermal Energy* described in [19], with a confidence level of 95 %, is ± 0.2 °C (0.4 °F) and ± 9.4 %, respectively. Assuming that internal loads and solar gain are small compared to the conductive and convective heat losses,

$$\dot{Q}_{hp} \approx UA\left(T_{\text{outdoor}} - T_{\text{setpoint}}\right).$$

Thus the slope of linear fit to the data provides an estimate for *UA*. From these data it was found that *UA = 180 ± 8 W/K* with a confidence of 95 %. This result confirms that learned value of UA_e = 172 W/K is a reasonable estimate.

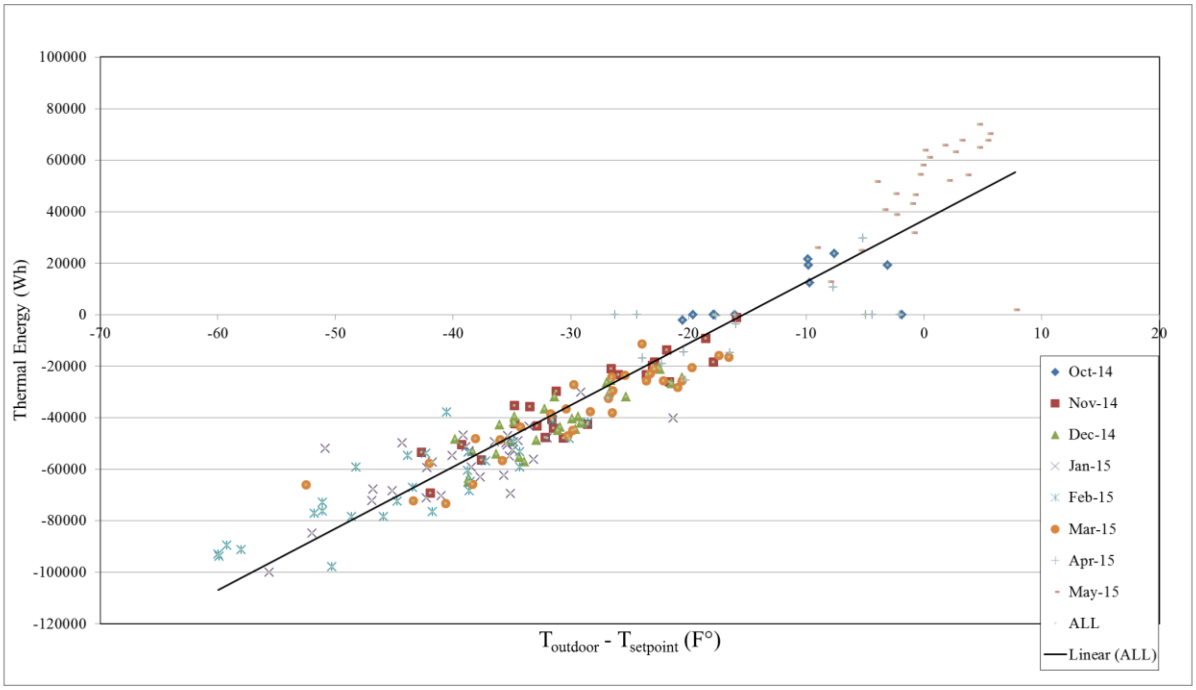

Figure 12. Heat pump load vs. temperature difference, courtesy of William V. Payne

3.3. Estimating Solar Gain

An estimate of solar heat gain is needed to apply Eq. (1.13). Detailed procedures for estimating solar heat gain are provided in [20]. Modeling solar heat gain is a complex process that involves many details about window size, orientation, shading, and materials along with estimates of direct and indirect solar radiation. For the application intended in this work, these details are not likely to be available and the custom configuration needed to use them is not practical to obtain. The solution proposed is to develop a mathematical representation for solar heat gain with a small number of parameters that capture the unknown details, and then learn those parameter values by observation. One representation for solar heat gain is adapted from [21].

$$q_{sol} = E_{DN} \cos(\theta)(T - NA)W_A, \tag{1.17}$$

where:

q_{sol} is the total solar heat gain;

E_{DN} is the direct normal irradiance per unit area;
θ is the incidence angle;
T is the transmittance;
A is the absorptance;
N is the inward-flowing fraction; and
W_A is the window area.

The quantity ($T - NA$) is the solar heat gain coefficient (SHGC). Because the optical properties of T and A varies as a function of incidence angle (θ) and wavelength (λ) the SHGC is [21]

$$SHGC(\theta,\lambda) = T(\theta,\lambda) - NA(\theta,\lambda), \tag{1.18}$$

and Eq. (1.17) can be written as

$$q_{sol} = E_{DN}\cos(\theta)SHGC(\theta,\lambda)W_A. \tag{1.19}$$

In residential buildings we can assume that the windows are of the clear glass type and therefore not strongly spectrally selective so that the wavelength dependence of SHGC can be neglected. Thus, Eq. (1.19) can be re-written as

$$q_{sol} = E_{DN}\cos(\theta)SHGC(\theta)W_A. \tag{1.20}$$

Eq. (1.20) is the total solar heat gain, at every time step, added to a house and the SHGC (as function of the incidence angle) is given in [21]

$$SHGC(\theta) = T(\theta) - \sum_{k=1}^{L} N_k A_k(\theta), \tag{1.21}$$

where, L is the number of glazing layers, N_k and A_k are the inward-flowing fraction and absorptance of layer k, respectively. Assuming a single layer window, a modified version of Eq. (1.21) is

$$SHGC(\theta) = T(\theta) - NA(\theta). \tag{1.22}$$

Since the type of the windows installed in a house is not known a priori; therefore, Eq. (1.22) becomes

$$SHGC_e(\theta) = T(\theta) - N_e A(\theta), \tag{1.23}$$

where, N_e (effective N) is an approximation of N and $SHGC_e$ (effective $SHGC$) is an approximation of the $SHGC$. Normally, in order to convert beam radiation measured on one surface to another (i.e., on a tilted surface to that on a horizontal surface) a dimensionless geometric factor; that is, a ratio between the two surfaces is computed and the beam radiation is multiplied by that ratio. For further description of calculating this ratio see [22]. It is further assumed that the orientation and size of the windows is unknown. The objective is to modify Eq. (1.20) such that the details of window size and orientation, shading effects, and the fraction of direct or diffuse solar radiation are represented by parameters that can be learned by observation. This eliminates the need for detailed custom configuration by the user. The modified solar heat gain Eq. is

$$q_{sol} = I \times SHGC_e(\theta) \times AR_e, \tag{1.24}$$

where:

I is the solar irradiance in W/m^2; and

AR_e is an approximation (effective) window area and the ratio of solar irradiance to the vertical surfaces of the windows in units of m^2.

We utilize a moving window optimization technique, described later, to learn the N_e and AR_e parameters.

In order to calculate $SHGC_e$ given in Eq. (1.23) the transmittance and absorptance must be calculated based on the angle of incidence. The angle of incidence is calculated using Eq. (1.25) described in [22].

$$\begin{aligned}\cos(\theta) = {} & \sin(\delta)\sin(\phi)\cos(\beta) - \sin(\delta)\cos(\phi)\sin(\beta)\cos(\gamma) \\ & + \cos(\delta)\cos(\phi)\cos(\beta)\cos(\omega) + \cos(\delta)\sin(\phi)\sin(\beta)\cos(\gamma)\cos(\omega) \\ & + \cos(\delta)\sin(\beta)\sin(\gamma)\sin(\omega),\end{aligned} \tag{1.25}$$

where:

δ is the declination, the angular position of the sun at solar noon;

ϕ is the latitude, the angular location north or south of the equator;

β is the slope, the angle between the plane of the surface in question and the horizontal (windows or solar radiation measuring angle);

γ is the surface azimuth angle, the deviation of the projection on a horizontal plane of the normal to the surface from the local meridian;

ω is the hour angle, the angular displacement of the sun east or west of the local meridian due to rotation of the earth on its axis at 15° per hour; and

θ is the angle of incidence, the angle between the beam radiation on a surface and the normal to that surface.

For a detailed explanation of computation of the values δ, ω, and θ see [22]. While the latitude, slope, longitude, local meridian, local time zone, surface azimuth angle are inputs and based on the geographical location of the NZERTF in Gaithersburg Maryland. The list of inputs and their associated values are given in Table 2.

Table 2. List of inputs and their associated values to calculate the angle of incidence

Inputs	Values based on location of NZERTF
ϕ	39.14°
β (windows tilt $\angle$)	90°
Longitude	77.2°
Local Meridian	75°
Local Time Zone	Eastern
γ	0°

In this application, the incidence angle is computed based on the timestamp associated with the measured data. According to [23], the transmittance and absorptance of a variety of window types can be computed using Eq.s (1.26) and (1.27).

$$T(\theta) = \sum_{i=0}^{3} c_i \cos^i(\theta), \tag{1.26}$$

$$A(\theta) = \sum_{j=0}^{3} c_j \cos^j(\theta). \tag{1.27}$$

The coefficients c_i and c_j for a single layer glass, $3.2\ \text{mm}\ (1/8 - inch)$, double strength float are adopted from Table I of [23] and reported in Table 3.

Table 3. Coefficients of a glass window used to calculate transmittance and absorptance

Windows Structure	Solar Properties	c_0	c_1	c_2	c_3
Glass	$T(\theta)$	-0.0372	3.0392	-3.6360	1.4784
	$A(\theta)$	0.0738	0.2370	-0.4364	0.2168

With the transmittance and absorptance calculated, the two unknown parameters are the inward-flowing fraction N_e (from Eq. (1.23)) and AR_e (from Eq. (1.24)). The total heat gain ($Q_h = q_{sol} + q_{hp} + q_l$) inside the NZERTF with q_{sol} given by Eq. (1.24) is

$$Q_h = \left(I \times SHGC_e(\theta) \times AR_e\right) + q_{hp} + q_l. \tag{1.28}$$

To calculate N_e and AR_e a moving window optimization algorithm was developed and implemented.

3.4. Moving Window Prediction Algorithm

The moving window algorithm utilizes Eq. (1.13) and Eq. (1.28) to learn the N_e and AR_e parameters from measured data over a training window, the size of which is discussed later. These parameters are then used to predict the next day's indoor temperature. Training is repeated daily using a fixed-size sliding window of data. This approach allows any shading effects and the seasonal variation in sun position to be accounted for. The moving window prediction approach is illustrated in Figure 13. The red rectangles depict the sliding training data window. The green rectangles depict the corresponding prediction horizon.

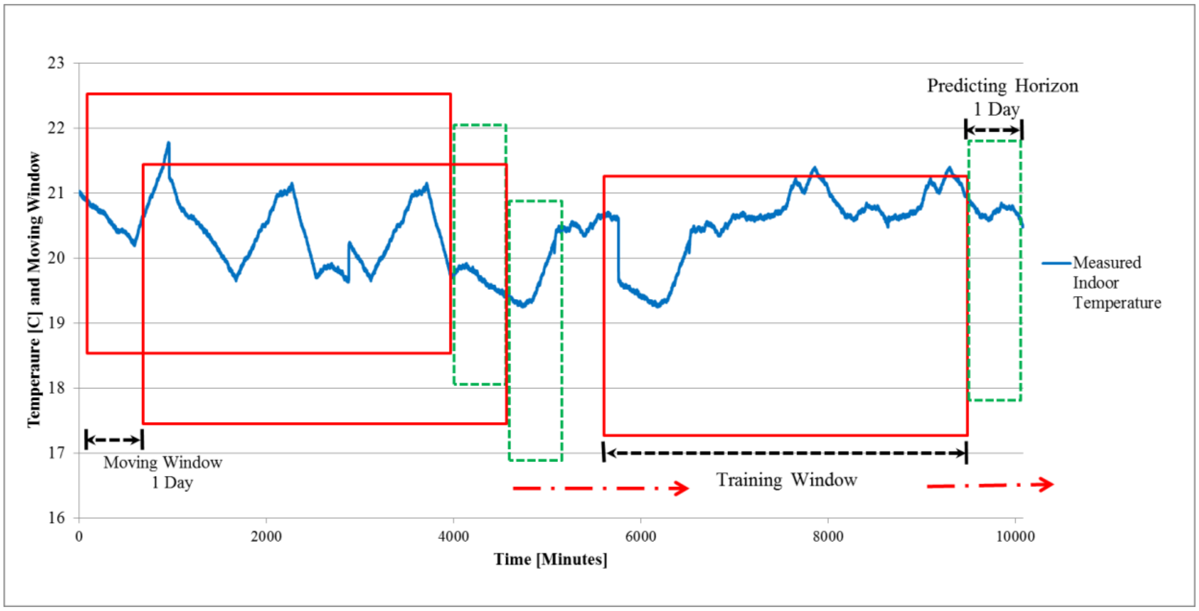

Figure 13. The concept of the moving window prediction algorithm, note that the sizes of the windows are not to scale

The objective function for the moving window algorithm is defined as the SSE between the measured average first floor temperature (T_m) and the predicted temperature (T_p) obtained from Eq. (1.13). This can be expressed as

$$f\left(N_e, AR_e\right) = \left\| T_m - T_p \right\|_2^2 \ . \tag{1.29}$$

The optimization problem is defined as

$$\begin{aligned} \min_{N_e, AR_e} \quad & f(N_e, AR_e) \\ & 0 \le N_e \le 1 \\ & 1 \le AR_e \le \infty, \end{aligned} \tag{1.30}$$

where, the N_e is a unitless quantity, and the AR_e is in units of m^2. The upper and lower bounds of the N_e is between [0, 1] because it only represents the fraction of the solar irradiance absorbed into the interior spaces. The lower bound of the AR_e is set to1 for numerical stability. The upper bound is allowed to float because it is not known a priori.

In order to find N_e and AR_e a Matlab non-linear optimization function (*fmincon*) with its default interior-point algorithm was used to minimize Eq. (1.30). Initially the algorithm was trained on one day of data and predicted the next day's temperature. But since the N_e and especially

AR_e parameters greatly affect the total solar heat gain of the model, the prediction accuracy was highly influenced by the variability of the solar irradiance from one day to the next due to cloud cover. For example, if the parameters were learned on a cloudy day and applied to a day that was sunny the model over predicted the temperature. The model under predicted when the opposite was true. Figure 14 shows the measured solar irradiance for a cloudy training day followed by measured solar irradiance on the prediction day. Figure 15 shows the impact of this situation on predicting the next day's temperature.

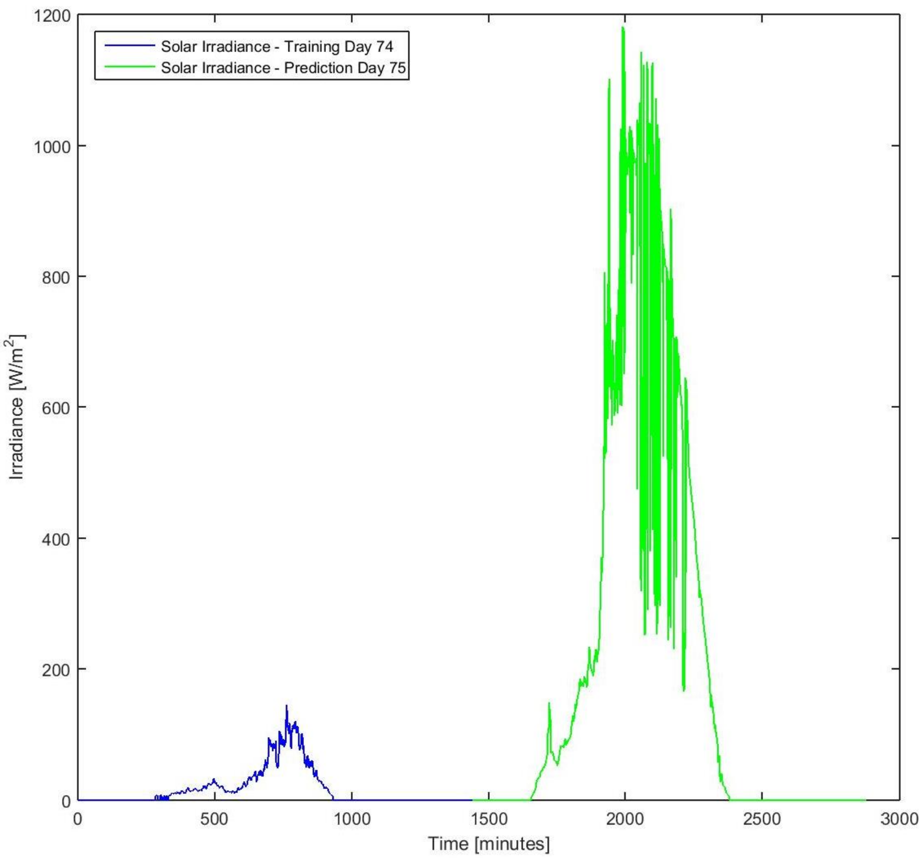

Figure 14. Available solar irradiance – training and prediction days

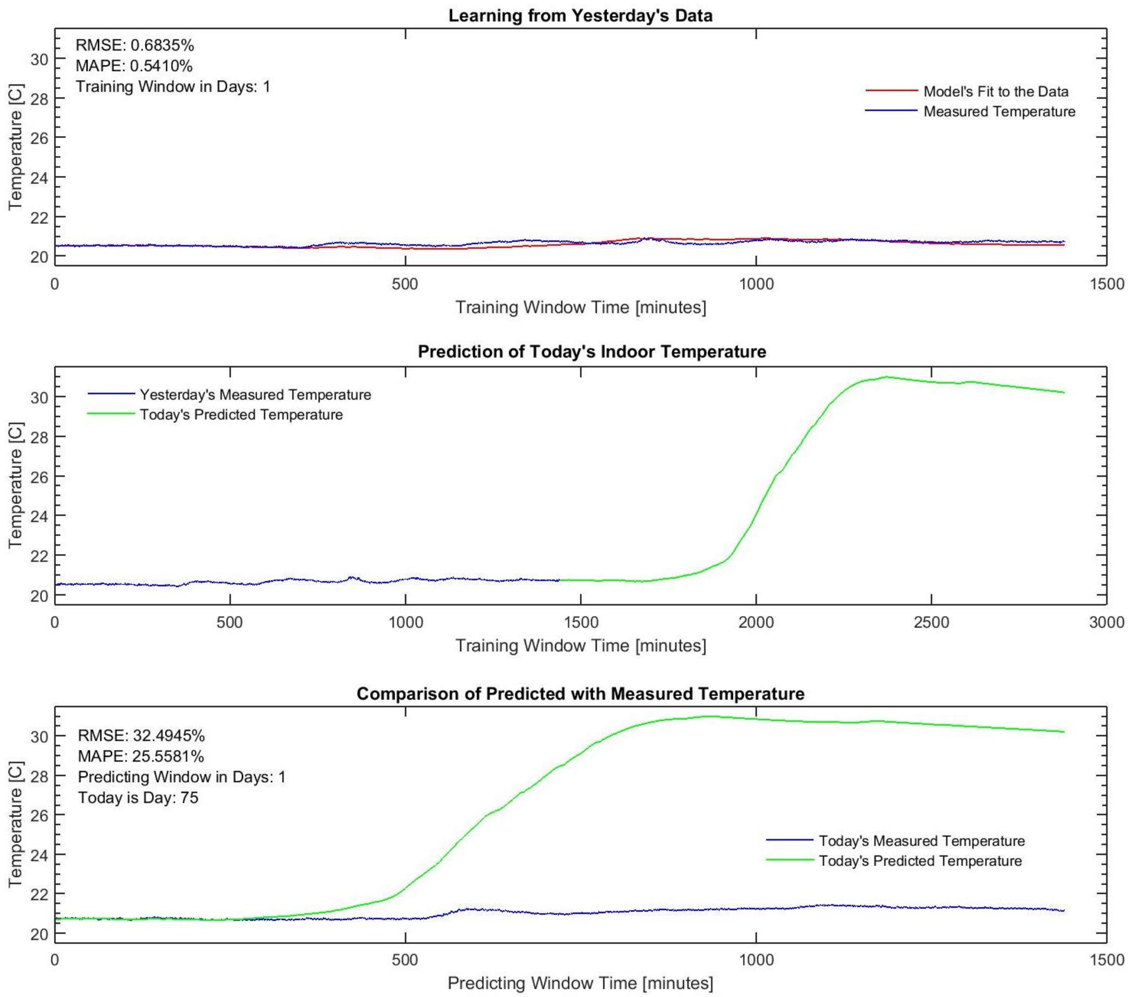

Figure 15. Learning parameters on a cloudy day and applying it to a sunny day (1-day training window)

There is a good agreement between the predicted and measured temperatures, shown in the top plot of Figure 15, because, by adjusting the N_e and AR_e parameters, the learning algorithm minimizes the SSE between the model and the measured data. The second plot shows the model's predicted indoor temperature at the beginning of the day and the third plot shows the comparison between the predicted and the actual measured temperatures for the same day.

It was found that if the parameters were learned on a cloudy or a sunny day and applied to a day with a similar solar condition, the predicted and measured temperatures were close. Figure 16 shows the solar irradiance for the training and prediction days while Figure 17 shows the influence of learning a parameter on such a day and applying it to a day with a similar solar condition.

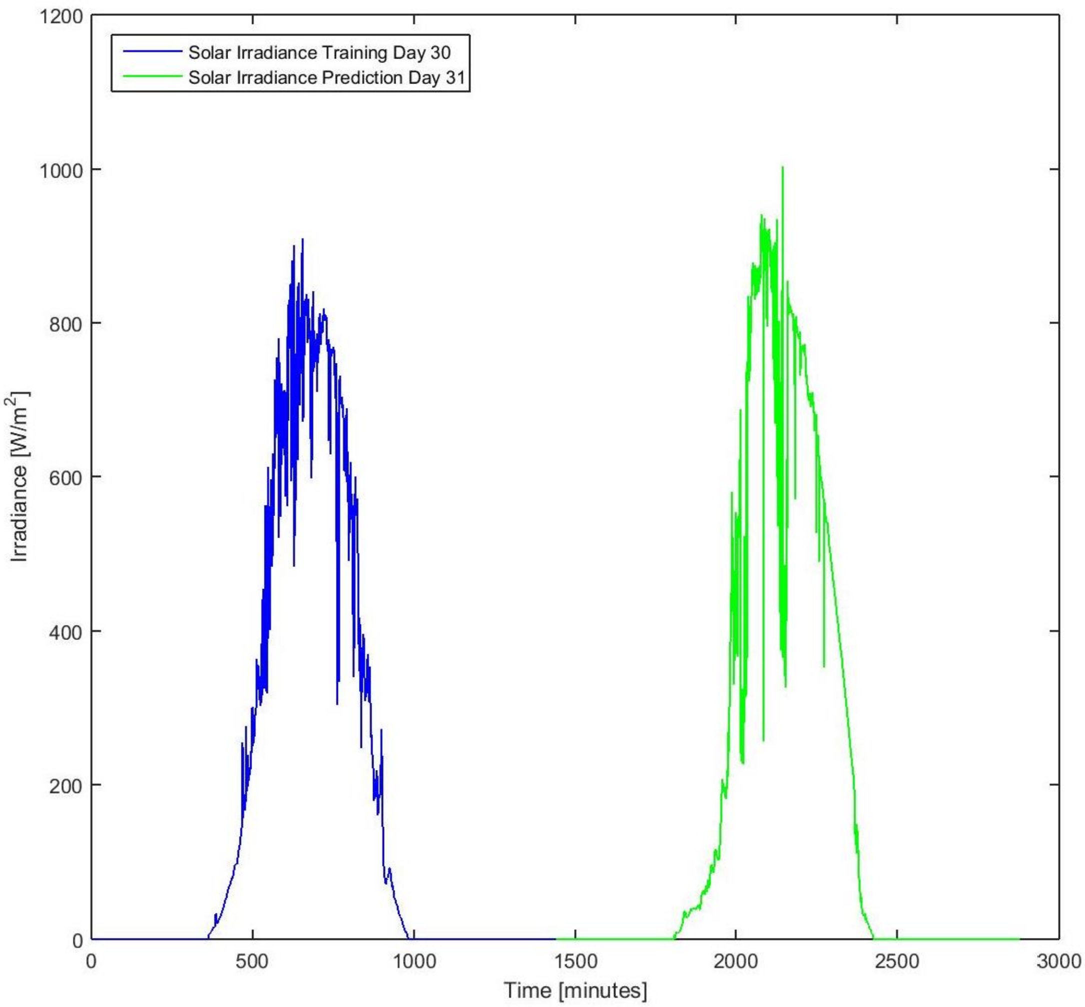

Figure 16. Available solar irradiance – training and prediction days

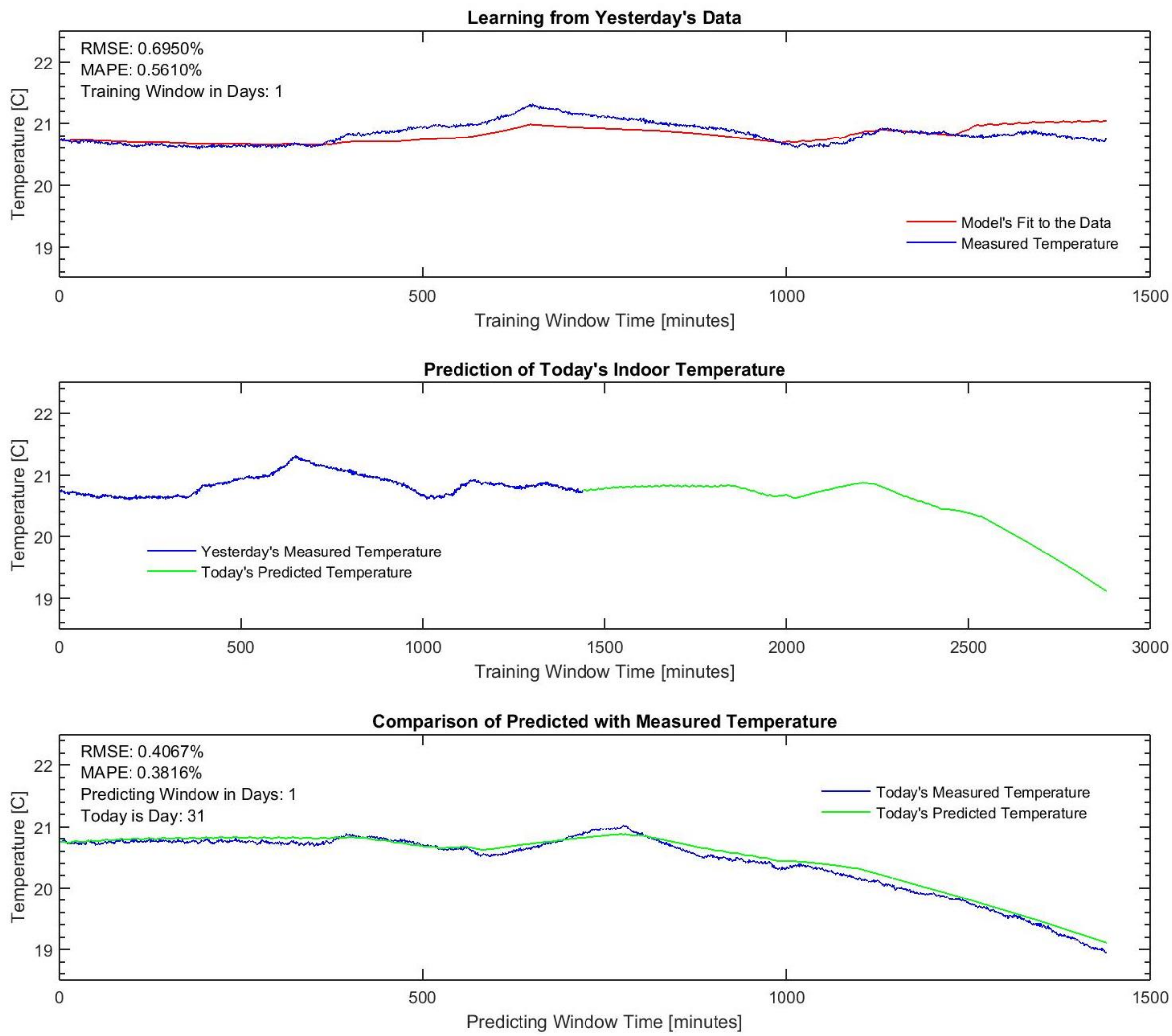

Figure 17. Learning parameters on a sunny day and applying it to a sunny day (1-day training window)

These results clearly indicate that a larger training window is required. In order to evaluate the merit of various training window sizes two statistical measures (relative root mean square error (*% RMSE*) [24] and mean absolute percentage error (*MAPE*) given in [25] are defined as follows

$$\%RMSE = \frac{\sqrt{\dfrac{\sum_{i=1}^{n}\left(T_m^i - T_p^i\right)^2}{n}}}{\overline{T_m}} \times 100\,, \tag{1.31}$$

and

$$MAPE = \frac{1}{n}\sum_{i=1}^{n}\left|\frac{T_m^i - T_p^i}{T_m^i}\right| \times 100\,, \tag{1.32}$$

where:

n is the number of samples;

T_m^i is the i^th^ measured temperature;

$\overline{T_m}$ is the mean of the measured temperature; and

T_p^i is the i^th^ predicted temperature.

Both *% RMSE* and *MAPE* are dimensionless quantities, and a measure of closeness of the predicted and measured temperatures. The output of Eq. (1.31) and (1.32), reported in Table 4, confirms the observation that the prediction accuracy of the model is significantly improved when the training and prediction days had identical solar conditions.

Table 4. Prediction horizon *% RMSE* and *MAPE* (1-day training window)

Figure #	**% RMSE**	**MAPE**
Figure 15	29	23
Figure 17	0.4	0.4

Using these metrics an optimal window size can be determined. The prediction algorithm was tested for various training window sizes over the 85-days data set. The average *% RMSE*, for each training window size, was calculated and reported in Figure 18. Figure 18 also shows the average elapsed time (in minutes) that the optimization algorithm took while learning the N_e and AR_e parameters. It is noted that the elapsed time is specific to our implementation of the algorithm. Faster times may be possible but in general the larger the training window the slower the optimization.

Figure 18 shows that there is large reduction in *% RMSE* when the size of the training window is increased from 1 to 3 days. The error is further reduced, gradually, until the size of the training window is 7 days long. There is a slight increase in the error for the 14 and 21 days of training, however the increase is minimal. Even though the 42 days training window has the lowest *% RMSE,* the time that the optimization requires to learn N_e and AR_e is significantly larger compared to the rest of the training windows. Considering the elapsed times, number of training data required, and smaller prediction error, it was decided that the 7-day training window was an appropriate size.

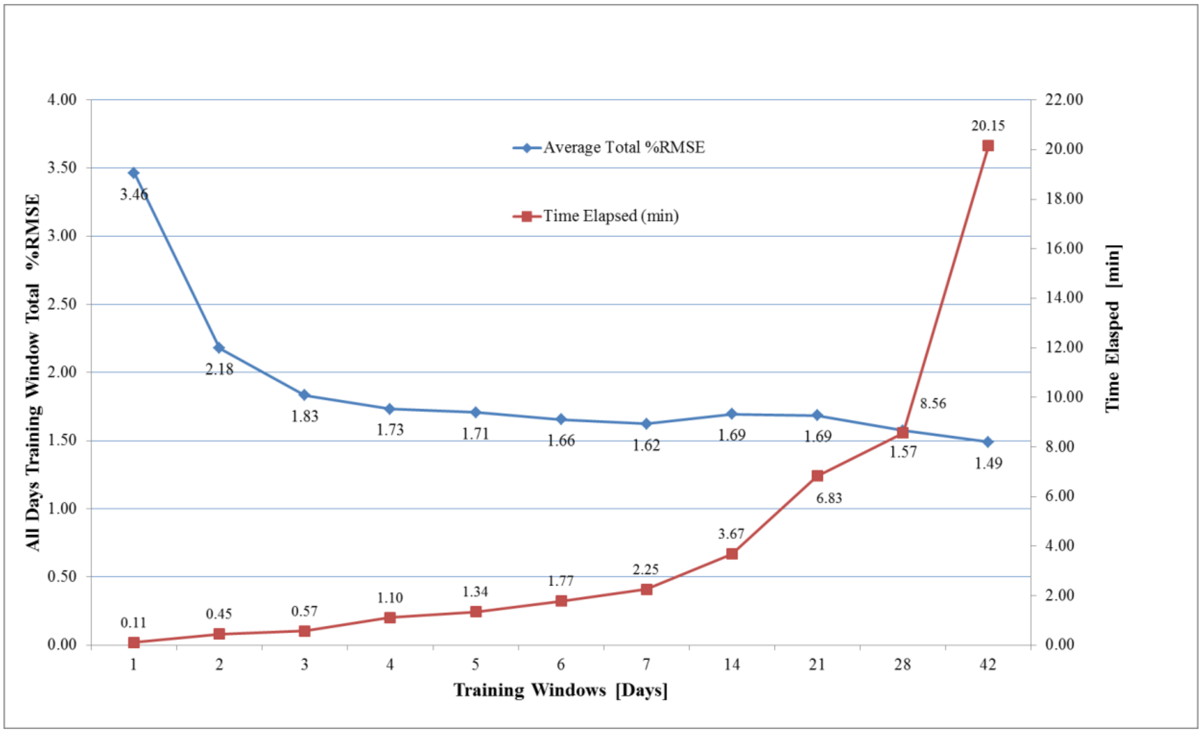

Figure 18. Average *% RMSE* for various training window sizes (UA_e = 172 W/K and τ_e = 104 h)

The impact of using the seven-day vs. one-day of training is shown for the same days, previously depicted in Figure 15 and Figure 10, are given in Figure 19 and Figure 20, respectively.

The *% RMSE* and *MAPE* shown in Figure 19 have significantly improved over the values reported, for the same days, in Figure 15. However, the *% RMSE* and *MAPE* shown in Figure 20 have slightly increased over the same days reported in Figure 17. The slight increase in *% RMSE* and *MAPE* were expected because the N_e and AR_e parameters were effectively average values vs. a day where the solar conditions were similar to the conditions of the day being predicted.

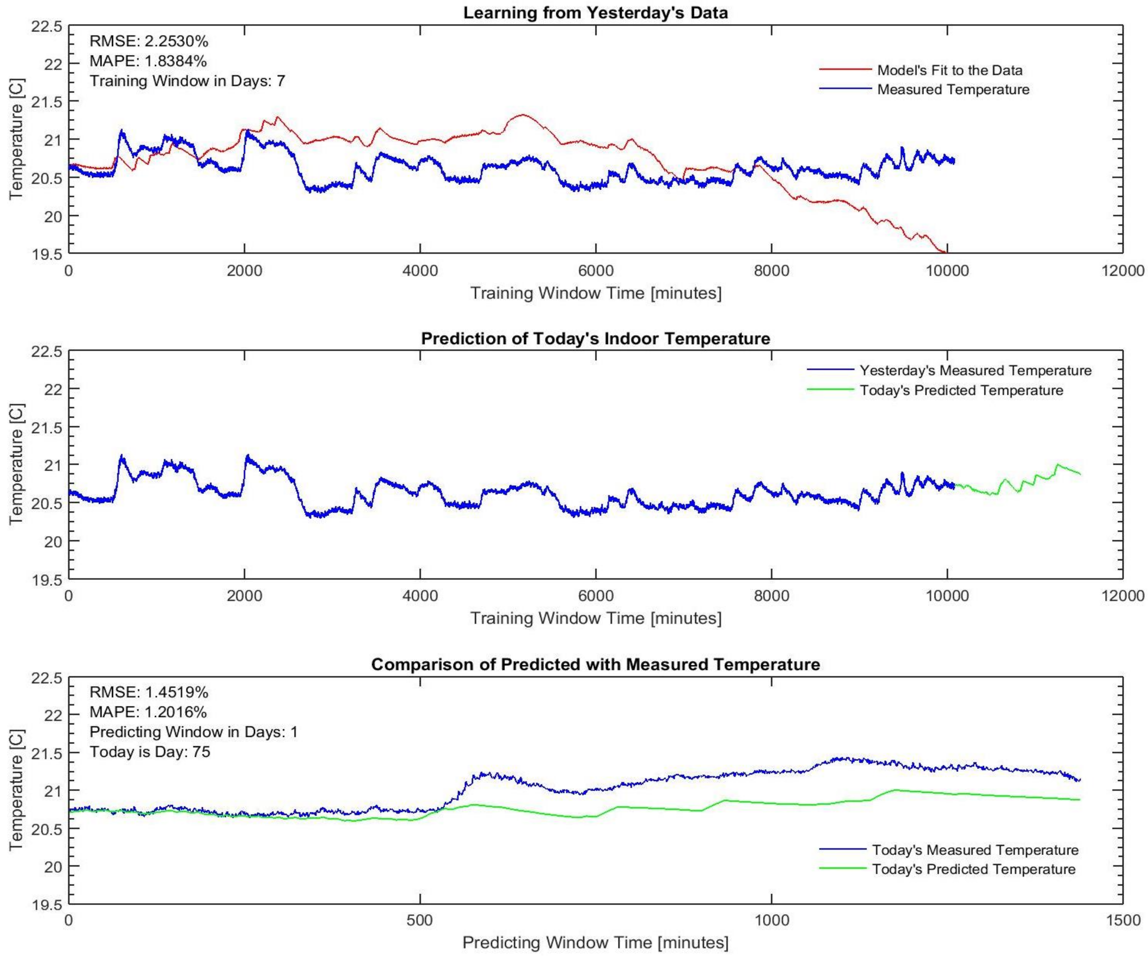

Figure 19. Learning parameters over a 7-day training window and applying to a sunny day

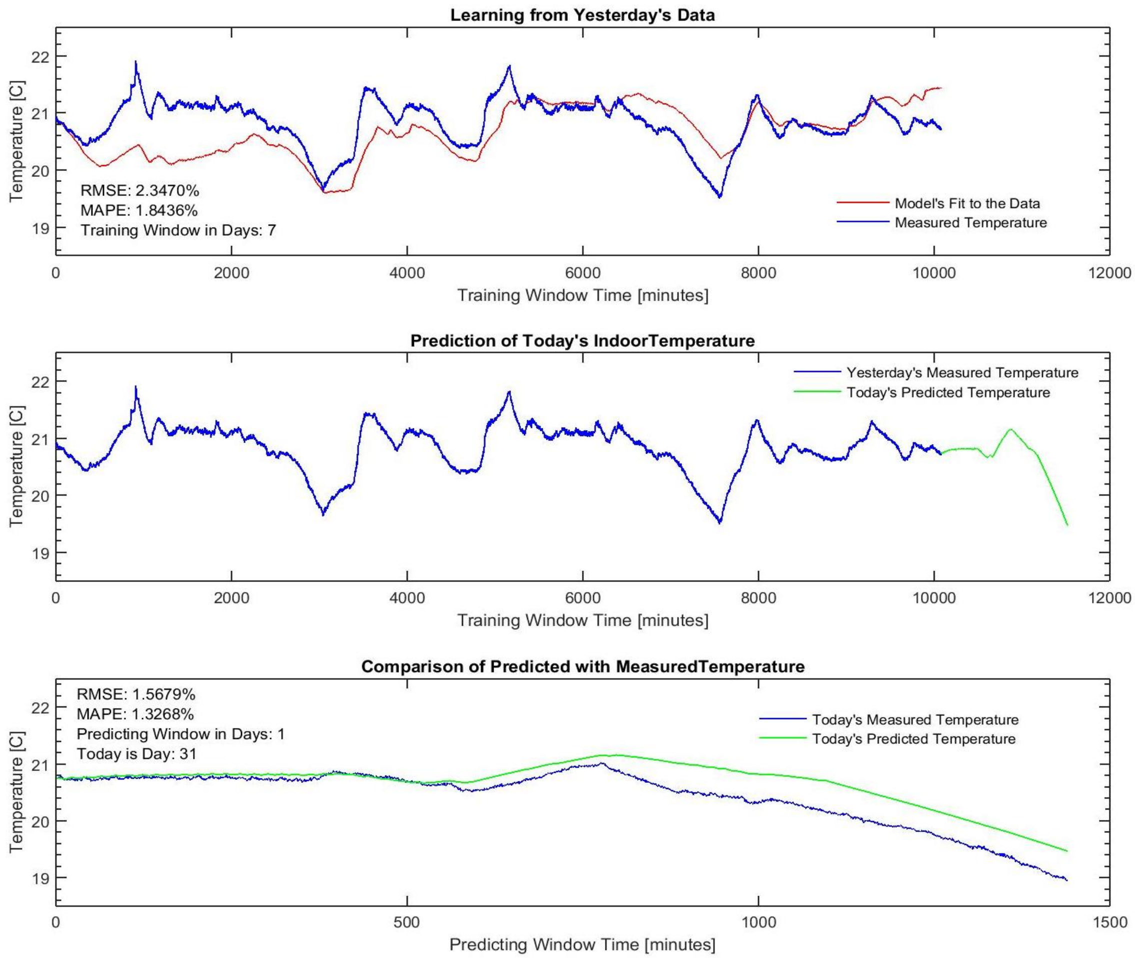

Figure 20. Learning parameters over a 7-day training window and applying it to a sunny day

The *% RMSE* and *MAPE*, for the temperature prediction algorithm, and their average errors are shown for the entire data set in Figure 21. The maximum *% RMSE* and *MAPE* errors over the 362-day data set are *12 %* and *10 %*, respectively. The 95 % confidence interval on the mean of *% RMSE* and *MAPE* errors are *2.24 ± 0.17 and 1.86 ± 0.14*, respectively.

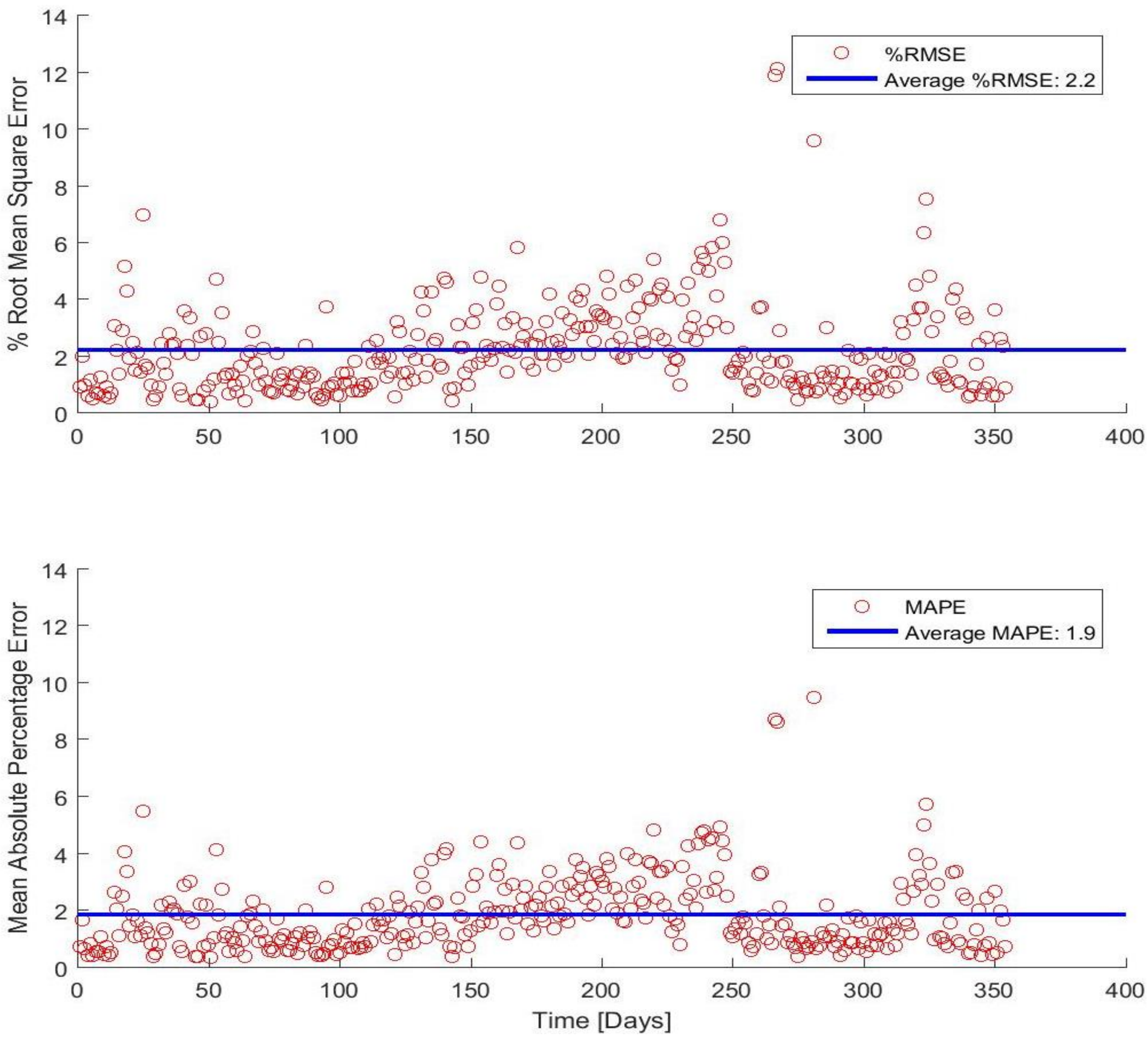

Figure 21. The % RMSE, MAPE and the average error for both metrics (7-day training window)

In order to visually depict the behavior of the learning algorithm and its prediction capabilities, three different prediction scenarios were identified to represent the worst (Figure 22), a typical (Figure 23), and the best case (Figure 24).

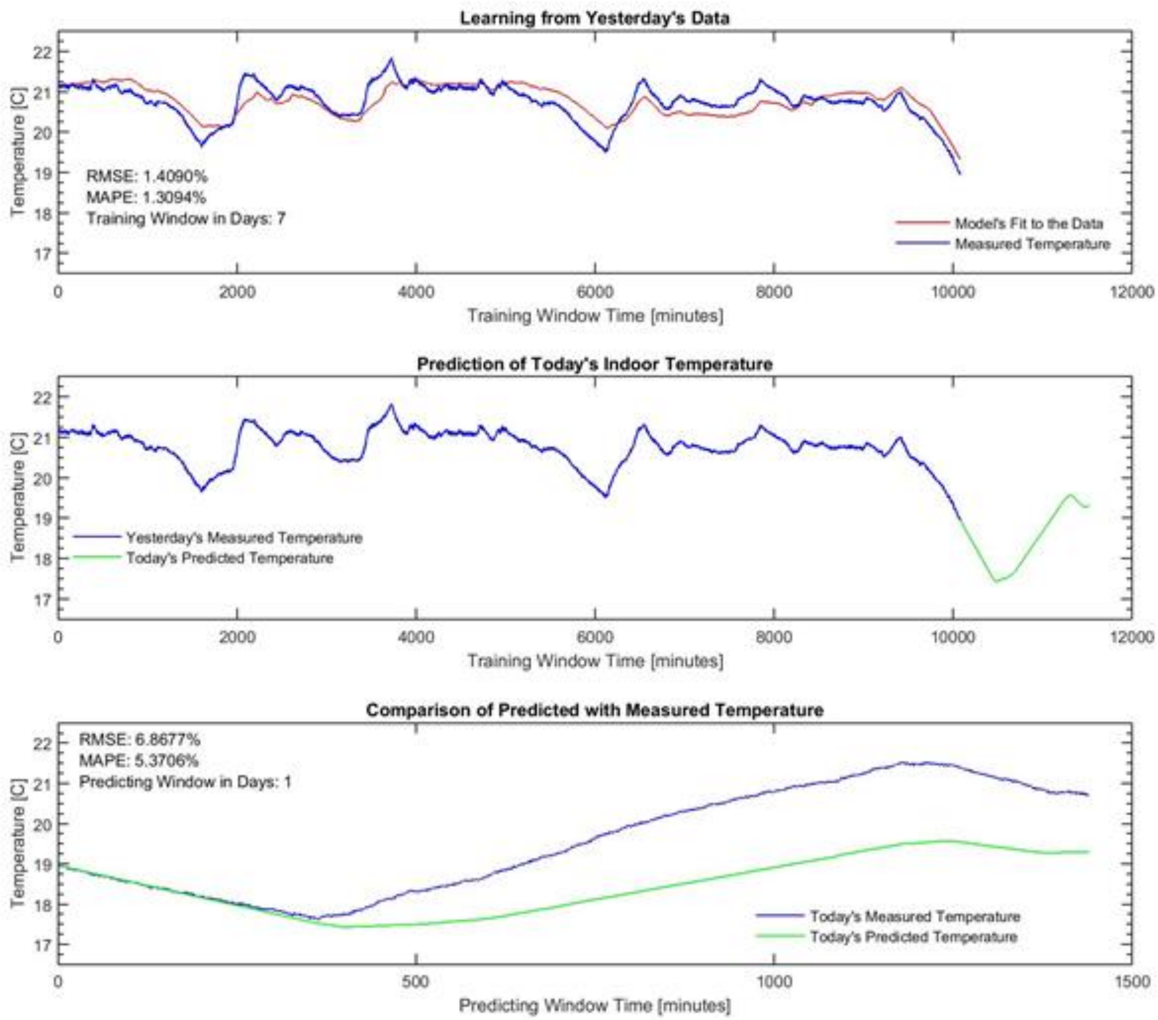

Figure 22. The worst-case prediction scenario (7-day training window)

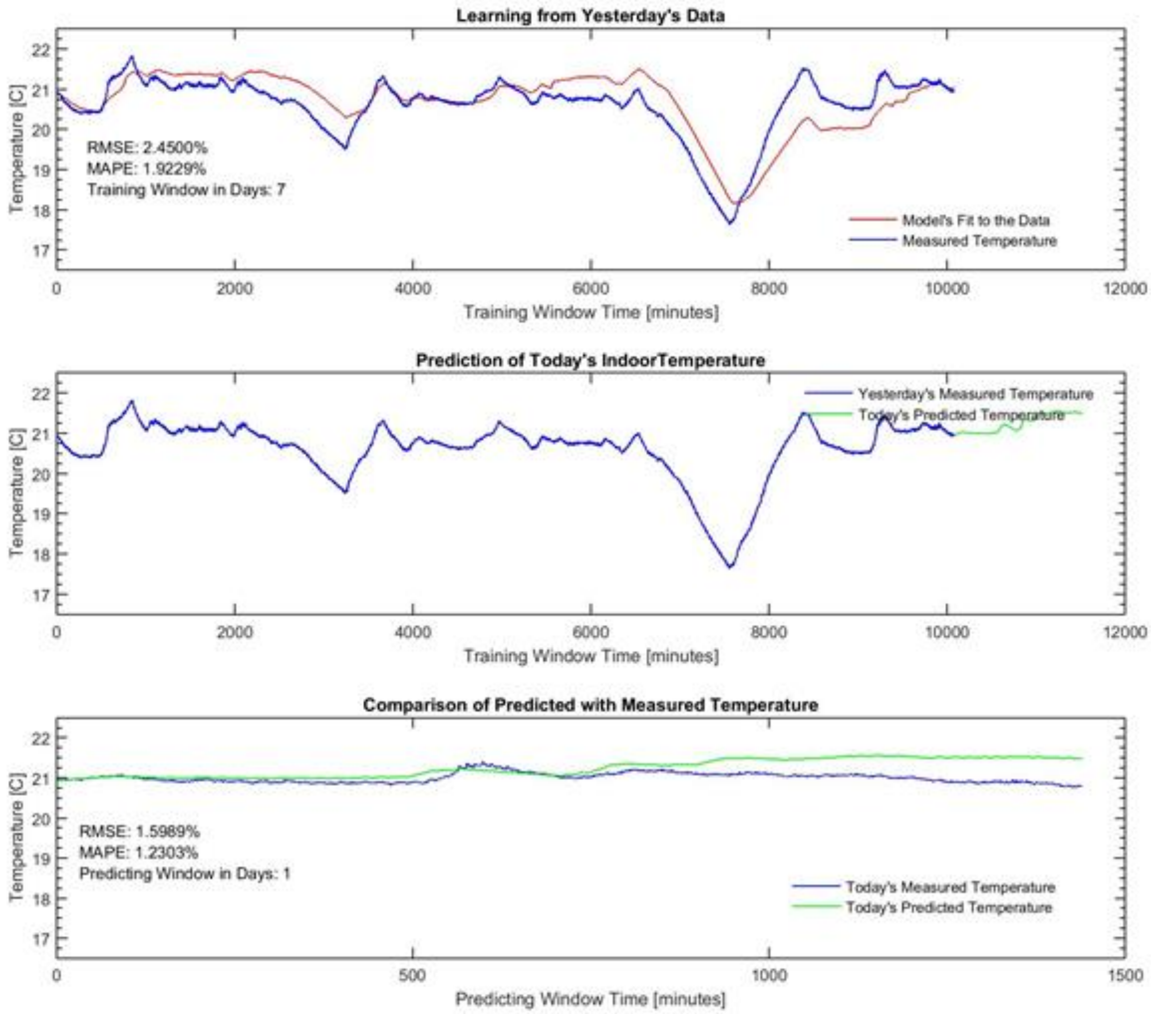

Figure 23. A typical case prediction scenario (7-day training window)

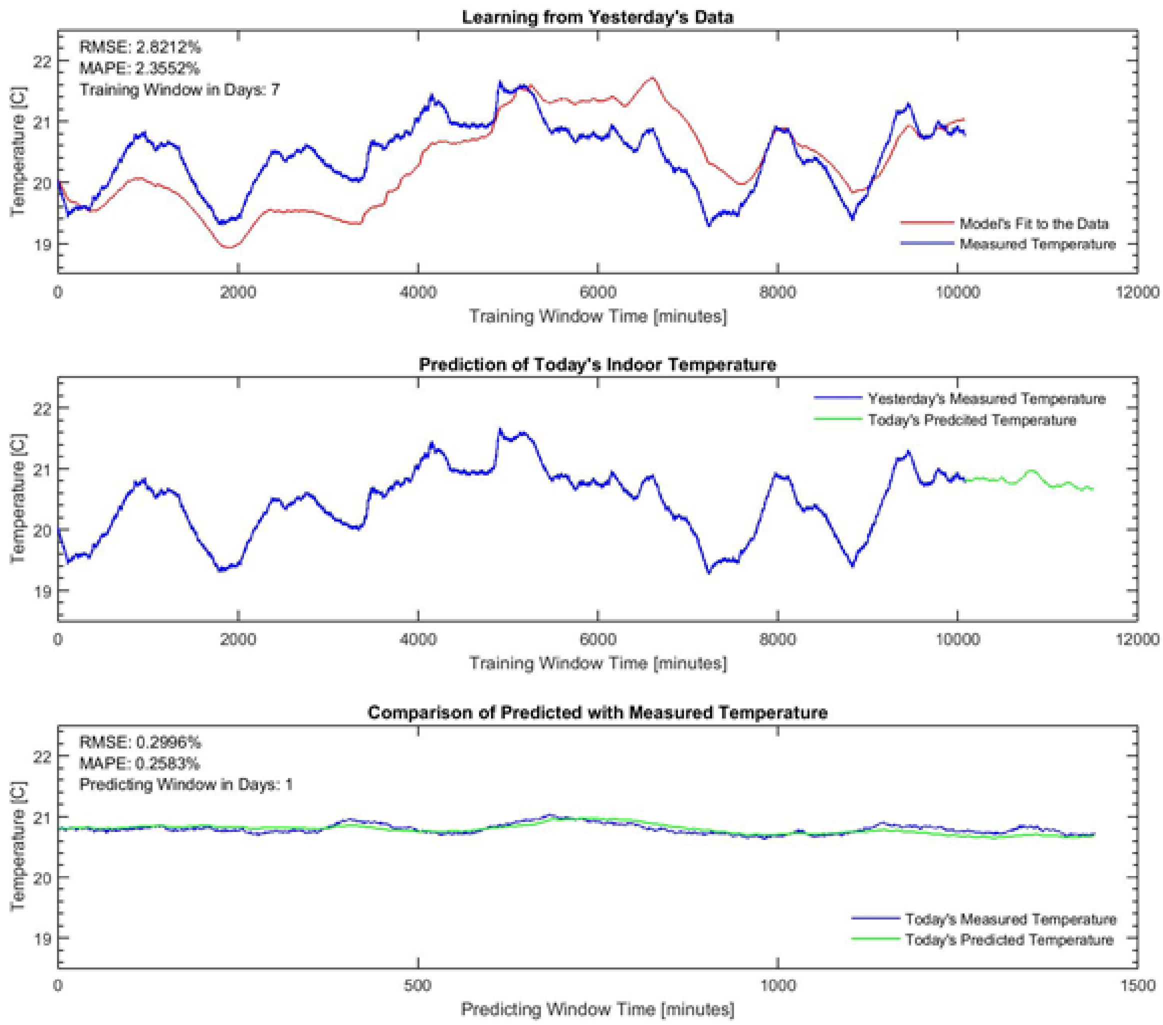

Figure 24. The best-case prediction scenario (7-day training window)

Chapter 4

4. Energy Management Control Algorithms

Realizing a smart electric grid requires intelligent control algorithms to facilitate autonomous interaction between a homeowner and the grid. Common optimization objectives include cutting cost, reducing energy consumption, or both while trying to maintain thermal comfort. The actions resulting from the optimization include controlling appliances, performing temperature setbacks, and preheating or precooling residential buildings. This chapter describes the development and performance of six residential EMCAs with different performance characteristics that were developed to control a residential heat pump and test the assessment framework described in Chapter 5. Each algorithm was integrated with the TRNSYS model of the NZERTF. The HVAC system of the NZERTF consists of an air-source heat pump with a dedicated dehumidification function and a heat recovery ventilator (HRV) [19]. The heat pump provides space conditioning while the HRV provides ventilation by bringing fresh air into the NZERTF. In this study, only options for controlling the heat pump were considered.

Selecting the appropriate stage for operating the heat pump depends on the deviation of the indoor temperature from the setpoint and the time-out associated with each stage. The heating and cooling setpoint temperatures are 20.5 °C and 23.89 °C, respectively. In the heating season, the 1st Stage is turned on when the indoor temperature, as measured by the thermostat in the living room, drops 0.1 °C below the heating setpoint. The 2nd Stage turns on when either the 1st Stage has been running for 10 min or the indoor temperature falls 1.1 °C below the heating setpoint. The 3rd Stage turns on when either the 2nd Stage has been running for 40 min or the indoor temperature drops 3.3 °C below the heating setpoint.

In the cooling season, the 1st Stage is turned on when the indoor temperature rises 0.2 °C above the cooling setpoint. The 2nd Stage turns on when either the 1st Stage has been running for 40 min or the indoor temperature rises 2.8 °C above the cooling setpoint. A TRNSYS model of the NZERTF was developed that implemented this control logic using several differential controllers [10]. The model is shown schematically in Figure 25 with the differential controllers highlighted.

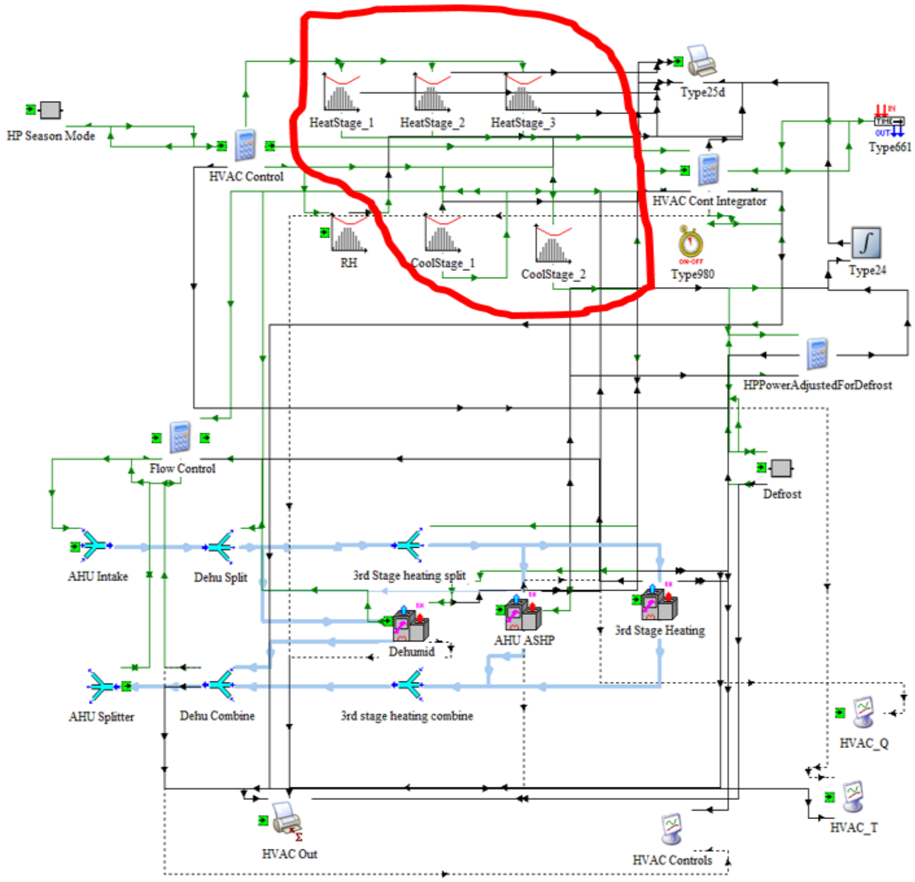

Figure 25. Schematic of the TRNSYS heat pump model for the NZERTF

Although, minor parameter adjustments can be made with the differential controllers, future research requirements for residential EMCAs necessitate the use of software tools that are flexible for developing, testing, debugging, and integrating complex and sophisticated learning and optimization techniques to control the operation of the heat pump. All residential EMCAs, for this study, were developed using a 64-bit version of MATLAB software. Using Type277 described in Chapter 2, the NZERTF model was linked with MATLAB environment. TRNSYS simulated the dynamics of the NZERTF in response to the control actions generated in MATLAB. Figure 26 shows an instance of using Type277 replacing the differential controllers used in the simulation model of the NZERTF.

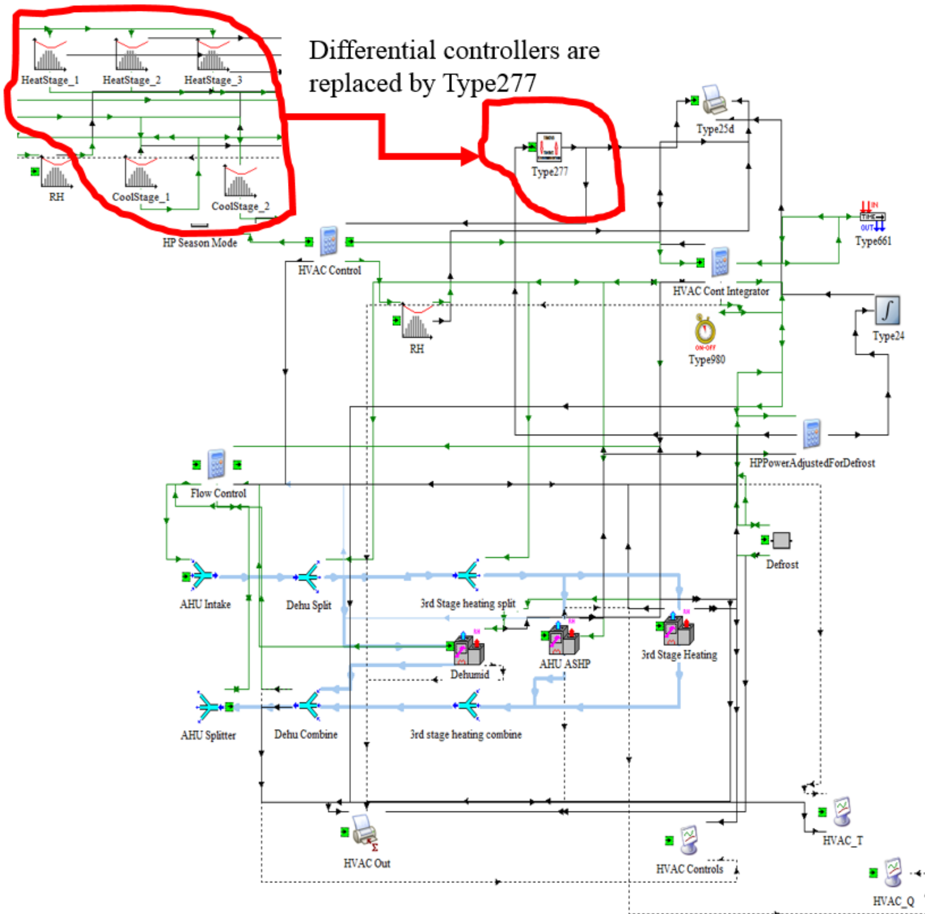

Figure 26. Schematic of the modified TRNSYS heat pump model for the NZERTF

As previously mentioned, six residential EMCAs with different performance characteristics and control objectives were developed for use in testing a performance the AE. One algorithm was designed to match a real heat pump controller used in the NZERFT. A second was the same as the first with relaxed comfort deadbands. Four others use linear integer optimization with varying optimization objectives. The algorithms were compared by analyzing their performance over a year based on energy consumption, cost, and comfort as measured by predicted mean vote and percentage of dissatisfied occupants.

A summary of important characteristics and parameters for the six residential EMCAs is presented in Table 5. The (✓,Yes) and (×, No) markers are used to indicate whether an algorithm is single-objective, multi-objective, or limited by the upper or lower bound constraints. For example, residential EMCA3 used optimization, was not limited by upper and lower bound constraints and was multi-objective.

Table 5. Summary Description of Residential EMCAs

Residential EMCAs	Optimization Used	Objective Description	Thermostat Setpoints (°C) (heating, cooling)	Heating Lower Bound (°C)		Cooling Upper Bound (°C)		Multi-Objective	Dominance Factor (λ, 1-λ)	Forecast Horizon (min)
1	✓	Minimize Energy	(20.5, 23.9)	20.2		24.2		×	×	30
2	✓	Minimize Cost	(20.5, 23.9)	20.2		24.2		×	×	1440
3	✓	Minimize Discomfort + Cost	(20.5, 23.9)	×		×		✓	(0.45, 0.55)	240
4	✓	Minimize Discomfort + Cost	(20.5, 23.9)	×		×		✓	(0.55, 0.45)	240
5	×	NZERTF Case	(20.5, 23.9)	1st Stage	20.4	1st Stage	24.1	×	×	×
				2nd Stage	19.4	2nd Stage	27.1			
				3rd Stage	17.2	×	×			
6	×	NZERTF Case with Relaxed Deadbands	(20.5, 23.9)	1st Stage	20.0	1st Stage	24.5	×	×	×
				2nd Stage	19.0	2nd Stage	27.1			
				3rd Stage	16.8	×	×			

4.1. Default Controller

In this work the logic of a Default Controller is defined. This controller is the basis for EMCA 5 and, with relaxed deadband constraints, EMCA 6. The Default Controller is designed to replicate an actual controller used in the NZERTF. The optimization algorithms in the other cases also use this controller during learning periods and if the optimization fails to find a better solution. Table 6 defines key input parameters used by the Default Controller.

Table 6. Default Controller Input Parameters

Input Data Description	**Value [unit]**	**Source of Data**
First floor drybulb indoor temperature (T_{ind})	Variable [°C]	Simulation Model
Heating temperature setpoint (HS_p)	20.5 [°C]	User preference
Cooling temperature setpoint (*CSp*)	23.9 [°C]	User preference
Heat to cooling season deadband (*heatToCool*)	1.67 [°C]	Differential controller setting
Cool to heating season deadband (*coolToHeat*)	1.67 [°C]	Differential controller setting
Heating 1st Stage deadband (*hLSD*)	0.1 [°C]	Differential controller setting
Heating 2nd Stage deadband (*hHSD*)	1.1 [°C]	Differential controller setting
Heating 3rd Stage deadband (*hASD*)	3.3 [°C]	Differential controller setting
Heating 1st Stage time-out (*hLSTO*)	10 [min]	Differential controller setting
Heating 2nd Stage time-out (*hHSTO*)	40 [min]	Differential controller setting
Cooling 1st Stage deadband (*cLSD*)	0.2 [°C]	Differential controller setting
Cooling 2nd Stage deadband (*cHSD*)	2.8 [°C]	Differential controller setting
Cooling 1st Stage time-out (*cLSTO*)	40 [min]	Differential controller setting

Figure 27 is a flowchart depicting a high-level overview of the process for selecting heat pump control actions

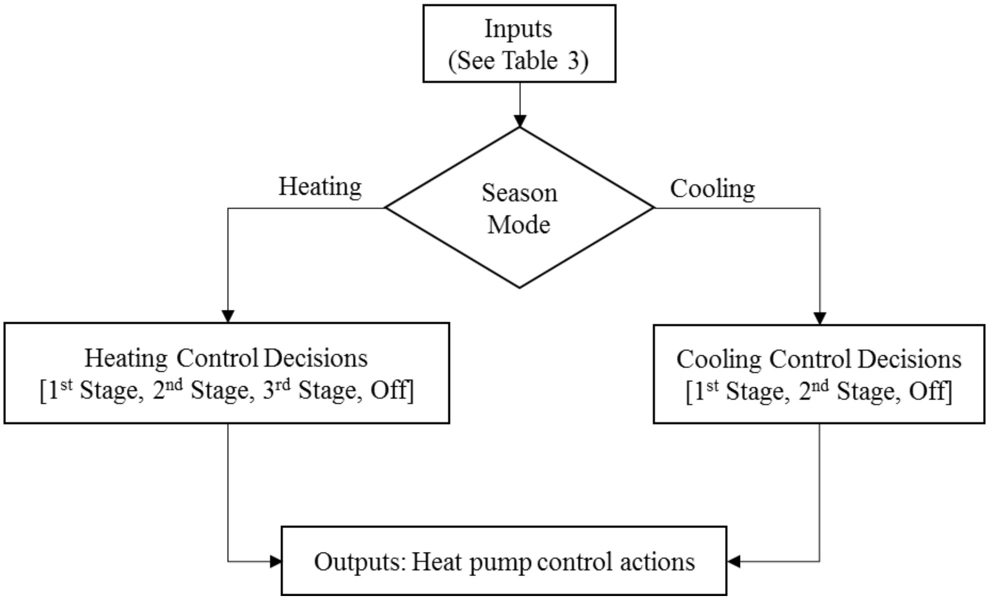

Figure 27. Overview of the heat pump control action selection process

As can be seen from Figure 27, there are three main functions that enables the Default Controller to make heat pump control decisions. These functions are the Season Mode, Heating Control Decisions (HCD), and Cooling Control Decisions (CCD). At the first stage, the Season Mode function determines the operating season (heating or cooling). The Default Controller then calls either the HCD function of the CCD function to determine the next appropriate operating stages.

The HCD function is designed to maintain the T_{ind} close to the HS_p by choosing from the three heating stages or turning the heat pump off. The CCD function is designed to maintain the T_{ind} close to the CS_p by choosing from the two cooling stages or turning the heat pump off.

4.1.1. Season Mode Function

The Season Mode function determines the operating season of the Default Controller. Figure 28 is a flowchart describing the decision process.

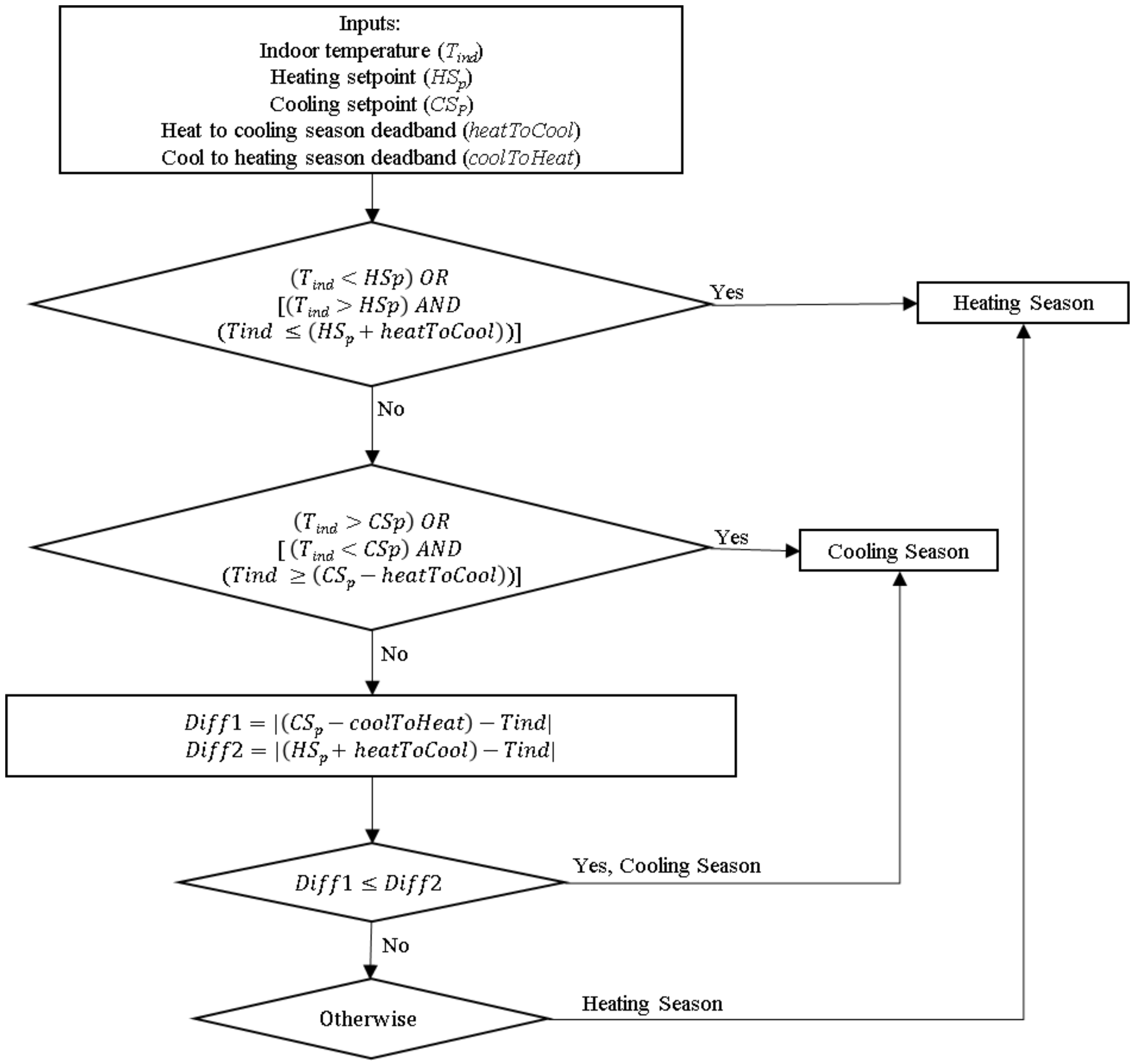

Figure 28. The Season Mode function flowchart used for determining the operating season

Figure 29 shows the resulting temperature regions. If T_{ind} is less than the HS_p or if T_{ind} is greater than the HS_p by an amount less or equal to the *heatTtoCool* deadband, then the output of the Season Mode function is the heating season (shaded in blue). If T_{ind} is above the CS_p or if it is less than the CS_p by an amount less than the *coolToHeat* deadband, then the output of the Season Mode function is the cooling season (shaded in green).

If neither of these conditions are true, there is some ambiguity about whether heating or cooling season is appropriate and there may be a transition between seasons. This ambiguity is resolved by selecting Cooling Season if T_{ind} is closer to the Cooling Season boundary and selecting Heating Season if T_{ind} is closer to the Heating Season boundary. Figure 29 depicts this ambiguous region (shaded in oragne).

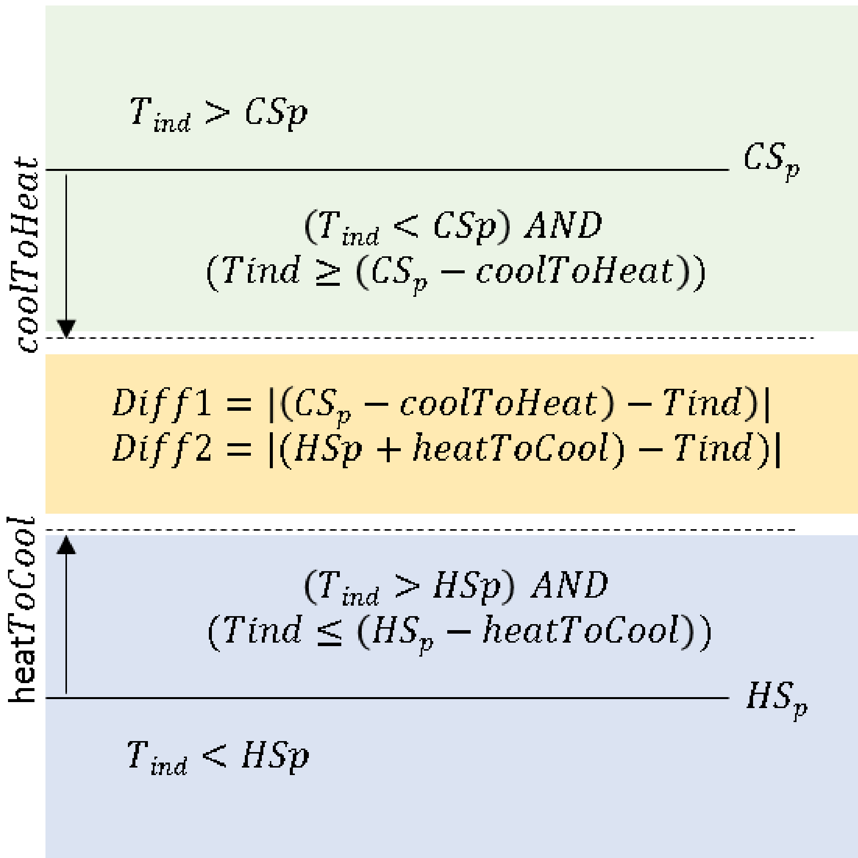

Figure 29. The heating (blue), ambiguous (orange), and cooling (green) regions

4.1.2. Heating Control Decision

The HCD function is used to determine appropriate heat pump control actions during the heating season. Figure 30 is a finite state diagram that describes the behavior of the heat pump operation in the heating season. Using the information provided in Table 6, the HCD function determines the current state of the system by choosing from the three heating stages or turning the heat pump off. Each arrow shows the direction of transition from one state to another or to itself, provided that the logical condition alongside the arrow is true. *TimerLow* and *TimerHigh* are simple counters. They keep track of the elapsed time in 1st Stage and 2nd Stage states, respectively.

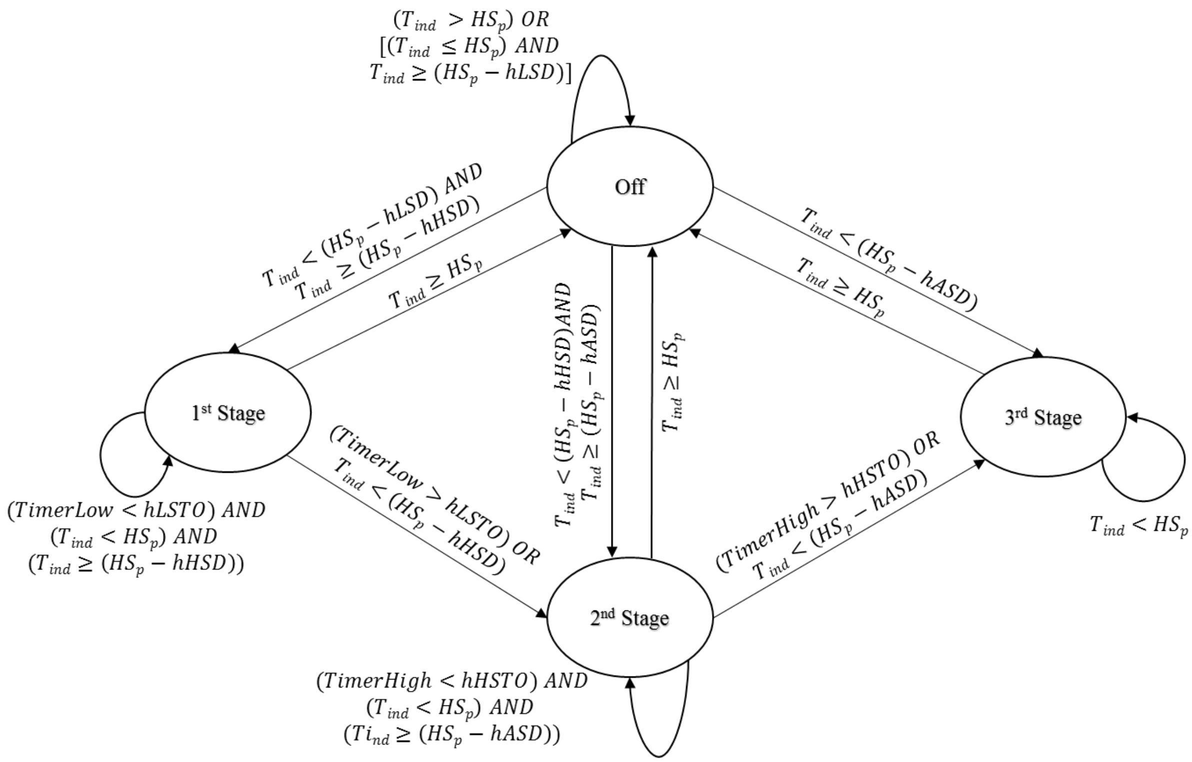

Figure 30. Finite state diagram for determining heating control actions

4.1.3. Cooling Control Decisions

The CCD function is used to determine appropriate heat pump control actions during the cooling season. Figure 31 is a finite state diagram that describes the behavior of the heat pump operating in the cooling season. Using the information provided in Table 6, the CCD function determines the current state of the system by choosing from the two cooling stages or turning the heat pump off. Each arrow shows the direction of transition from one state to another or to itself, provided that the logical condition alongside the arrow is true. *TimerLow* is a simple counter that keeps track of the elapsed time in the 1st Stage state.

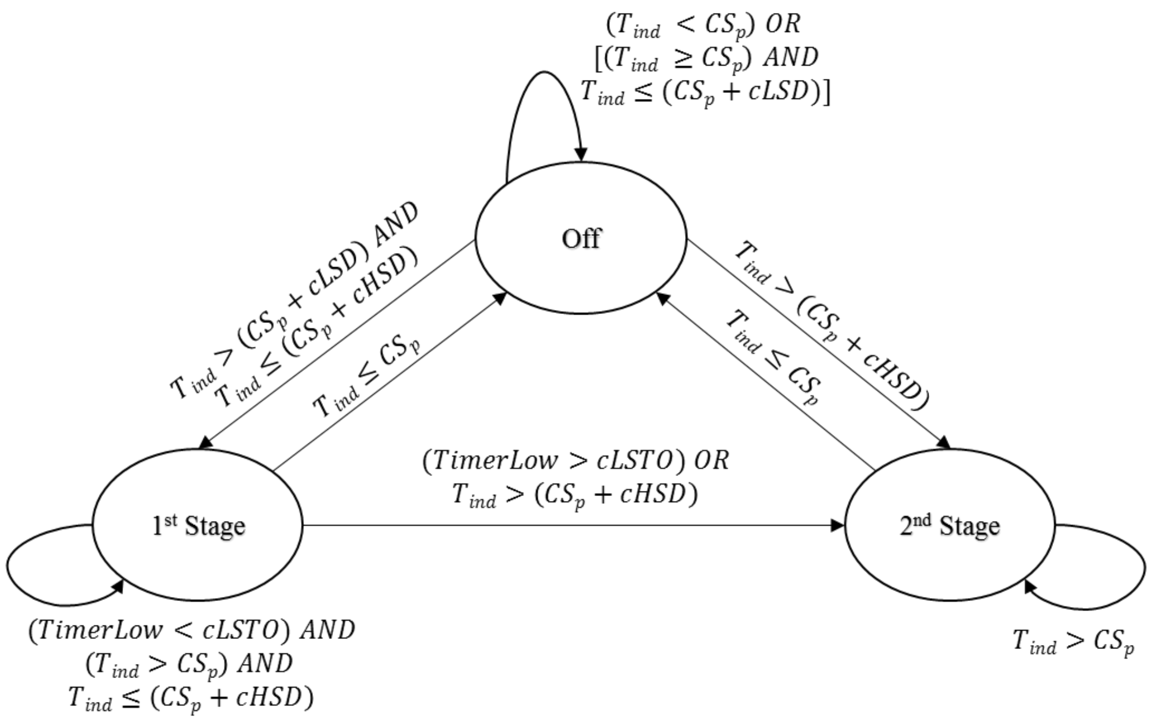

Figure 31. Finite state diagram for determining cooling control actions

4.2. Control Optimization Framework

The control optimization framework realization involved developing and integrating three components: A Default Controller, a learning algorithm, and an optimization algorithm to generate heat pump control actions. These components were selected to perform specific tasks, but collectively they form the foundation for residential EMCA1 through residential EMCA4. The optimization algorithm uses indoor temperature forecast models (ITFM) to predict T_{ind} in response to heat pump control actions for a given forecast horizon. The mathematical descriptions of the ITFMs for heating and cooling seasons are given in Sec. 4.2.1.1 and Sec. 4.2.1.2, respectively. Application of the ITFM requires estimated values of key parameters of a residential house that must be learned from observation. The control optimization framework utilizes a learning algorithm to update these parameters using historical data.

The learning algorithm is a sliding-window algorithm that was derived to forecast the next day's indoor temperature profile [26], [27]. It is formulated in such a way that key design details of a residential house such as window size and configuration, thermal insulation, and airtightness that effect heat loss and solar heat gain are combined into effective parameters that can be learned from observation. The sliding-window of learning data accounts for both seasonal variations in the sun position and daily cloud cover fluctuations. Using measurement data from the NZERTF, it was determined that a training window size of seven days produced good results for forecasting T_{ind} [26], [27]. Therefore, during the first week of the simulation, the Default Controller is used to generate heat pump control actions, while data needed for the learning algorithm is being stored. The Default Controller is also used for one week before the end of the simulation to prevent abrupt termination of the simulation for not having sufficient data to accommodate the learning algorithm's sliding-window requirement. Once the simulation time step moves beyond the first week but has not reached the week before the end of the simulation, the control optimization framework immediately runs the learning algorithm. The learning algorithm is triggered because sufficient data has been collected to satisfy the seven-days requirement. After the initial run, the learning algorithm is triggered only once every day at the beginning of the day to update parameters with the data from the new seven-day window. This continues until the simulation time step reaches the one week before the end of the simulation when there is no longer seven days of data to process.

The optimization algorithm uses the ITFMs to forecast the indoor temperature for a given forecast horizon. The optimization algorithm is only triggered based on the size of the forecast horizon. For example, if the size of the forecast horizon is 60 min, then the optimization algorithm is triggered at every hour. The number of forecasted control actions are also determined by the length of the forecast horizon. The control optimization framework is designed to account for situations where the optimization algorithm cannot find a feasible solution. If the solution is infeasible, then the control reverts to the Default Controller. This condition persists until the optimization algorithm runs again. If the solution is feasible, it outputs the forecasted control actions for the current simulation time step and stores the remaining forecasted control actions for subsequent calls to the framework. In subsequent time steps before the optimization algorithm runs gain, previously found forecasted control actions are used. Figure 32, is a flowchart depicting this process graphically.

Residential EMCA1 though residential EMCA4 are modeled as pure integer optimization problems and implemented in YALMIP [28], a modeling and optimization toolbox developed for MATLAB. The optimization problems were solved by applying the linear integer programming algorithm (intlinprog) from MATLAB's optimization toolbox [29]. The intlinprog algorithm is simulated with its default settings except for the MaxTime, which is the maximum time that intlinprog runs to find a solution. The default value for MaxTime is 7200 s, which can prohibit a year-long simulation to complete in a reasonable time. In this study, the value for MaxTime was set to 300 s.

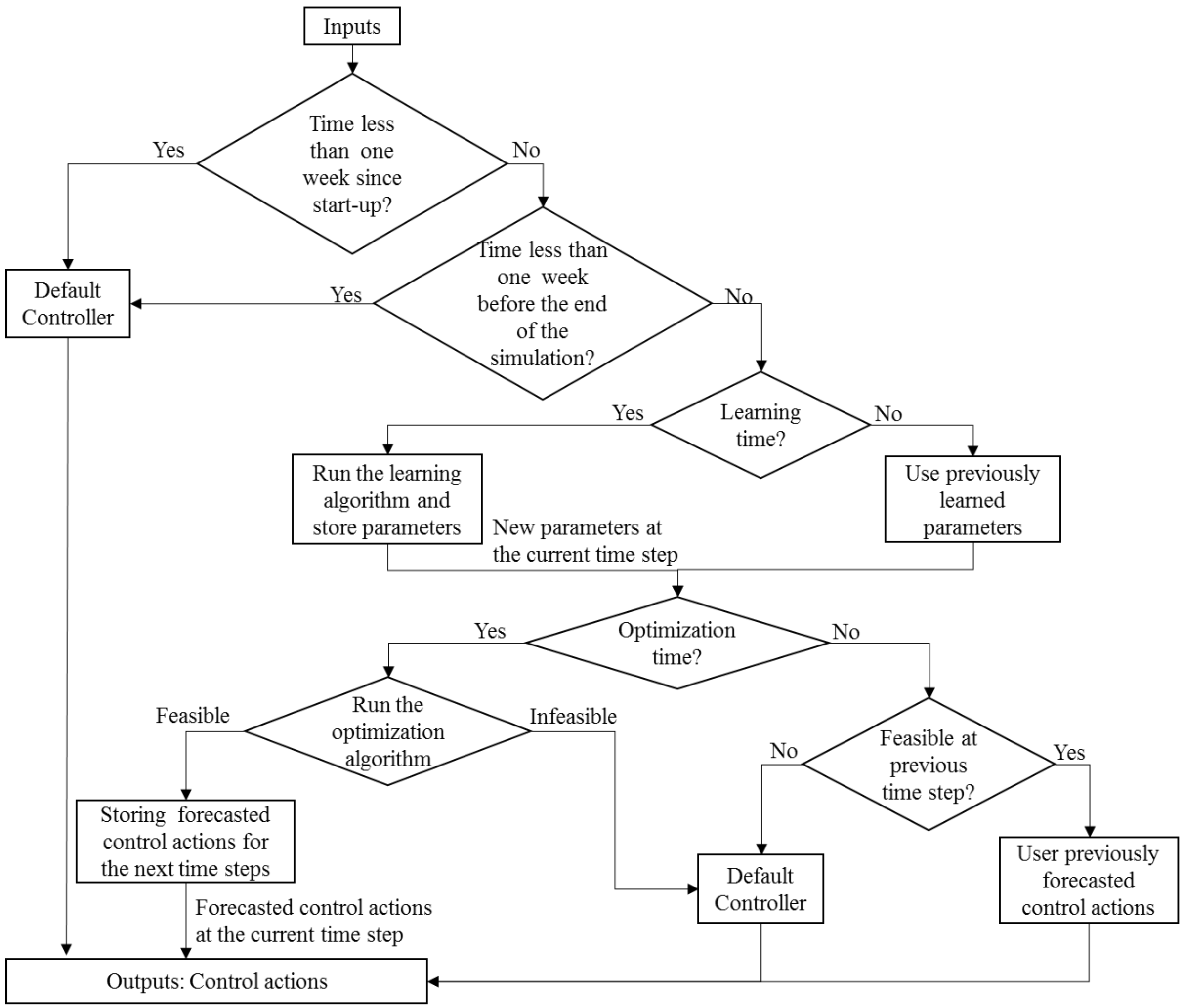

Figure 32. The control optimization framework flowchart, describing the process of obtaining heat pump control actions

The following subsections involve describing the development process of the optimization algorithm. A description of the optimization algorithm falls into two main categories: the single objective and multi-objective optimization problems. Detailed description of the Default Controller was provided in Sec. 4.1 of this document. Detailed description of the learning algorithm is given in Ch. 3 and published in [26], [27].

4.2.1. Optimization Algorithms

Realization of the optimization algorithm involved developing a common structure for solving both single and multi-objective optimization problems. The common structure implementation involves two main functions: the optimization heating controller (OHC) and the optimization cooling controller (OCC). Figure 33 describes the process of generating forecasted heat pump control actions.

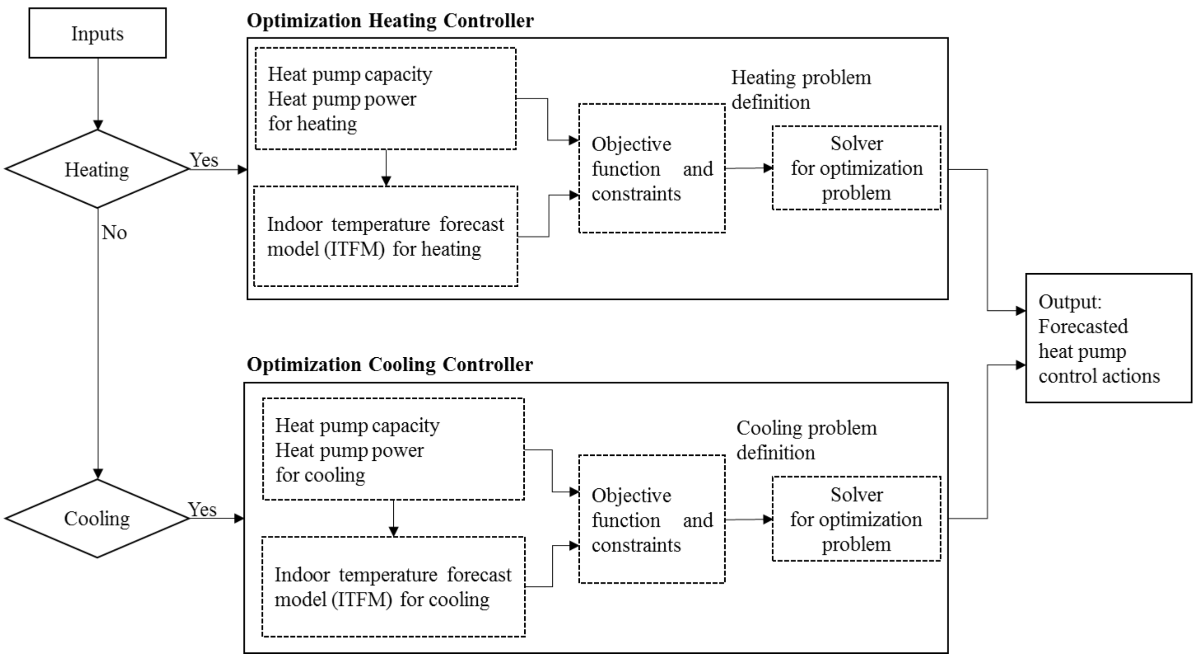

Figure 33. The process for obtaining forecasted heat pump control actions in both heating and cooling seasons

The OHC and OCC functions utilize the ITFMs, objective function and constraints, and the *intlinprog* solver to obtain forecasted heat pump control actions. The optimization problem is formulated in such a way that the solver is selecting control actions such that the overall value of the objective function is minimized while constraints are satisfied. The selected operating state is used in the ITFMs to forecast T_{ind}. The output of the OHC and OCC functions is a vector of forecasted heat pump control actions for the forecast horizon. In addition, the application of OHC and OCC functions also require forecasted data to predict heat pump control actions (Table 7).

Table 7. Forecasted Data Needed for Predicting the Indoor Temperature

Forecasted Data	**Description**
Solar irradiance (W/m^2)	Derived from an hourly 2013 typical meteorological year (TMY3) weather data file collected at the Dulles International Airport.
Plug-loads (W)	The values for forecasted plug-loads were known through a fixed occupancy schedule used in the operation of the NZERTF and described in [14].
Ambient outside dry-bulb temperature, T_∞ (°C)	Derived from the hourly 2013 TMY3 weather data file collected at the Dulles International Airport. The same TMY3 weather file was used for simulating the NZERTF model in TRNSYS [10].
Real-time price (RTP)	The RTP tariff was derived from the day-ahead wholesale hourly price of electricity from a regional transmission organization, the Pennsylvania-New Jersey-Maryland Interconnection (PJM). The RTP tariff data was from January 2013 to December 2013. The day-ahead wholesale price was scaled to generate a forecasted retail RTP tariff, resulting in an average of 15 ¢/kWh. The average cost of consuming energy in a residential home in Gaithersburg, Maryland is approximately 15 ¢/kWh (that includes the transmission, distribution, taxes, and fees).
Heat pump thermal capacity (*E*) and electrical power (*P*)	The values of *E* (Btu/h) and *P* (W) for heating and cooling seasons are obtained from equations in Sec. 4.2.1.1 and Sec. 4.2.1.2, respectively. The *E* and *P* equations used in this study were derived from measurement data obtained from the operation of the NZERTF [30]. In general, the capacity of a heat pump to deliver thermal energy and electrical power is a strong function of T_∞. The association between T_∞ and the output of an *E* and *P* equations can be characterized by a linear relationship.

The ITFMs use linear correlations of heat pump thermal capacity and power consumption as a function of outdoor temperature to predict T_{ind} and to account for the power consumption in the objective function of the optimization algorithms.

4.2.1.1. Components of OHC

The heat pump thermal capacity and electrical power consumption for the 1st Stage and 2nd Stage operation during the heating season are defined as

$$\begin{aligned} E_{h1} &= 339.33 \times T_{\infty} + 1617.3 \\ E_{h2} &= 323.24 \times T_{\infty} + 10576 \\ P_{h1} &= 6.9632 \times T_{\infty} + 1046.8 \\ P_{h2} &= 6.7257 \times T_{\infty} + 1747.6, \end{aligned} \tag{1.33}$$

where:

E_{h1} and E_{h2} are thermal capacities in (Btu/h);
P_{h1} and P_{h2} are electrical power in (W); and
T_{∞} is in °F.

Note that, because the correlations were developed using degrees Fahrenheit and Btu/h, some unit conversions are necessary to apply the result in the IFTM.

The ITFM utilizes a discrete form of the first order lumped capacitance model for forecasting T_{ind} given in Eq. (1.13). The value of q_{hp} in Eq. (1.13) is the sum of the three heat pump stages ($q_{hp} = E_{h1} + E_{h2} + E_{h3}$). Recall that the 3rd Stage heating capacity (E_{h3}) is a 10 kW electric resistance element. Substituting the heat pump stages for q_{hp} in Eq. (1.13) gives the one-step ITFM for the heating season, expressed as

$$\begin{aligned} T_{i,k+1} = T_{\infty,k} &+ \frac{(q_{sol,k} + E_{h1,k} + E_{h2,k} + E_{h3,k} + q_{l,k})}{UA_e} \\ &+ \left(T_{i,k} - T_{\infty,k} - \frac{(q_{sol,k} + E_{h1,k} + E_{h2,k} + E_{h3,k} + q_{l,k})}{UA_e} \right) \exp\left(-\frac{\Delta t}{\tau_e} \right). \end{aligned} \tag{1.34}$$

4.2.1.2. Components of OCC

The E and P equations and the ITFM used in the cooling season are described below. The heat pump thermal capacity and electrical power for the 1st Stage and 2nd Stage are E_{c1}, E_{c2}, P_{c1}, and P_{c2}, respectively. These equations are expressed as

$$\begin{aligned} E_{c1} &= -79.593 \times T_{\infty} + 25259 \\ E_{c2} &= -94.151 \times T_{\infty} + 32471 \\ P_{c1} &= 16.32 \times T_{\infty} - 105.6 \\ P_{c2} &= 19.331 \times T_{\infty} + 438.57, \end{aligned} \tag{1.35}$$

where:

E_{c1} and E_{c2} are thermal capacities in (Btu/h);
P_{c1} and P_{c2} are electrical power in (W); and
T_{∞} is in °F.

To forecast the indoor air temperature of the NZERTF, the OCC function utilizes the modified version of Eq. (1.34) because in the cooling season thermal energy is removed from the model instead of added. The one-step ITFM for the cooling season is expressed as

$$T_{i,k+1} = T_{\infty,k} + \frac{q_{sol,k} - (E_{c1,k} + E_{c2,k}) + q_{l,k}}{UA_e} + \left(T_{i,k} - T_{\infty,k} - \frac{q_{sol,k} - (E_{c1,k} + E_{c2,k}) + q_{l,k}}{UA_e} \right) \exp\left(-\frac{\Delta t}{\tau_e} \right). \tag{1.36}$$

The information obtained from Sec. 4.2.1.1 and Sec. 4.2.1.2 are used to develop the objective functions and constraints describing the single-objective optimization problems for residential EMCAs in Sec. 4.2.1.3 and multi-objective optimization problems in Sec. 4.2.1.4.

4.2.1.3. Single objective Optimization

Residential EMCA1 and residential EMCA2 are single-objective optimization problems. The optimization objectives are to minimize energy consumption and cost, respectively.

4.2.1.3.1. Optimization Problem for Residential EMCA1

The objective function of the residential EMCA1 is formulated in such a way that it attempts to minimize energy consumption of the heat pump over the forecast horizon given in Table 5. The objective function for residential EMCA1 is expressed by

$$\min_{k \in [2,n]} \sum_{i=1}^{m} u_{i,k-1} P_{i,k-1} \cdot w_{i,k-1} , \tag{1.37}$$

where:

m represents the number of stages of the heat pump, (m = 3) in the heating and (m = 2) in the cooling season [unit less];
k represents the discrete simulation time steps [min];
n represents the forecast horizon given in Table 5 [min];
u represents the binary decision variable [unit less], and at each simulation time step it is defined as

$$u \in \begin{cases} 1, \text{ if a heat pump stage is selected} \\ 0, \text{ otherwise;} \end{cases}$$

P represents the electrical power associated with each stage of the heat pump [W]; and
w represents heat pump stage weight factors [1/W] described in Sec. 4.2.1.3.1.1.

Practical implementation of Eq. (1.37) requires a set of constraints, enabling the optimization solver to minimize energy consumption, maintain thermal comfort, and consider equipment efficiency and longevity. These constraints are described below.

Only one stage of the heat pump to be activated at a time. This constraint is given by

$$\sum_{i=1}^{m} u_{i,k-1} \leq 1, \forall k \in [2,n]. \tag{1.38}$$

The solver must not be allowed to arbitrarily cycle the heat pump on and off at each simulation time step because it can adversely affect its efficiency and longevity. To prevent such cycling, each stage *i* of the heat pump has a minimum on-time U_i and a minimum off-time D_i constraint. Thus, if stage *i* is off at *k-1* and turned on in time step *k*, then it must remain on until time step $k + U_i - 1$ [28]. Similarly, if stage *i* is on at *k-1* and turned off in time step *k*, then it must remain off until time step $k + D_i - 1$ [28]. The minimum on-time constraint is given by the following linear inequalities

$$\begin{aligned} u_{i,k} - u_{i,k-1} &\leq u_{i,y} \\ &\forall y \in \left[k, \min\left(n, k + U_i - 1\right) \right] \\ &\forall i \in [1, m] \\ &\forall k \in [2, n], \end{aligned} \tag{1.39}$$

where:

u, *m*, *n*, and *k* were described in Eq. (1.37); and
U represents the vector of minimum on-times for each stage of the heat pump [min].

The minimum off-time constraint is given by the following linear inequalities

$$\begin{aligned} u_{i,k-1} - u_{i,k} &\leq 1 - u_{i,g} \\ &\forall g \in \left[k, \min\left(n, k + D_i - 1\right) \right] \\ &\forall i \in [1, m] \\ &\forall k \in [2, n], \end{aligned} \tag{1.40}$$

where:

D represents the vector of minimum off-times for each stage of the heat pump [min].

The minimum on-time and off-time constraints of residential EMCA1 in the heating season are *U = [10, 10, 5]* and *D = [5, 5, 5]*, and in the cooling season are *U = [10, 10]* and *D = [5, 5]* minutes. The entries in *U* and *D* vectors correspond to the first, second, and third (heating only) stages of the heat pump, respectively.

The optimization problem is further constrained such that the forecasted T_{ind} must remain between an arbitrary defined lower bound and the HS_p in the heating season, and the CS_p and an arbitrary selected upper bound in the cooling season. The values for HS_p and CS_p as well as the upper and lower bounds are given in Table 5. These constrains are given by

$$\begin{aligned} lb \le T_k \le HS_p \\ CS_p \le T_k \le ub, \end{aligned} \quad (1.41)$$

where:

lb represents the T_{ind} lower bound [°C]; and
ub represents the T_{ind} upper bound [°C].

4.2.1.3.1.1. Weight Factors

The weight factors are applied to Eq. (1.37) to reduce the average solution time of the optimization solver. The optimization solver time is the amount of time in seconds that the intlinprog algorithm, on average, used to solve the optimization problems and generate heat pump control actions. The weight factors are formulated in such a way that using the 2nd Stage of heat pump is prioritized over the 1st Stage in both heating and cooling seasons. In the heating season, the 3rd Stage is prioritized the least because it is the least efficient mode of operation.

For the heating season, at each simulation time step they are defined as

$w_1 = 1 / mean(P_{h1}, P_{h2}, P_{h3})$, where w_1 is the weight factor for the 1st Stage [1/W];
$w_2 = 1 / \max(P_{h1}, P_{h2}, P_{h3})$, where w_2 is the weight factor for the 2nd Stage [1/W];
$w_3 = 1 / \min(P_{h1}, P_{h2}, P_{h3})$, where w_3 is the weight factor for the 3rd Stage [1/W]; and

for the cooling season, they are defined as

$w_1 = 1 / mean(P_{c1}, P_{c2})$, where w_1 is the weighting factor for the 1st Stage [1/W]; and
$w_2 = 1 / \max(P_{c1}, P_{c2})$, where w_2 is the weighting factor for the 2nd Stage [1/W].

4.2.1.3.2. Optimization Problem for Residential EMCA2

The objective function of the residential EMCA2 is formulated in such a way that it attempts to minimize the cost of energy consumption of the heat pump over a forecast horizon of one day. The objective function for residential EMCA2 is expressed by

$$\min_{k \in [2,n]} \sum_{i=1}^{m} u_{i,k-1} P_{i,k-1} \cdot w_{k-1} \cdot x_{k-1}, \quad (1.42)$$

where:

m, k, n, u, and P are previously defined in Eq. (1.37); and
x represents the vector of normalized values of the price of electricity [unit less], and is given by
$x = p_e / \max(p_e), \forall p_e \in [k,n]$, where p_e is a vector of price of electricity in [¢/kWh];
w represents heat pump stage weight factors [1°C/W].

In the heating season the weight factors are defined as

$w_1 = 1^\circ C / \max(P_{h1}, P_{h2}, P_{h3})$, where w_1 is the weigh factor for the 1st Stage;
$w_2 = 1^\circ C / \max(P_{h1}, P_{h2}, P_{h3})$, where w_2 is the weight factor for the 2nd Stage; and
$w_3 = 1^\circ C / \min(P_{h1}, P_{h2}, P_{h3})$, where w_3 is the weight factor for the 3rd Stage.

In the cooling season the weight factors are defined as

$w_1 = 1^\circ C / \max(P_{c1}, P_{c2})$, where w_1 is the weighting factor for the 1st Stage; and
$w_2 = 1^\circ C / \max(P_{c1}, P_{c2})$, where w_2 is the weighting factor for the 2nd Stage.

Unlike residential EMCA1, no preferential treatment for a particular stage was considered in Eq. (1.42). Normalizing the price and power consumption stages of the heat pump are not necessary to solve the optimization problem. It is an implementation preference to obtain unitless objective function and create a common structure for reusability in multi-objective optimization algorithms.

Practical implementation of Eq. (1.42) requires a set of constraints, enabling the optimization solver to minimize the cost of energy consumption, maintain thermal comfort, and consider equipment efficiency and longevity. Mathematical descriptions of these constraints are identical to the descriptions given for the residential EMCA1 in Eq. (1.38) to Eq. (1.41).

The objective or residential EMCA2 is to minimize the cost of operating the heat pump using the RTP tariff. A forecast horizon of one day was chosen for this algorithm to take advantage of the full range of variability in the structure of the RTP tariff. Since the optimization problem is defined over one day, it is computationally difficult for the optimization solver to forecast heat pump control actions for each simulation time step in a reasonable amount of time. Therefore, the forecast horizon was divided into 60 bins, each bin holding 24 min of data. Average values of all forecasted variables in each bin was computed and used as a representative sample. This effectively reduced the forecast horizon to 60 min, which is computationally less time consuming. Since the new forecast horizon is 60 min, the output of the optimization solver is also a vector of length sixty. Each element of the vector represents 24 forecasted control actions. For example, if the first element of the output vector is the 2nd

Stage, then in the 2nd Stage is simulated for the next 24 min. For this reason, the values for the minimum on-time and off-time constraints in residential EMCA2 are set to unity. More explicitly, in both heating and cooling seasons the values for minimum on-time and off-time constraints are *U = [1, 1, 1]* and *D = [1, 1, 1]*, and *U = [1, 1]* and *D = [1, 1]* minutes, respectively.

4.2.1.4. Multi-Objective Optimization

Residential EMCA3 and residential EMCA4 are multi-objective optimization problems. The objectives of these control algorithms are to maintain a balance between thermal comfort and minimize the cost of energy consumption of the heat pump over a forecast horizon of 4 h. The following subsections discuss the objective functions and constraints of residential EMCA3 and residential EMCA4.

4.2.1.4.1. Optimization Problem for Residential EMCA3

The objective function of the residential EMCA3 is expressed by

$$\min_{k\in[2,n]} \lambda \cdot \left|T_k - T_{SP}\right| + \left(1-\lambda\right) \cdot \sum_{i=1}^{m} u_{i,k-1} P_{i,k-1} \cdot w_{i,k-1} \cdot x_{k-1}\ . \qquad (1.43)$$

Note that the objective function defined in Eq. (1.43) contains a non-linear term, the absolute value of T_{ind} minus the indoor temperature setpoint. In its current form, it cannot be solved using linear optimization methods. Application of linear programming requires that the objective function and all its constraints are expressed in a linear form. To linearize the objective function given in Eq. (1.43), the absolute value term is replaced with a variable Z in the objective function and adding two additional linear constraints to the problem definition. The linear form of the objective function is given by

$$\min_{k\in[2,n]} \lambda \cdot Z_{k-1} + \left(1-\lambda\right) \cdot \sum_{i=1}^{m} u_{i,k-1} P_{i,k-1} \cdot w_{i,k-1} \cdot x_{k-1}, \qquad (1.44)$$

where:

m, k, n, u, and P are previously defined in Eq. (1.37);
λ is a value between 0 and 1 that represents the relative dominance between comfort and cost [unit less, fixed at 0.45];
x is previously defined in Eq. (1.42);
w represents heat pump stage weight factors described in Sec. 4.2.1.3.1.1 with one minor difference of having units of [°C/W] similar to the residential EMCA2.

The linear constraints replacing the absolute value term of the objective function are expressed as

$$\begin{aligned} T_k - T_{SP} &\le Z_{k-1} \\ -\left(T_k - T_{SP}\right) &\le Z_{k-1}, \end{aligned} \qquad (1.45)$$

where Z has a unit of [°C].

Together with linear constraints of Eq. (1.45), practical implementation of Eq. (1.43) requires a set of constraints, enabling the optimization solver to minimize energy consumption, maintain thermal comfort, and consider equipment efficiency and longevity. Mathematical descriptions of these constraints are identical to the descriptions given for the residential EMCA1 in Eq. (1.38) to Eq.(1.40). In residential EMCA3, there are no upper and lower bound constraints because the thermal comfort term is explicitly defined in the objective function. The values for U and D vectors in residential EMCA3 are identical to values given for residential EMCA2.

4.2.1.4.2. Optimization Problem for Residential EMCA4

The mathematical description of the optimization problem of residential ECMA4 is identical to the formulation of residential EMCA3 including all constraints. The only difference is the value of the dominance factor $\lambda = 0.55$ instead of $\lambda = 0.45$ given for residential EMCA3.

The results of applying residential EMCA1 through residential EMCA6 for managing the heat pump operation of the NZERTF are presented in Appendix A through Appendix G.

Chapter 5

Disclaimer: The material presented in this chapter has previously been published in:

1. F. Omar, S. T. Bushby, and R. D. Williams, “Assessing the Performance of Residential Energy Management Control Algorithms: Muti-Criteria Decision Making Using the Analytical Hierarchy Process,” NIST Tech. Note 2017, 2018.

Credit to my co-authors:

1. Steven T. Bushby, National Institute of Standards and Technology, steven.bushby@nist.gov
2. Ronald D. Williams, University of Virginia, rdw@virginia.edu

5. Assessment Engine

The assessment framework realization is the core of this research project. Every component of the reCAAT was developed to support this process. The main challenge in creating the assessment framework is developing a methodology that can effectively compare different residential EMCAs and rank them with respect to a set of user defined preferences and goals. This chapter discusses the development of the assessment methodology and its implementation in the AE.

There is an extensive literature describing approaches for comparing residential EMCAs. A unifying theme throughout the literature is centered on comparing the performance of proposed residential EMCAs on energy cost savings [31]–[36], energy savings [33], [35], [37], [38], peak load reduction [31], [32], [35], [39], and thermal comfort [33], [35], [37] to an established baseline. In [40] the authors proposed a data-driven framework for comparing the energy performance of residential thermostats controlling central HVAC systems. Using thermostat field data, the proposed framework applied different assessment techniques to separately consider behavioral attributes (setpoint-related) from non-behavioral attributes such as HVAC control strategies and fault detection and diagnostics (FDD). Setpoint-related energy impacts were evaluated from a data-driven method using a building simulation model, while HVAC and FDD control impacts were determined using traditional testing methods such as field experiments. The results were integrated to determine typical energy performance of residential thermostats relative to a specified baseline. The baseline was a fixed seasonal temperature that a typical homeowner would prefer to maintain if setbacks were not available. Using historical data, a user’s preferred baseline was determined from seasonal hourly setpoints by calculating the 90th percentile value for heating season and 10th percentile value for the cooling season.

However, little has been reported on a comprehensive framework for assessing the performance of residential EMCAs considering multiple objectives and users’ subjective preferences simultaneously. Developing a comprehensive framework requires the use of a multi-criteria decision-making mechanism that can handle both subjective preferences from users and objective analyses from performance data generated because of using residential EMCAs. A few examples of using such a hybrid mechanism (subjective and objective analyses) have been given in the literature. The authors in [41], [42] presented an assessment framework based on the Analytical Hierarchy Process (AHP) that combines subjective analyses from expert judgments with objective data derived from analytical methods to rank alternatives. The assessment framework in [41] was used to choose the best sustainable building envelope design among alternatives, while in [42] a case study was presented for choosing the best HVAC system design for a building. The decision was informed by incorporating uncertainty analysis into selecting building design parameters.

Although the frameworks presented in [41], [42], in concept, are similar to the work described in this study, the domain of the problems are fundamentally different. The objective of [41], [42] was to make design decisions, but the main objective of this study is to develop an assessment framework capable of comparing and ranking different residential EMCAs. Assessing the performance of residential EMCAs is a multi-criteria decision making problem because multiple and conflicting objectives (such as minimizing cost while maintaining comfort or other user preferences) apply simultaneously.

Unlike prior studies, the proposed framework will:

1. Provide a systematic mechanism for comparing the overall performance of residential EMCAs in terms of energy consumption, cost, and comfort while actively allowing users to interact with the framework to capture the impact of their preferences on the ranking and decision making;
2. Provide an algorithm for mapping quantitative performance data to the comparison scale of the AHP and consequently creating a matrix of pairwise comparison (MPC); and
3. Calculate all relative weights (priorities) for both subjective (user's preferences) and objective performance data using the methodology described in the AHP framework.

To implement the proposed framework, an AE was developed as shown schematically in Figure 34. The AE incorporates subjective and objective analyses, deriving priorities from user's input and performance data resulting from different residential EMCAs. It performs the evaluation and ranking of residential EMCAs using AHP. A case study of the proposed AE, applied to six residential EMCAs described in Chapter 4, is presented.

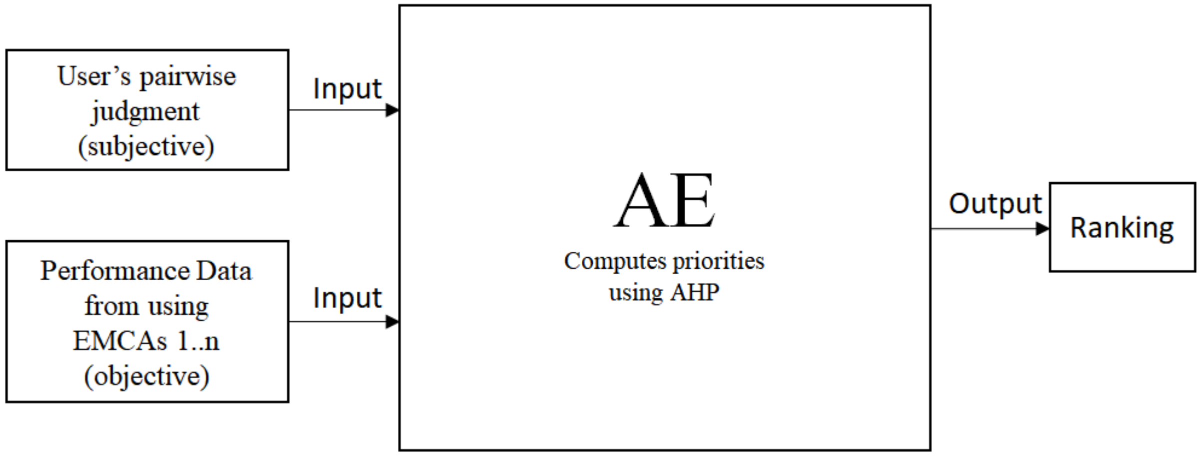

Figure 34. A schematic representation of the assessment process

5.1. Analytical Hierarchy Process

AHP is a multi-criteria decision-making (MCDM) method developed by Saaty [43]. It has been commonly used in solving decision-making problems that consider both quantitative and qualitative analysis [41], [42], [44], [45]. A comprehensive review of the application of AHP to planning, choosing among alternatives, allocating resource, etc., is presented in [46]. The American Society for Testing and Materials (ASTM) Standard E1765 documents a procedure for applying AHP to investments related to buildings and building systems [47]. The main principles of the AHP are hierarchy, pairwise comparison, and principle eigenvector. AHP decomposes a MCDM problem into a hierarchy to handle its numerous or multi-faceted criteria and to keep the number of pairwise comparisons manageable [45]. The goal (objective) of the problem is placed at the top of the hierarchy. The alternatives are positioned at the bottom of the hierarchy, while the criteria and sub-criteria occupy the intermediate levels. To illustrate this, consider a hypothetical example of a couple that is purchasing a house. The couple decided to use the AHP and follow its prescribed steps to achieve their goal. At the first step, they have determined their goal. The goal is to find the house that best suits their needs. At the second step, they have identified the three most important criteria (building size, location, and price) for selecting their desired home. At the third step, they identified three existing homes (alternatives) labeled as *H1*, *H2*, and *H3*. Figure 35 shows the decomposition of this hypothetical problem into a hierarchical arrangement. Each line shows a relationship between an alternative and the criterion above it, or the relationship between the criterion and the goal. These relationships are mathematically represented by priorities, for example, $P_{H1,Size}$ is the priority of the alternative *H1* with respect to the criterion Size and $P_{Size,Goal}$ represents the priority of the criterion Size to the Goal.

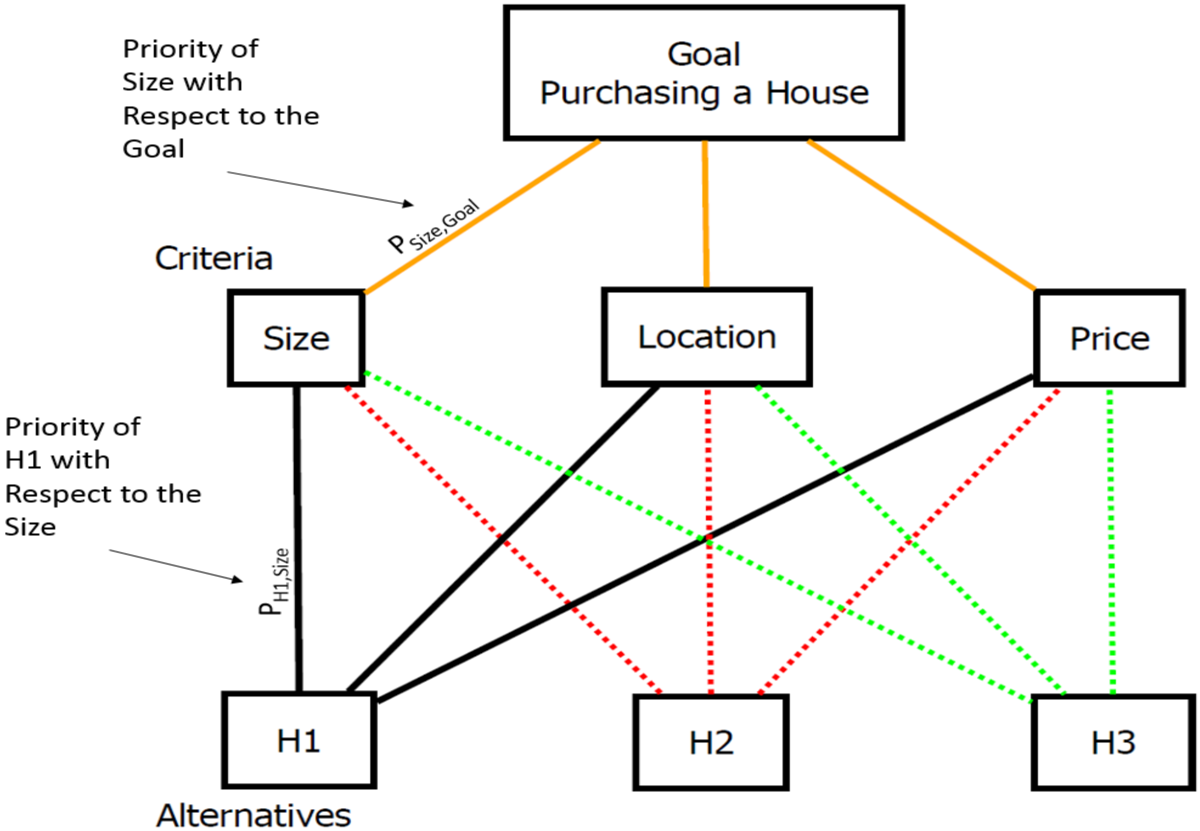

Figure 35. Decomposition of the hypothetical problem of purchasing a house into a hierarchy

At the fourth step, the couple needs to build an MPC (decision matrix) for comparing criteria to each other with respect to the goal of purchasing a house. Each element of an MPC is created by comparing one criterion with another criterion i.e., Size (activity *i*) is compared with Location (activity *j*). To create an MPC, the couple must first judge which criterion is more desirable with respect to reaching their goal. After much discussion, the couple expresses their subjective judgments (expert knowledge) as follows:

1. Location of the house is strongly preferred over the size of the house because of a desire to be near schools and shopping centers;
2. Price of the house is slightly preferred over the size of the house because the budget is fixed; and
3. Location of the house is slightly preferred over the price of the house because of a desire to be near schools and shopping centers.

AHP enables the couple (decision makers) to translate their preferences (subjective judgments) into precise numbers using a 1-9 numerical scale shown in Table 8.

Table 8. The AHP Fundamental Scale, Adapted from Table 3-1 p. 54 of [43]

The Fundamental Scale for Pairwise Comparisons		
Intensity of Importance	**Definition**	**Explanation**
1	Equal importance	Two activities contribute equally to the objective
3	Weak importance of one over another	Experience and judgment slightly favor one activity over another
5	Essential or strong importance	Experience and judgment strongly favor one activity over another
7	Very strong or demonstrated importance	An activity is favored very strongly over another; its dominance demonstrated in practice
9	Absolute importance	The evidence favoring one activity over another is of the highest possible order of affirmation
2,4,6,8	Intermediate values between adjacent scale values	When compromise is needed

Using AHP's fundamental scale, the couple translated their subjective preferences into numeric values as shown in Table 9. For example, since the location of the house is strongly preferred over its size, the table entry for the intersection of the Location row and Size column is assigned the value 5, indicating that location is five times more important than size. The inverse value, 1/5, is assigned to the table entry for the intersection of the Size row and Location column. The couple translates all preferences to numerical values in a similar manner.

Table 9. Criteria compared with respect the Goal for purchasing a house

	Size	**Location**	**Price**
Size	1	1/5	1/3
Location	5	1	3
Price	3	1/3	1

At the fifth step, the couple needs to build an MPC for comparing alternatives to each other with respect to each criterion. Each element of an MPC is created by comparing one alternative with another alternative i.e., H1 (activity *i*) is compared with H2 (activity *j*). To create an MPC, the couple must first judge which alternative is more desirable with respect to the criterion that is being considered i.e., Size. After much discussion, the couple expresses their subjective judgments as follows:

1. H1 is very strongly preferred over H2 because it meets the space requirement of our family;

2. Although H1 and H3 meets the space requirement, the bathroom in H3 is somewhat smaller so H1 is strongly preferred over H3; and
3. H3 is slightly preferred over H2 because the kitchen is somewhat bigger.

Using the procedure highlighted in the step four, the couple forms the following MPC for comparing alternatives with respect to the criterion Size:

Table 10. Alternatives compared with respect the criterion Size

	H1	**H2**	**H3**
H1	1	7	5
H2	1/7	1	1/3
H3	1/5	3	1

The MPCs for comparing alternatives with respect to Location and Price criteria are obtained in a similar manner. In general, the result of pairwise comparisons between activity *i* and activity *j* are stored in an MPC (*n-by-n* matrix) of the form

$$A = \begin{bmatrix} 1 & a_{12} & \cdots & a_{1n} \\ 1/a_{12} & 1 & \cdots & a_{2n} \\ \vdots & \vdots & \vdots\vdots\vdots & \vdots \\ 1/a_{1n} & 1/a_{2n} & \cdots & 1 \end{bmatrix},$$

where a_{ij} is the numerical representation of the quantified judgments on pairs (activity *i*, activity *j*) for all activities (i, j = 1, 2, …, n) [43] where *i* denotes a row and *j* denotes a column entry of the matrix A. The diagonal of the matrix A is equal to one because activity *i* is always as important as itself. The activities below the diagonal are the reciprocal values of the corresponding activities above the diagonal because if activity *i* is four times as important as activity *j*, then activity *j* is one fourth as important as activity *i*. More explicitly, the following rules adapted from [43] define the a_{ij} entries:

Rule 1. If $a_{ij} = \sigma$ then $a_{ji} = 1/\sigma$, $\sigma \neq 0$; and
Rule 2. If activity *i* is judged to be of equal relative importance as activity *j*, then $a_{ij} = 1$, $a_{ji} = 1$, and $a_{ii} = 1$ for all *i*.

Once the judgments are recorded in the matrix A, AHP uses the principle eigenvector method to derive priorities or weights (normalized to sum to one) for the criteria and alternatives. It also uses the principle eigenvalue, λ_{max}, to check for consistency between pairwise comparisons. The eigenvalue/eigenvector in matrix notation is given by

$$Aw = \lambda_{\max} w, \tag{1.46}$$

where:

A is the reciprocal matrix with entries a_{ij} for all ($i, j = 1, 2, \ldots, n$);
w is the eigenvector; and

λ_{max} is the principle eigenvalue.

If the judgments in the matrix A are perfectly consistent, then the value of λ_{max} is equal to n (number of activities). In AHP, the deviation from consistency is a violation of proportionality [43] and shows an inherent possibility of bias and errors in the judgements [45]. Two metrics are recommended in [43] as measure of the consistency of pairwise comparisons, the consistency index (CI) and consistency ratio (CR). *CI* is the difference between the principle eigenvalue and *n*, and is mathematically defined as $(\lambda_{max} - n)/(n-1)$. *CR* is a measure of the goodness of *CI* and it is defined as *CI/RI*. The random index *RI*, is an average *CI* of randomly generated reciprocal matrices [43] as shown in Table 11. A *CR* of 10 % or less is desirable, indicating good judgments when activities are pairwise compared.

Table 11. The Average RI for Matrices of Order 1-15, Adopted from p. 21of [43]

Matrix Order	1	2	3	4	5	6	7	8	9	10	11	12	13	14	15
Average RI	0.00	0.00	0.58	0.90	1.12	1.24	1.32	1.41	1.45	1.49	1.51	1.48	1.56	1.57	1.59

The final step in AHP is to calculate the overall score for each alternative with respect to the goal. Consider the hierarchical arrangement of the hypothetical problem of purchasing a house with three levels: the goal, criteria, and alternatives. Let *wg* represent the vector of priorities derived for each criterion with respect to the goal (that is, the principal eigenvector of the MPC for the goals), and *m* be the number of criteria. Let p_a represent the vector of priorities derived for an alternative with respect to criteria in the level above it (that is, the principal eigenvector of the MPC for each of the criteria). The overall score for alternative *a* (S_a) with respect to the goal is computed by

$$S_a = \sum_{k=1}^{m} p_a(k) wg(k) . \tag{1.47}$$

Using Eq. (1.47), the overall scores for all alternatives are computed. The sum of priorities at each level of the hierarchy must equal one. The alternative with the highest score is the most desirable one. Applying these definitions to the hypothetical problem of purchasing a house, give us the following results:

$$wg = [0.11, 0.63, 0.26]$$

$$p_{size} = [0.73, 0.08, 0.19],$$

where:

wg is the vector of priorities derived for each criterion with respect to the *Goal* and is computed from the MPC shown in Table 9; and

p_{size} is the vector of priorities derived for each alternative with respect to the criterion *Size* from the MPC shown in Table 10.

The vector of priorities for each alternative with respect to the criteria *Location* and *Price* are obtained in a similar manner as p_{size}. These priorities are given below:

$$p_{location} = [0.16, 0.59, 0.25]$$
$$p_{price} = [0.25, 0.50, 0.25],$$

where:

$p_{location}$ is the vector of priorities derived for each alternative with respect to the criterion Location; and

p_{price} is the vector of priorities derived for each alternative with respect to the criterion Size.

Therefore, the vector of priorities for each alternative with respect to the criteria is given by

$$p_{\mathrm{H1}} = [0.73, 0.16, 0.25]$$
$$p_{\mathrm{H2}} = [0.08, 0.59, 0.50]$$
$$p_{\mathrm{H3}} = [0.19, 0.25, 0.25],$$

The relationship between alternative houses, criteria, and the goal of purchasing a house are shown in Figure 36.

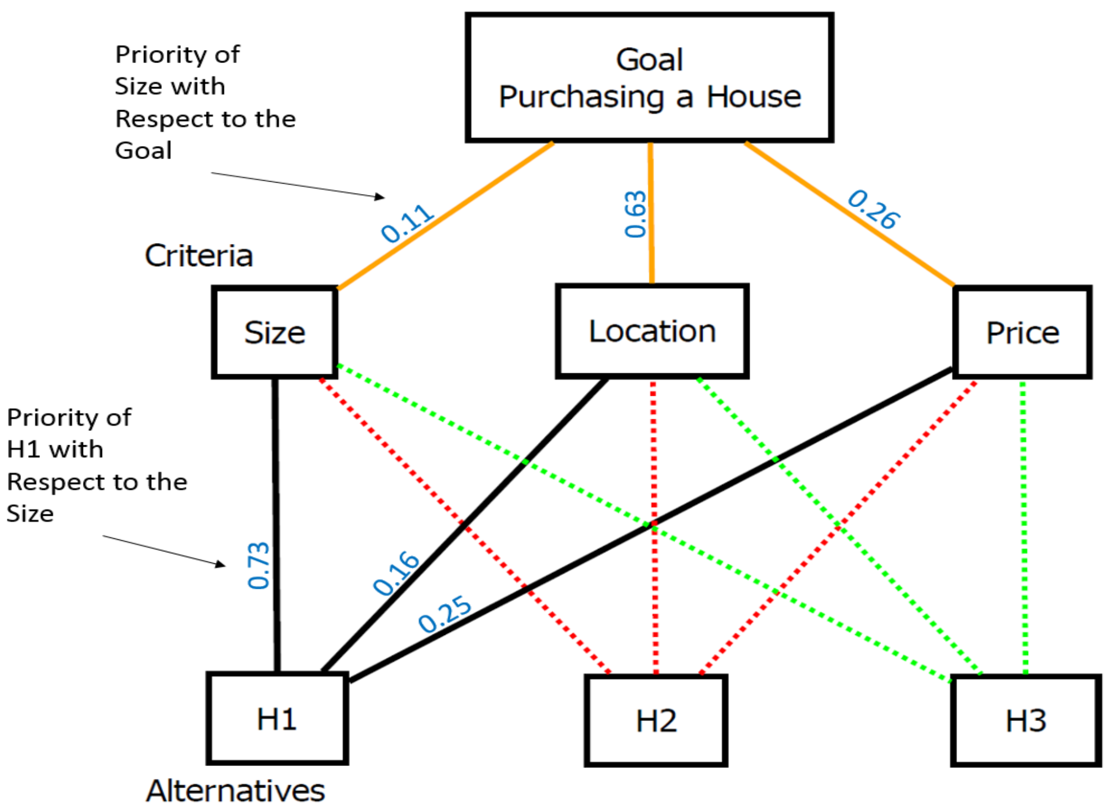

Figure 36. Summary figure showing the relationship between alternatives, criteria, and the goal using priorities for one alternative

Applying Eq. (1.47) to the derived priorities, the overall scores for each alternative with respect to the Goal is given in Table 12. For example, the overall score for H1 is computed by

$$S_{\mathrm{H1}} = \sum_{k=1}^{3} p_{\mathrm{H1}}(k) wg(k)$$
$$= 0.25.$$

Table 12. The overall scores of alternatives for purchasing a house

Alternatives	Overall Score (S_a)
H1	0.25
H2	0.51
H3	0.24

Based on the overall scores in Table 12, the most desirable outcome for the couple is to purchase the second house (H2).

5.2. Problem Hierarchy Assessing EMCAs

The proposed AE splits the problem of assessing the performance of residential EMCAs into a three-level hierarchy: the goal, criteria, and alternatives as shown in Figure 37.

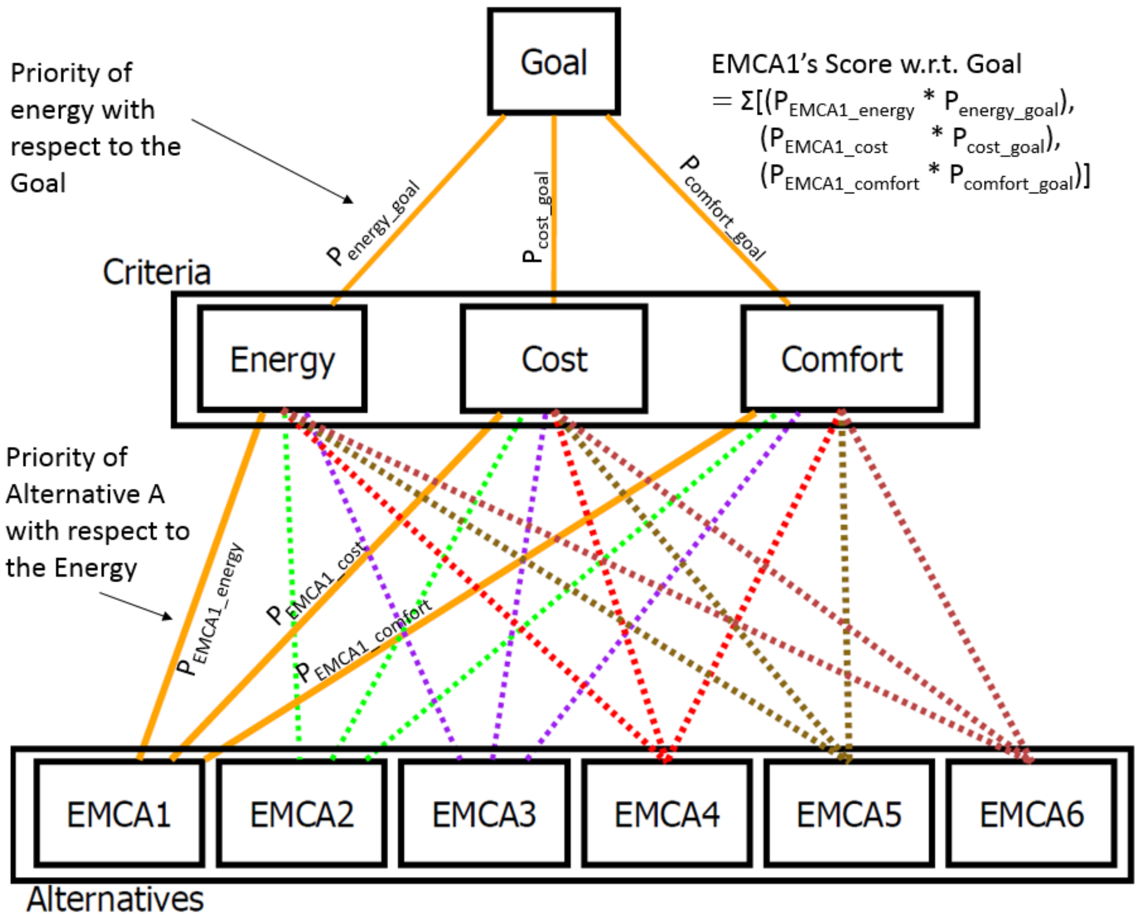

Figure 37. The assessment problem hierarchy showing the relationship of the alternatives to the criteria and the goal

The goal is to identify the best alternative given the user's preferences and the performance data resulting from the use of residential EMCAs. Energy, cost, and comfort were selected as the criteria because they can be controlled by a residential EMCA and have a significant impact on the overall well-being of the occupants and because they can help utilities with peak demand reduction. The main objective of developing the residential EMCAs was to create a diverse set of realistic operating scenarios for the AE to evaluate and rank.

5.3. The AE User Interface

The AE utilizes subjective preferences (inputs from a user) and objective performance data (generated in response to the use of a residential EMCA) to perform pairwise comparisons and ultimately help users select the best alternative among all alternatives. The AE user interface

(AEUI), shown in Figure 38, was developed to capture user's preferences and obtain/process performance data. In its current form, users can perform the following tasks:

1. Import up to six hourly and minutely performance data files;
2. Solicit a user's preferences (expert knowledge or judgments) for pairwise comparison of energy, cost, and comfort; and
3. Perform an overall ranking of the residential EMCAs with respect to the goal.

Additionally, the AEUI provides a set of diagnostic analyses and plots comparing the residential EMCAs with respect to a base case. Any residential EMCA can be used as a base case. The diagnostic analyses can be used as a benchmarking tool, independent of the assessment and ranking.

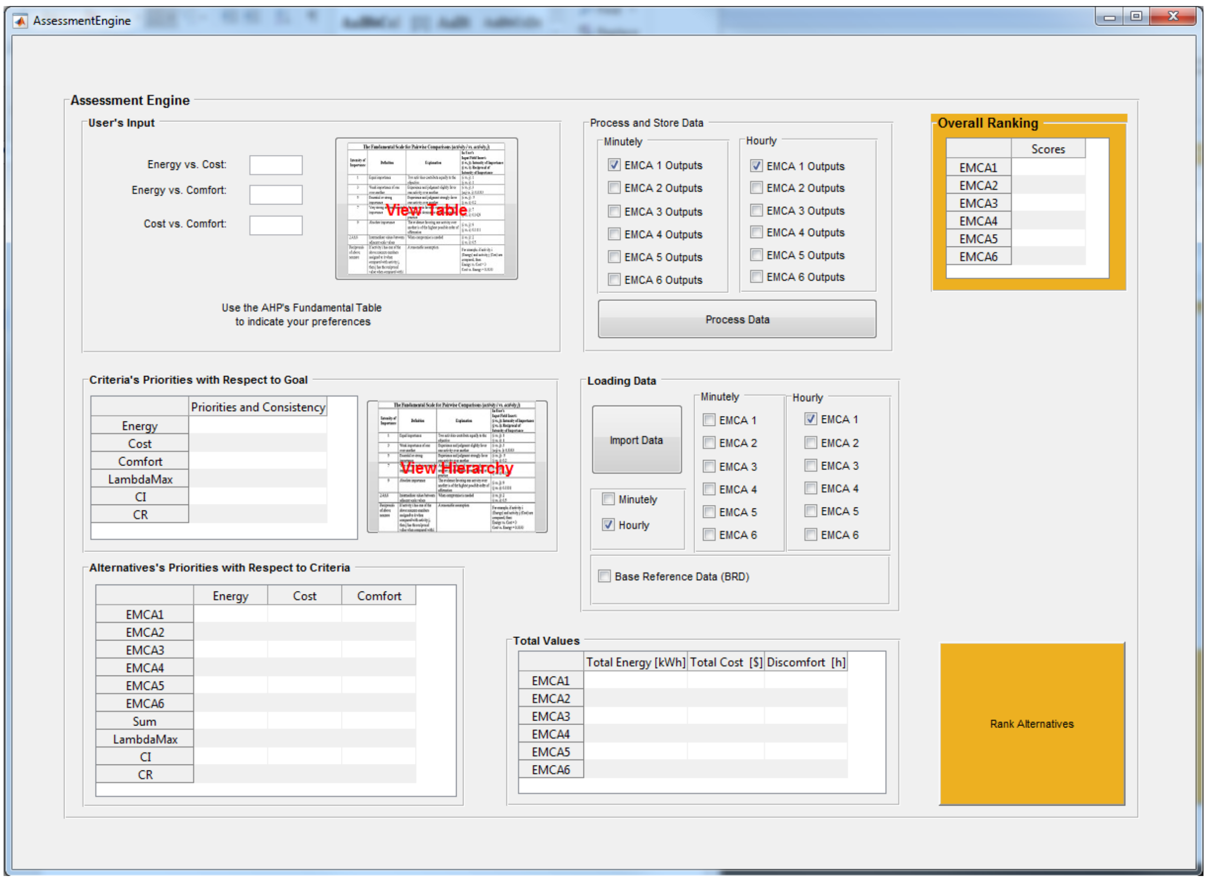

Figure 38. The AE user interface captures user's input, loads performance data, and performs ranking

5.4. Priorities from User's Judgments

Using a user's input, the AE computes the relative priorities of the criteria with respect to the goal. A user uses the AHP's fundamental scale shown in Table 8 to express his/her desire (or expert judgment) for comparing two criteria in pairs. For example, when the cost criterion is favored very strongly over the energy criterion, the user would enter 0.1429 (1/7) in the Energy vs. Cost input field. However, if the cost criterion is slightly favored over the comfort criterion, the user would enter 3 in the Cost vs. Comfort input filed. The User's Input fields shown in Figure 39 captures these preferences.

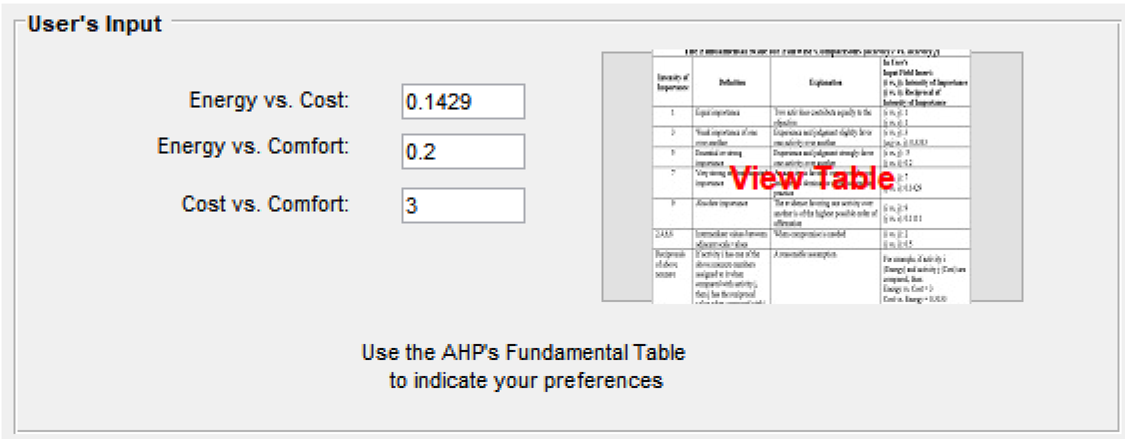

Figure 39. User's Input fields capturing preferences between criteria

Using the provided preferences, the AE forms the corresponding MPC for pairwise comparisons between selected criteria as shown in Table 13.

Table 13. MPC between Criteria

	Energy	**Cost**	**Comfort**
Energy	1	0.1429	0.2
Cost	7	1	3
Comfort	5	0.3333	1

From this user input, the AE uses the AHP's principle eigenvector method to compute the relative priorities of each criterion with respect to the goal and the consistency of a user in judging the intensity of importance when the criteria were compared in pairs. The results from the user input shown in Table 13 are summarized in Table 14.

Table 14. Priorities and Consistency metrics

Criteria and consistency metrics	**Priorities and consistency**
Energy	0.07
Cost	0.65
Comfort	0.28
λ_{max}	3.07
CI	0.03
CR	0.06

For this example, cost is the most important factor for the decision maker followed by comfort and energy. Recall from Table 11 that for a matrix of order 3, the *CR* value of 6 % indicates that the decision maker was consistent in providing subjective judgments.

5.5. Calculating Energy, Cost, and Comfort

Using the performance data, the AE calculates the total energy consumption, total cost, and a discomfort index for each residential EMCA. These calculations, collectively, form the basis for computing the relative priorities of each alternative EMCA with respect to each criterion.

5.5.1. Energy

The total energy consumption is computed by

$$E_{total,k} = \sum_{h=1}^{H} e_h \text{ for } k = 1,...,n\,, \tag{1.48}$$

where:

n is the number of alternatives (six residential EMCAs in this case);
H is the number of hours (i.e., 8760 h for one year); and
e_h is the energy consumed by the HVAC unit in hour h [kWh].

5.5.2. Cost

The cost of consuming energy is computed by

$$C_{total,k} = \sum_{h=1}^{H} e_h \times p_h \text{ for } k = 1,...,n\,, \tag{1.49}$$

where:

H, e_h and n are the same as described in Eq. (1.48); and
p_h is the RTP tariff in hour h [¢/kWh].

The RTP tariff was derived from the day-ahead wholesale hourly price of electricity from PJM. The data is from January 2013 to December 2013. The day-ahead wholesale price, shown in Figure 40, was scaled to generate a forecasted retail RTP structure, resulting in an average of 15 ¢/kWh. The average cost of consuming energy in a residential home in Gaithersburg, Maryland is approximately 15 ¢/kWh (including transmission, distribution, taxes, and fees).

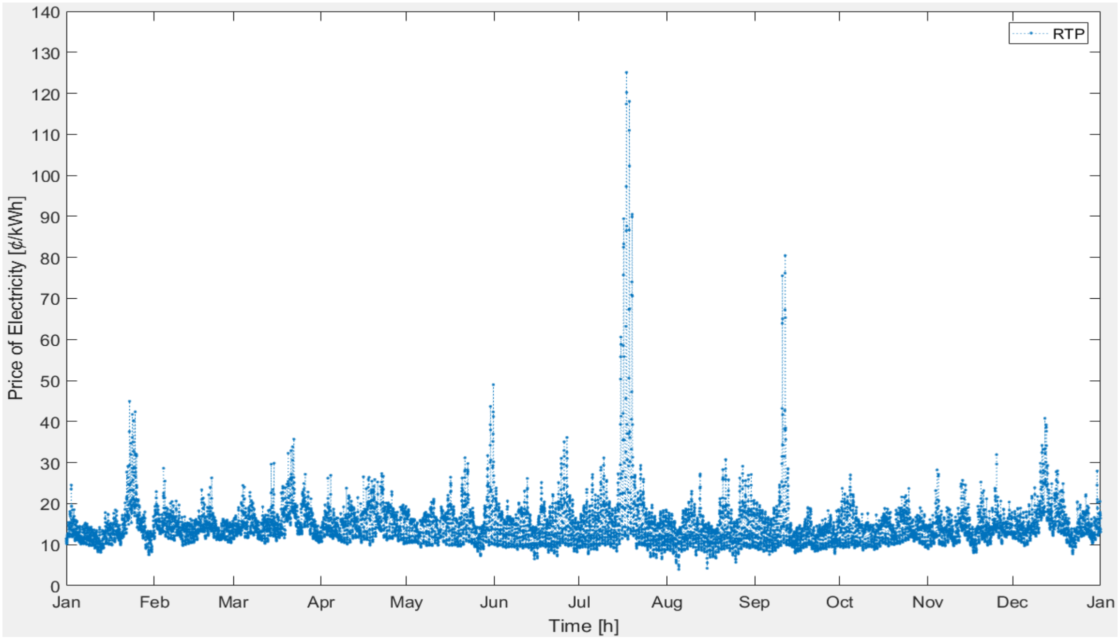

Figure 40. The hourly RTP tariff used to compute the cost of energy consumption

5.5.3. Comfort

Many long-term discomfort indices that evaluate the thermal response of humans to changes in indoor climatic conditions have been reported in the literature and standards. A review of these indices, their strengths and weaknesses are documented in [48]. In this study, a discomfort index was chosen that produced a single value, was based on well-known thermal comfort standards, and considered both the duration and severity of the thermal discomfort. The AE computes the long-term discomfort index using a methodology that is based on predicted mean vote (PMV) and predicted percentage of dissatisfied (PPD). The methodology for computing the long-term index is the PPD-weighted criterion (PPD_{wc}) documented in Method C of International Organization for Standardization standard 7730 (ISO 7730) [49] and summarized in [48]. This measure of discomfort index is described as "the time during which the actual PMV exceeds the comfort boundaries is weighted with a factor that is a function of the PPD" [49].

5.5.3.1. Calculating PMV and PPD

The *PMV* index is the mean value that predicts the response of a large group of people on the seven-point thermal sensation scale defined in [49], [50] and shown in Table 15.

Table 15. Seven-point Thermal Sensation Scale

+3	Hot
+2	Warm
+1	Slightly warm
0	Neutral
-1	Slightly Cool
-2	Cool
-3	Cold

Using heat balance principles, the *PMV* index relates key primary thermal factors such as metabolic rate, clothing insulation, air temperature, radiant temperature, air speed, and humidity to the thermal sensation scale in Table 15. Many assumptions must be made about some of the inputs for calculating *PMV*, including that the difference between T_{air} and T_{mrt} is negligible. This assumption is common in previous indoor climate studies [51], [52]. Table 16 shows the input values used in this study to calculate *PMV*.

Table 16. **Assumed Values for Calculating PMV**

Input data (unit)	**Assumed Value**	
Clothing (clo)	Summer months (May, June, July, August, September)	0.36 (Walking shorts, short-sleeve shirt [50])
	Other months	0.6 (Trousers, long-sleeve shirt [50])
Metabolic rate (met)	1.7 (Office activities, walking about [50])	
External work (met)	0 [50]	
Air temperature T_{air} (°C)	Indoor dry bulb temperature	
Mean radiant temperature T_{mrt} (°C)	Indoor dry bulb temperature	
Relative air velocity (m/s)	0.05 [53]	
Relative humidity (%)	Indoor relative humidity	

The *PMV* metric is iteratively calculated by using of the following four equations given in ISO 7730 [49]

$$PMV = [0.0303\times\exp(-0.036\times M)+0.028]\times\left\{\begin{array}{l}(M-W)-3.05\times10^{-3}\\ \times[5733-6.99\times(M-W)-p_a]\\ -0.42\times[(M-W)-58.15]\\ -1.7\times10^{-5}\times M\times(5867-p_a)\\ -0.0014\times M\times(34-t_a)\\ -3.96\times10^{-8}\times f_{cl}\times[(t_{cl}+273)^4\\ -(\bar{t}_r+273)^4]-f_{cl}\times h_c\times(t_{cl}-t_a)\end{array}\right\}, \quad (1.50)$$

$$t_{cl} = 35.7 - 0.028 \times (M - W) - I_{cl} \times \left\{ \begin{array}{l} 3.96 \times 10^{-8} \times f_{cl} \\ \times \left[(t_{cl} + 237)^4 - (\bar{t}_r + 273)^4 \right] \\ + f_{cl} \times h_c \times (t_{cl} - t_a) \end{array} \right\}, \qquad (1.51)$$

$$h_c = \begin{cases} 2.38 \times |t_{cl} - t_a|^{0.25} & \text{for } 2.38 \times |t_{cl} - t_a|^{0.25} > 12.1 \times \sqrt{v_{ar}} \\ 12.1 \times \sqrt{v_{ar}} & \text{for } 2.38 \times |t_{cl} - t_a|^{0.25} < 12.1 \times \sqrt{v_{ar}}, \end{cases} \qquad (1.52)$$

$$f_{cl} = \begin{cases} 1.00 + 1.290\, l_{cl} & \text{for } l_{cl} \le 0.078\, m^2 \times K/W \\ 1.05 + 0.645\, l_{cl} & \text{for } l_{cl} > 0.078\, m^2 \times K/W, \end{cases} \qquad (1.53)$$

where:

- M is the metabolic rate in (W/m^2), 1 metabolic unit = 1 met = 58.2 W/m^2;
- W is the effective mechanical power in (W/m^2);
- I_{cl} is the clothing insulation in (m^2 K/W), 1 clothing unit = 1 clo = 0.155 m^2 °C/W;
- f_{cl} is the clothing surface area factor;
- t_a is the air temperature in (°C);
- $\bar{t}_r$ is the mean radiant temperature in (°C);
- v_{ar} is the relative air velocity in (m/s);
- p_a is the water vapor partial pressure in (P$_a$);
- h_c is the convective heat transfer coefficient in [W/(m^2 K)]; and
- t_{cl} is the clothing surface temperature in (°C).

It is noted that the conversion of 1 met equals to 58.2 W/m^2 is based on (ANSI/ASHRAE) Standard 55 [50]. This conversion neglects body size, sex, and age of an individual, for more information regarding this conversion and topic see [54].

The *PPD* index is determined from the *PMV*. It is a quantitative prediction of thermally dissatisfied people in percentage (%) and it is computed by

$$PPD = 100 - 95 \times \exp(-0.03353 \times PMV^4 - 0.2179 \times PMV^2). \qquad (1.54)$$

Computer instructions for calculating *PMV* and *PPD* is provided in Appendix D of American Nation Standards Institute /American Society of Heating, Refrigerating, and Air-Conditioning Engineers (ANSI/ASHRAE) Standard 55 [50]. The instructions were implemented in Matlab [53]. In a typical application, ANSI/ASHRAE Standard 55 also defines a recommended *PMV* and *PPD* range, shown in Table 17, for general thermal comfort. If the calculated values for the *PMV* and hence for the *PPD* are within the defined ranges, the conditions are considered to be comfortable.

Table 17. The PMV and PPD Ranges for Thermal Comfort

PMV Range	PPD (%)
-0.5 < PMV < +0.5	< 10

Figure 41 shows the annual results from calculating *PMV* and *PPD* when residential EMCA1 is applied.

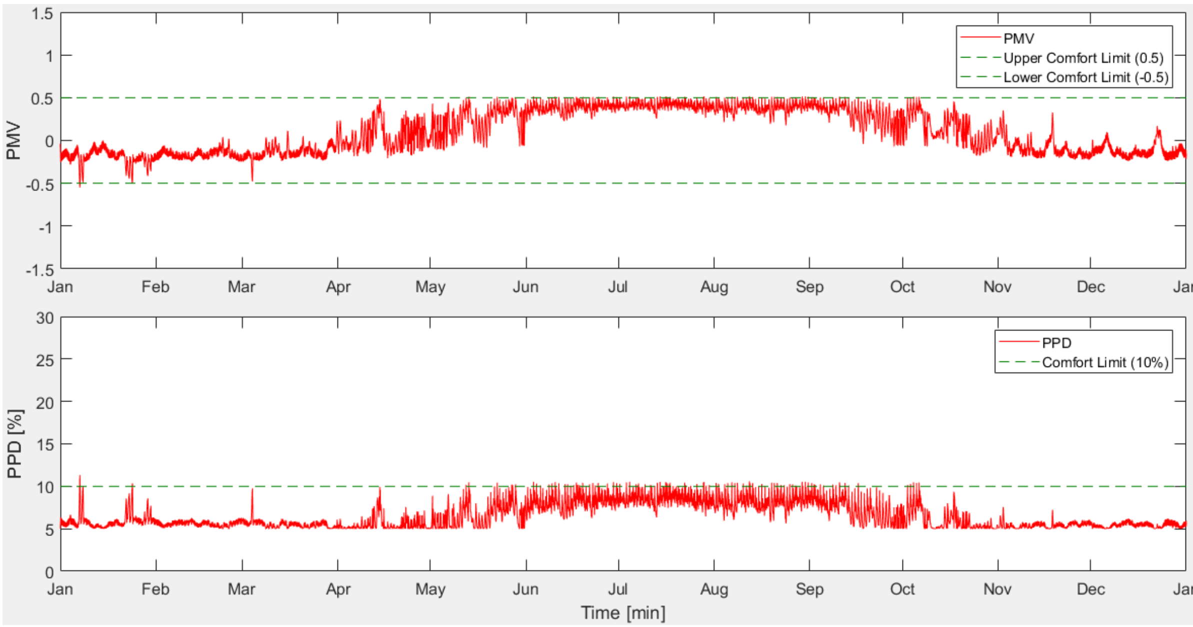

Figure 41. Annual comfort results for residential EMCA1 as measured by PMV and PPD

5.5.3.2. Calculating the Discomfort Index

The discomfort index (PPD_{wc}) is the sum of the product of a weighting factor and time when a building is occupied. In this study, the value of PPD_{wc} is computed in every occupied minute and the result is reported in hours. PPD_{wc} is computed by

$$PPD_{wc,k} = \sum_{j=1}^{om} \left(wf_j \cdot t_j \right) \text{ for } k = 1, \ldots, n \, , \tag{1.55}$$

where:

n is the number of alternatives;
wf_j is the weighting factor in each occupied minute;
om is the total number of occupied minutes; and
t_j is the time step, 1 min.

The weighting factor is computed by

$$wf_j = \begin{cases} \dfrac{PPD_{\mathrm{actualPMV}}}{PPD_{\mathrm{PMVlimit}}}, & |PMV| > |PMV_{\mathrm{limit}}| \\ 1, & PMV = PMV_{\mathrm{limit}} \\ 0, & |PMV| < |PMV_{\mathrm{limit}}|, \end{cases} \tag{1.56}$$

where:

$PPD_{actualPMV}$ is the *PPD* corresponding to the actual *PMV*; and

$PPD_{PMVlimit}$ is the *PPD* corresponding to PMV_{limit}.

5.6. Priorities from Performance Data

The results of applying Eq. (1.48), Eq. (1.49), and Eq. (1.55) to the performance data for each residential EMCA are shown in Table 18. In this document, Table 18 is referred to as the Performance Table. The values in the Performance Table are used to derive priorities for each residential EMCA relative to the criteria.

Table 18. Summary of Results for key Performance Metrics

Residential EMCA	**Total Energy (E_{total}) [kWh]**	**Total Cost (C_{total}) [$]**	**Discomfort Index (PPD_{wc}) [h]**
1	5605	901	9
2	5588	880	339
3	5484	847	1176
4	5762	918	222
5	5882	938	0
6	6589	1050	37

Having computed the total energy consumption (E_{total}), cost of consuming energy (C_{total}), and the discomfort index (PPD_{wc}) for all residential EMCAs, the next step is to compute a set of relative priorities when alternatives are pairwise compared. To compute these priorities, an algorithm was developed to first map each column of the Performance Table to the Intensity of Importance in Table 8 then form an MPC using the derived quantified judgements a_{ij} in matrix A. Using AHP's standard procedure described in Sec. 5.1 on matrix A will result in relative priorities (a set of weights) with respect to criteria along with λ_{max}, *CI*, and *CR*. When creating the MPC, the following main assumptions form the basis of the computations:

1. Lower energy consumption is desired over higher energy consumption;
2. Lower monetary cost is desired over higher cost; and
3. More comfortable environment is desired over less comfortable environment.

The following steps describe the algorithm for computing priorities:

1. For each entry in each column in the Performance Table, scale the values by dividing the maximum of each column by the value of each entry in the column. Let R_E, R_C, and R_{DC} represent energy, cost, and discomfort ratios, respectively. These ratios are mathematically represented by:

$$R_{E,k} = {\beta_{\max}}\big/{E_{total,k}}, \forall\ k = 1,\dots,n, \tag{1.57}$$

where $\beta_{\max} = \max\left(\left\{E_{total,k} : k = 1,\dots,n\right\}\right)$.

$$R_{C,k} = {\gamma_{\max}}\big/{C_{total,k}}, \forall\ k = 1,\dots,n, \tag{1.58}$$

where $\gamma_{\max} = \max\left(\left\{C_{total,k} : k = 1,\dots,n\right\}\right)$.

$$R_{DC,k} = {\delta_{\max}}\big/{PPD_{wc,k}}, \forall\ k = 1,\dots,n, \tag{1.59}$$

where $\delta_{\max} = \max\left(\left\{PPD_{wc,k} : k = 1,\dots,n\right\}\right)$ and for numerical stability

$$PPD_{wc,k} = \begin{cases} PPD_{wc,k}, & \text{if } PPD_{wc,k} > 0 \\ 1, & \text{if } \mathrm{PPD}_{wc,k} = 0. \end{cases} \tag{1.60}$$

For instance, the energy ratios $R_{E,k}$ (for $k = 1,\dots, n$), where n is the number of residential EMCAs, is computed by Eq. (1.57) and is shown in Table 19.

Table 19. Energy Ratio (R_E)

Residential EMCA	**E_{total} (kWh)**	**R_E (dimensionless)**
1	5605	1.18
2	5588	1.18
3	5484	1.20
4	5762	1.14
5	5882	1.12
6	6589	1.00

2. Define scale factors for energy (S_{Ef}), cost (S_{Cf}), and discomfort (S_{Df}). Let C_{scale} represent the AHP Intensity of Importance shown in Table 8.

$$S_{Ef} = {\left(\max\left(C_{scale}\right) - \min\left(C_{scale}\right)\right)}\big/{\left(\eta_{\max} - \eta_{\min}\right)}, \tag{1.61}$$

where $\eta_{\max} = \max\left(\left\{R_{E,k} : k = 1,\dots,n\right\}\right)$ and $\eta_{\min} = \min\left(\left\{R_{E,k} : k = 1,\dots,n\right\}\right)$.

$$S_{Cf} = {\left(\max\left(C_{scale}\right) - \min\left(C_{scale}\right)\right)}\big/{\left(\nu_{\max} - \nu_{\min}\right)}, \tag{1.62}$$

where $\nu_{\max} = \max\left(\left\{R_{C,k} : k = 1,\dots,n\right\}\right)$ and $\nu_{\min} = \min\left(\left\{R_{C,k} : k = 1,\dots,n\right\}\right)$.

$$S_{Df} = {\left(\max\left(C_{scale}\right) - \min\left(C_{scale}\right)\right)}\big/{\left(\mu_{\max} - \mu_{\min}\right)}, \tag{1.63}$$

where $\mu_{\max} = \max\left(\left\{R_{DC,k} : k = 1,\dots,n\right\}\right)$ and $\mu_{\min} = \min\left(\left\{R_{DC,k} : k = 1,\dots,n\right\}\right)$.

For instance, using Eq. (1.61), the S_{Ef} for the values in R_E (given in Table 19) is 39.68.

3. Map energy consumption (M_E), cost (M_C), and discomfort (M_{DC}) to C_{scale} to create a vector of preferences, rounded to the nearest integer

$$M_{E,k} = round\left(\left(R_{E,k} - \eta_{\min}\right) \times S_{Ef} + \min\left(C_{scale}\right), 0\right), \forall\, k = 1, ..., n\,. \qquad (1.64)$$

$$M_{C,k} = round\left(\left(R_{C,k} - \nu_{\min}\right) \times S_{Cf} + \min\left(C_{scale}\right), 0\right), \forall\, k = 1, ..., n\,. \qquad (1.65)$$

$$M_{DC,k} = round\left(\left(R_{DC,k} - \mu_{\min}\right) \times S_{Df} + \min\left(C_{scale}\right), 0\right), \forall\, k = 1, ..., n\,. \qquad (1.66)$$

For instance, using Eq. (1.64), mapping the values in R_E (given in Table 19) to C_{scale} resulted in $M_E = [8,8,9,7,6,1]$.

4. Find the differences between each element of M_E, M_C, and M_{DC} with respect to all other elements of the same vector. The result is an n x n matrix of the form $D_E(d_{ij})$, $D_C(d_{ij})$, and $D_{DC}(d_{ij})$. More explicitly

Let d represent a vector of mapped preferences (i.e., M_E)

$$d_{ij} = d(i) - d(j)\,,$$

and

$$D(i,j) = \begin{bmatrix} d_{11} & d_{12} & \cdots & d_{1n} \\ d_{21} & d_{22} & \cdots & d_{2n} \\ \vdots & \vdots & \ddots & \vdots \\ d_{n1} & d_{n2} & \cdots & d_{nn} \end{bmatrix},$$

where n is the number of elements in d. For instance, finding the differences between each element of vector M_E results in the matrix $D_E(d_{ij})$

$$D_E(i,j) = \begin{array}{c|cccccc} & EMCA1 & EMCA2 & EMCA3 & EMCA4 & EMCA5 & EMCA6 \\ \hline EMCA1 & 0 & 0 & -1 & 1 & 2 & 7 \\ EMCA2 & 0 & 0 & -1 & 1 & 2 & 7 \\ EMCA3 & 1 & 1 & 0 & 2 & 3 & 8 \\ EMCA4 & -1 & -1 & -2 & 0 & 1 & 6 \\ EMCA5 & -2 & -2 & -3 & -1 & 0 & 5 \\ EMCA6 & -7 & -7 & -8 & -6 & -5 & 0 \end{array}\,.$$

The first row of $D_E(1,j)$ for $j=1,2,\ldots,6$ represents the differences between the first element of M_E (8 in this case) and all other elements of M_E, including the first element itself. $D_C(d_{ij})$ and $D_{DC}(d_{ij})$ are determined in a similar manner**.**

5. In the AHP framework, no MPC can contain any values (d_{ij}) that are less than or equal to zero. Since the $D_E(i,j)$ matrix contains entries that are equal to zero, the results from step 4 needs to be modified. Let q_{ij} represent the modified entries replacing d_{ij} and let $Q(i,j)$ represent the modified matrix replacing $D(i,j)$ where

$$q_{ij} = \begin{cases} d_{ij} + 1, \text{ if } d_{ij} \geq 0 \\ d_{ij} - 1, \text{ if } d_{ij} < 0, \end{cases} \tag{1.67}$$

the new matrix is

$$Q(i, j) = \begin{bmatrix} q_{11} & q_{12} & \cdots & q_{1n} \\ q_{21} & q_{22} & \cdots & q_{2n} \\ \vdots & \vdots & \vdots\vdots\vdots & \vdots \\ q_{n1} & q_{n2} & \cdots & q_{nn} \end{bmatrix},$$

and $D_E(i,j)$ becomes

$$Q_E(i, j) = \begin{array}{c|cccccc} & EMCA1 & EMCA2 & EMCA3 & EMCA4 & EMCA5 & EMCA6 \\ EMCA1 & 1 & 1 & -2 & 2 & 3 & 8 \\ EMCA2 & 1 & 1 & -2 & 2 & 3 & 8 \\ EMCA3 & 2 & 2 & 1 & 3 & 4 & 9 \\ EMCA4 & -2 & -2 & -3 & 1 & 2 & 7 \\ EMCA5 & -3 & -3 & -4 & -2 & 1 & 6 \\ EMCA6 & -8 & -8 & -9 & -7 & -6 & 1 \end{array}.$$

$Q(i,j)$ still contains entries q_{ij} that are less than zero and converting it to MPC requires a few additional modifications. Let f_{ij} represent the modified entries replacing q_{ij} and $F(i,j)$ replacing $Q(i,j)$, then

$$f_{ij} = \begin{cases} q_{ij}, \text{ if } q_{ij} > 0 \\ \dfrac{1}{|q_{ij}|}, \text{ if } q_{ij} < 0, \end{cases} \tag{1.68}$$

the new matrix is

$$F(i, j) = \begin{bmatrix} f_{11} & f_{12} & \cdots & f_{1n} \\ f_{21} & f_{22} & \cdots & f_{2n} \\ \vdots & \vdots & \vdots\vdots\vdots & \vdots \\ f_{n1} & f_{n2} & \cdots & f_{nn} \end{bmatrix},$$

and $Q_E(i,j)$ becomes

$$F_E(i,j) = \begin{array}{c|cccccc} & EMCA1 & EMCA2 & EMCA3 & EMCA4 & EMCA5 & EMCA6 \\ EMCA1 & 1.0000 & 1.0000 & 0.5000 & 2.0000 & 3.0000 & 8.0000 \\ EMCA2 & 1.0000 & 1.0000 & 0.5000 & 2.0000 & 3.0000 & 8.0000 \\ EMCA3 & 2.0000 & 2.0000 & 1.0000 & 3.0000 & 4.0000 & 9.0000 \\ EMCA4 & 0.5000 & 0.5000 & 0.3333 & 1.0000 & 2.0000 & 7.0000 \\ EMCA5 & 0.3333 & 0.3333 & 0.2500 & 0.5000 & 1.0000 & 6.0000 \\ EMCA6 & 0.1250 & 0.1250 & 0.1111 & 0.1429 & 0.1667 & 1.0000 \end{array}.$$

F(i,j) is an MPC that satisfies *Rule 1* and *Rule 2* described in Section 2 and reflects the derived objective judgments obtained from the performance data documented in the Performance Table for each alternative residential EMCA with respect to the energy, cost, and comfort criteria. Applying AHP's standard eigenvector and eigenvalue methods to *F(i,j)*, the relative priorities for each alternative with respect to the criteria, as well as consistency metrics *CI* and *CR*, are computed. For instance, the relative priorities of residential EMCAs with respect to the energy criterion, using $F_E(i,j)$, is given in Table 20.

Table 20. Priorities and Consistency Metrics

Residential EMCAs	**Priorities with respect to energy criterion and consistency metrics**	
1	0.21	Priorities
2	0.21	
3	0.34	
4	0.13	
5	0.08	
6	0.02	
λ_{max}	6.15	Consistency
CI	0.03	
CR	0.03	

In Table 20, residential EMCA3 has the highest priority with respect to the energy criterion compared to other alternatives, which is consistent with our assumption that less energy consumption is more desirable. The *CR* value of 3 % is less than the recommended consistency of 10 %, suggesting that the judgments for comparing alternatives are consistent.

5.7. Overall Scores

Having computed priorities of criteria with respect to the goal (*wg*) and priorities of each alternative with respect to criteria (p_a), the overall score for each alternative with respect to the goal is computed by Eq. (1.47). Recall that the priorities of criteria with respect to the goal along with consistency metrics were given in Table 14. The priorities (p_a) for each alternative with respect to the criteria for residential EMCAs and the consistency metrics are given in Table 21. For example, priorities of residential EMCA1 with respect to the energy, cost, and comfort criteria are $p_a = [0.21, 0.18, 0.12]$.

Table 21. Priorities and Consistency Metrics

Residential EMCAs and consistency metrics	Energy	Cost	Comfort	
1	0.21	0.18	0.12	Priorities
2	0.21	0.18	0.06	
3	0.34	0.42	0.06	
4	0.13	0.11	0.06	
5	0.08	0.08	0.63	
6	0.02	0.03	0.06	
λ_{max}	6.15	6.20	6.04	Consistency
CI	0.03	0.04	0.01	
CR	0.03	0.03	0.01	

The overall scores for residential EMCAs with respect to the goal are calculated using Eq. (1.47) and shown in Table 22.

Table 22. The Overall Scores

Residential EMCAs	Overall scores (ranking)
1	0.17
2	0.15
3	0.31
4	0.10
5	0.23
6	0.04

Based on the overall scores in Table 22, residential EMCA3 is the most desirable alternative with respect to the overall goal reflecting user's very strong preference in an alternative EMCA that saves the most money (lowest cost) followed by a strong desire for comfort over energy savings, and weak preference for comfort over cost. The relationship between alternatives, criteria, and the goal are shown in Figure 42. It shows the problem hierarchy, an example of computed priorities for two residential EMCAs, and the overall scores (ranking) for all residential EMCAs.

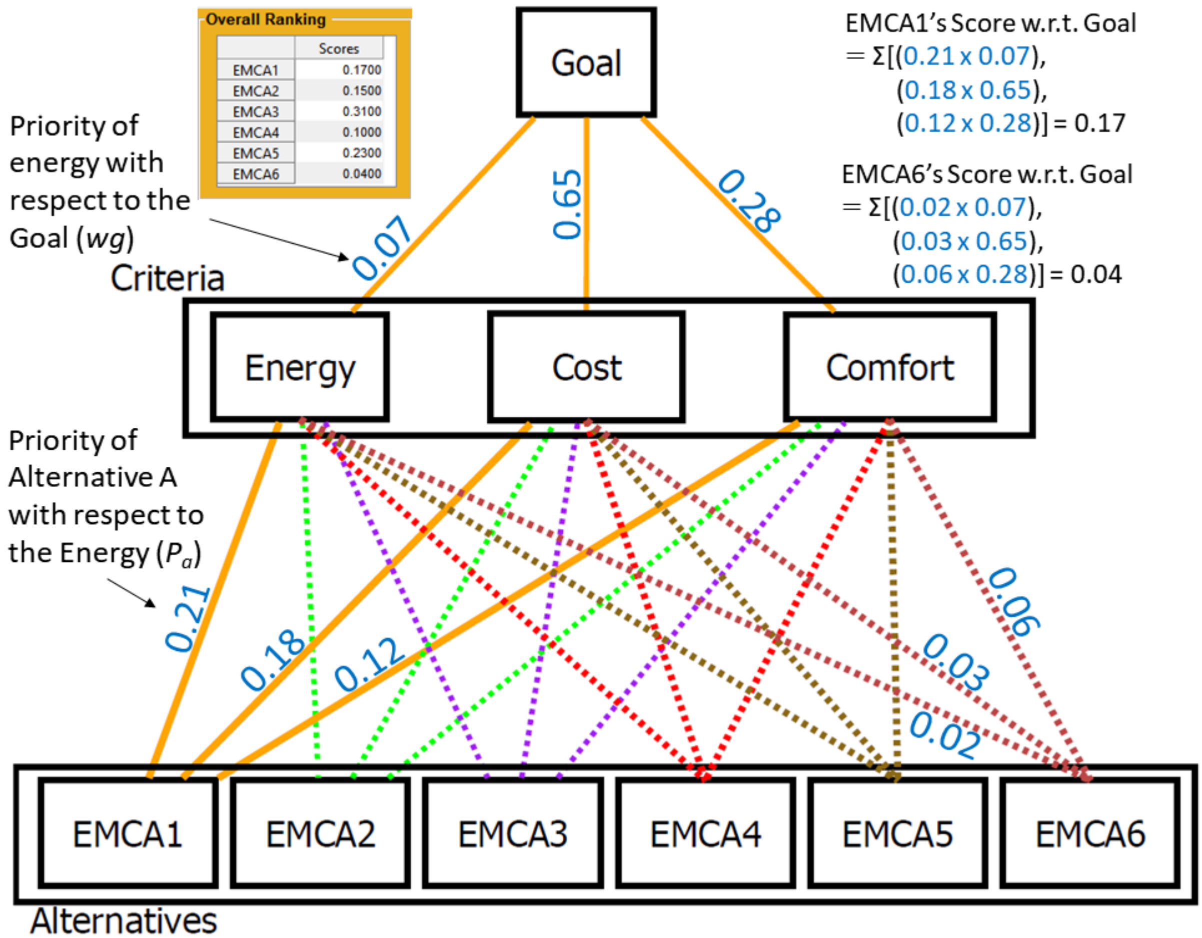

Figure 42. Summary figure showing the problem hierarchy, priorities and the overall scores for each alternative with respect to the goal

As previously mentioned, based on the performance data and user preferences, residential EMCA3 was ranked the highest by the AE. Depending on user preferences, a different algorithm other than residential EMCA3 can be ranked the highest by the AE. Recall that user preferences can only impact priorities of criteria with respect to the goal. For example, a user conveys a very strong desire in an alternative that provides the most comfort over cost, a strong preference for comfort over energy consumption, but a weak preference for energy consumption over cost. These preferences are captured by the AE in inputs fields of Figure 39 as following:

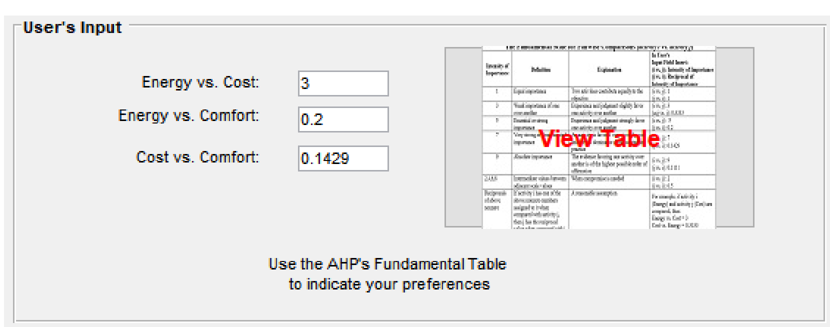

The AE forms the corresponding MPC for pairwise comparisons between criteria as shown in Table 23. It also calculates priorities for criteria with respect to the goal and the overall scores based on the new priorities.

Table 23. **MPC for Capturing User Preferences**

	Energy	**Cost**	**Comfort**
Energy	1	3	0.2
Cost	0.3333	1	0.1429
Comfort	5	7	1

The *CR* value of 5.6 % suggests that the user's judgments in Table 23 were consistent and the overall scores for residential EMCAs with respect to the goal are given in Table 24.

Table 24. The Overall Scores

Residential EMCAs	**Overall scores (ranking)**
1	0.14
2	0.10
3	0.14
4	0.08
5	0.48
6	0.05

The overall scores in Table 24 show that residential EMCA5 is the most desirable alternative. Residential EMCA5 is the top-ranked because it offers the best comfort among alternatives.

5.8. Limitations

Even though the AHP's theoretical foundations has been subject of debate in the literature [45], [55], it is the most widely used [46], [56] approach for solving practical multi-criteria decision making problems. Therefore, AHP was chosen for this study to develop the AE. Application of the AE requires hourly energy consumption data from HVAC equipment and the hourly price of electricity for computing the cost. It also requires one-minute sampling of indoor air temperature, mean radiant temperature, relative humidity, and an occupancy schedule. In the current study, to calculate PPD_{wc} the mean radiant temperature was assumed to be the same as the indoor air temperature. This assumption may not be valid for residential homes where the indoor temperatures are significantly impacted by direct solar radiation. Additionally, the current implementation of the AE only considers a three-level hierarchy (goal, criteria, and alternatives), while AHP provides a much more flexible framework for incorporating additional levels, criteria, and sub-hierarchies. The scope of this study was limited to three criteria and six residential EMCAs.

The algorithm used to derive priorities from the simulation performance data normalized the values for Energy, Cost, and Comfort with respect to the maximum value. This choice was arbitrary. Other possible choices for normalization could include the minimum, mean, or median value. It has been shown that, for some data sets, the approach used for normalization can affect the ranking [45].

Chapter 6

6. Conclusion and Future Work

6.1. Conclusion

For homes to become active participants in a smart grid, intelligent control algorithms are needed to facilitate autonomous interactions that take homeowner preferences into consideration. The objective of this dissertation was to develop an assessment tool that can rank the performance of these control algorithms, using a user's subjective preferences and objective performance data, representing energy consumption, cost, and comfort. It was established that a comprehensive assessment framework was needed to evaluate the performance of these algorithms by providing a figure of merit that enables policy makers, customers, and other stakeholders to make an informed decision by choosing a residential control algorithm that satisfied their need. Until now, it was not known if an effective comparison (ranking) between the residential control algorithms can be performed.

The key to a successful completion of this research was the design and implementation of the simulation manager and the assessment engine. The simulation manager facilitated the loosely-coupled integration of residential energy management control algorithms with the TRNSYS based residential simulation model. This loosely-coupled architecture provided an efficient mechanism for evaluating different types of residential energy management control algorithms without changing the core functionality of the simulation manager. The communication between the residential simulation model and other components of the simulation manager was established through a newly developed TRNSYS type (Type277). Type277 is written in C++ and compiled as a 32-bit Windows dynamic link library. To ensure a reliable exchange of information between the residential simulation model and other components of the simulation manager, the data is serialized using Google's protocol buffers. The key idea behind this approach was to enable a TRNSYS based simulation model to communicate with other applications that are likely to be written in different software languages. Since the data is serialized with Google's protocol buffers, Type277 enables a TRNSYS based simulation model to directly communicate with Java, C++, Python, and many more languages that are supported by the protocol buffers and indirectly with any software environment that communicates with these languages. The assessment engine was developed to rank the performance of residential energy management control algorithms using subjective judgements for pairwise comparisons of energy consumption, cost, and comfort criteria; and objective performance data for pairwise comparisons of residential EMCAs. This is a multi-criteria decision-making problem that required both qualitative and quantitative analyses. The AHP framework was used to solve this problem because it is a widely used framework for solving multi-criteria decision-making problems.

Testing and validation of the assessment engine was illustrated by applying the assessment process to six residential energy management control algorithms. The control algorithms were developed and tested using a simulation model of the Net-Zero Energy Residential Test Facility located on the campus of the National Institute of Standards and Technology in Gaithersburg, MD. Residential EMCA5 was designed to match a real heat pump controller used in the house model. Residential EMCA6 was the same as the first with relaxed comfort deadbands. Residential EMCA1 to residential EMCA4 used linear integer optimization with varying optimization objectives to generate forecasted heat pump control actions by utilizing the control optimization framework. The control optimization framework used three main components a default controller, a learning algorithm, and an optimization algorithm. The default controller was designed to maintain the indoor temperature close to the heating and cooling setpoints. The learning algorithm is a sliding-window algorithm that was designed to forecast the next day's indoor temperature using a first order lumped capacitance model. It was formulated in such a way that key design details of a residential house such as window size and configuration, thermal insulation, and airtightness that effect heat loss and solar heat gain were combined into effective parameters that could be learned from observation. The sliding-window of learning data accounted for both seasonal variations in the sun position and daily cloud cover fluctuations. The optimization algorithms used a common structure to solve both single and multi-objective optimization problems, utilizing heat pump power and capacity, an indoor temperature forecasting model, an objective function and constraints, and a linear integer programming solver to obtain forecasted heat pump control actions for a given horizon. The algorithms were compared by analyzing their performance over a year based on energy consumption, cost, and comfort as measured by predicted mean vote and predicted percentage of dissatisfied. Successful implementation of the assessment framework produced a figure of merit, which can be used to compare the performance of residential energy management control algorithms.

As discussed earlier in this dissertation, successful implementation of the assessment framework resulted in an assessment engine that can rank the performance residential energy management control algorithm. The assessment engine utilized a flexible hybrid mechanism based on the Analytical Hierarchy Process that derives a ranking from a combination of subjective user inputs representing preferences, and objective data from algorithms' performance related to energy consumption, cost and comfort. Such an assessment engine is a significant contribution for evaluating the performance of control algorithms, as it provides policy makers, homeowners, control algorithm engineers, and other stakeholder an efficient mechanism to evaluate the impact of new and existing smart grid ready residential energy management control technologies. By utilizing the Analytical Hierarchy Process to provide a single overall score the assessment engine delivers an effective mechanism for directly comparing alternative residential energy management control algorithms and rank them effectively.

6.2. Future Work

Application of the assessment framework was successfully demonstrated to rank EMCAs in single-family homes. Further research is needed to verify that the assessment framework is broadly applicable to evaluate the performance of EMCAs used in small commercial and residential buildings. The main idea is to explore the possibility of establishing a test procedure for evaluating these control algorithms. The objective of the test procedure is to provide unbiased information for stakeholders, policy makers, and consumers to make informed decisions, and ultimately lead to an industry run certification program. The certification program can help consumers in differentiating among available options and choosing an EMCA that meets their need. The test procedure realization involves exploring the following research topics:

1. Developing a test platform that is capable of interfacing real-time control hardware with a building simulation model;
2. Developing short-term test procedures that are applicable for long-term evaluation of these control algorithms; and
3. Developing metrics for assessing the consistency and reliability of the test procedures.

Furthermore, with the proliferation of distributed energy resources i.e., photovoltaics, buildings are expected to actively participate in the smart electric grid operation at the distribution level. Buildings can participate in the grid operation by provide ancillary services such as frequency response, real and reactive power consumption and supply, and voltage control. The key challenge facing the utilities and customers is the evaluation and verification of these services rendered to the grid. Further research is needed to investigate if the assessment framework, presented in this study, is also applicable for this application.

Appendix A

The aim of developing residential EMCAs was to control a residential heat pump, generating a set of performance data for testing and validating the AE. Each control algorithm was integrated and tested over the course of one year using a simulation model of the NZERTF. Using the performance data (i.e., power consumption and indoor temperature for each residential EMCA) the following key performance metrics are computed:

1. Total energy consumption, using Eq. (1.48);
2. Total cost of consuming energy, using Eq. (1.49); and
3. Thermal discomfort of the occupants, using Eq. (1.55).

The results for the annual total energy consumption, cost of total energy consumption, and discomfort for all EMCAs were reported in Table 18. In addition, the annual energy consumption across different operating modes of the heat pump, for all EMCAs, are also computed, given in Table 25.

Table 25. Annual Energy Consumption across Different Operating Modes of the Heat Pump with Respect to EMCAs

Residential EMCAs	3rd Stage [kWh]	Defrost Cycle [kWh]	1st and 2nd Stages of the Heat Pump in Heating Season [kWh]	Standby [kWh]	Dehumidification [kWh]	1st and 2nd Stages of the Heating Pump in Cooling Season [kWh]
1	34	323	2340	282	1322	1305
2	14	333	2452	278	1273	1238
3	3	283	2320	291	1261	1326
4	125	289	2288	284	1354	1421
5	405	356	2326	261	1287	1247
6	1538	269	1858	286	1295	1343

The annual energy consumption across different operating modes of the heat pump for the original simulation model of the NZERTF is given in Table 26.

Table 26. Annual Energy Consumption across Different Operating Modes of the Heat Pump with Respect to the Original Simulation Model of the NZERTF

Original Simulation Model	3rd Stage [kWh]	Defrost Cycle [kWh]	1st and 2nd Stages of the Heat Pump in Heating Season [kWh]	Standby [kWh]	Dehumidification [kWh]	1st and 2nd Stages of the Heating Pump in Cooling Season [kWh]
NZERTF	430	364	2471	255	1478	1193

To better quantify the performance of residential EMCAs reported in Table 18, the data for each residential EMCA is compared with respect to the original simulation model of the NZERTF. The total energy consumption of the original simulation model was 6190.4 kWh, the total cost of consuming energy was \$ 984.3, and total discomfort index was 297.2 h. A summary of this comparison is given in Table 27.

Table 27. Annual Performance Comparisons of Residential EMCAs and the Original Simulation Model

Residential EMCAs	Different in Annual Energy Consumption [%]	Difference in Annual Cost of Energy Consumption [%]	Difference in Annual Discomfort Index [%]
1	-9	-8	-97
2	-10	-11	14
3	-11	-14	296
4	-7	-7	-25
5	-5	-5	-100
6	6	7	-88

As can be seen in Table 27, using residential EMCA1 through residential EMCA5 resulted in energy and cost savings with varying degrees of thermal discomfort. Residential EMCA6, however, used more electrical energy, resulting in a 7 % higher cost but 88 % better thermal comfort compared to the original simulation model. All residential EMCAs improved thermal comfort except residential EMCA2 and residential EMCA3. Residential EMCA3 achieved the highest energy and cost savings, but at a greater discomfort to the occupants.

Similarly, to better quantify the performance of residential EMCAs across different operating modes of the heat pump, the annual energy consumptions reported in **Table** 25 is compared with respect to the annual energy consumption of the original simulation model reported in **Table** 26. The results of these comparisons are reported in **Figure** 43. For clarity, the ratios for the 3rd Stage are plotted on the secondary axis.

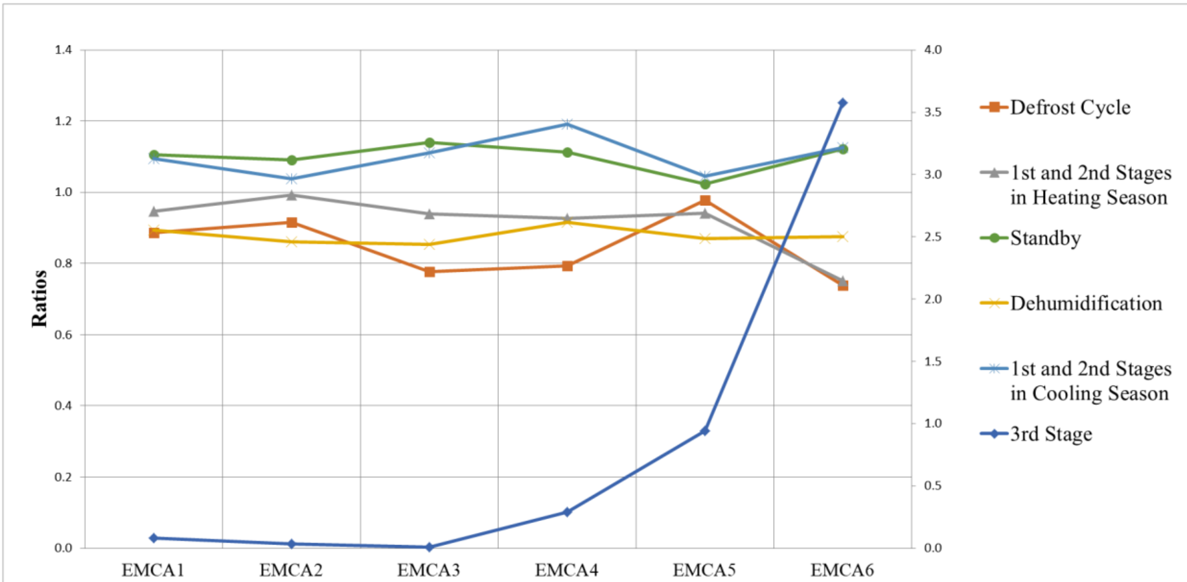

Figure 43. Ratios of residential EMCAs across different operating modes of the heat pump

As can be seen from Figure 43, all residential EMCAs resulted in lower energy consumption while operating in Defrost Cycle and Dehumidification modes. In the heating season, all residential EMCAs, except residential EMCA2 which consumed the same amount of energy as the original model, resulted in modest energy savings while the heat pump operated in the 1st and 2nd Stages. For all residential EMCAs, the energy consumption in the Standby mode slightly increased because the heat pump ran fewer minutes compared to the original simulation model. In the cooling season, all residential EMCAs resulted in modest energy increase while the heat pump operated in the 1st and 2nd Stages. Residential EMCA1 through residential EMCA4 resulted in a considerable reduction in energy consumption of the 3rd Stage. Meanwhile residential EMCA5 resulted in modest energy savings while operating in the 3rd Stage. In contrast, the energy consumption associated with the 3rd Stage of the residential EMCA6 significant increased compared to the original simulation model.

Further comparisons, with respect to the thermal performance as measured by the PMV and PPD metrics and indoor temperature, are also made between residential EMCAs and the original simulation model. The results of these comparisons are presented in Appendix B through Appendix G.

Appendix B

Residential EMCA1

The mathematical description of residential EMCA1 was given in Sec. 4.2.1.3.1.

Thermal Performance

The annual comparison of T_{ind} profiles of residential EMCA1 and the original simulation model is shown in Figure 44. In both heating and cooling seasons, T_{ind} is tightly controlled by the original simulation model based on the deadbands of the differential controllers given in Table 6. There are minor deviations from the setpoints in both heating and cooling seasons, but larger fluctuations during the shoulder seasons. The indoor temperature fluctuation during the shoulder seasons are due to the deadbands of the differential controllers as it switches between heating and cooling seasons. Residential EMCA1 shows slightly larger deviations in T_{ind} from the setpoints because it uses wider deadbands.

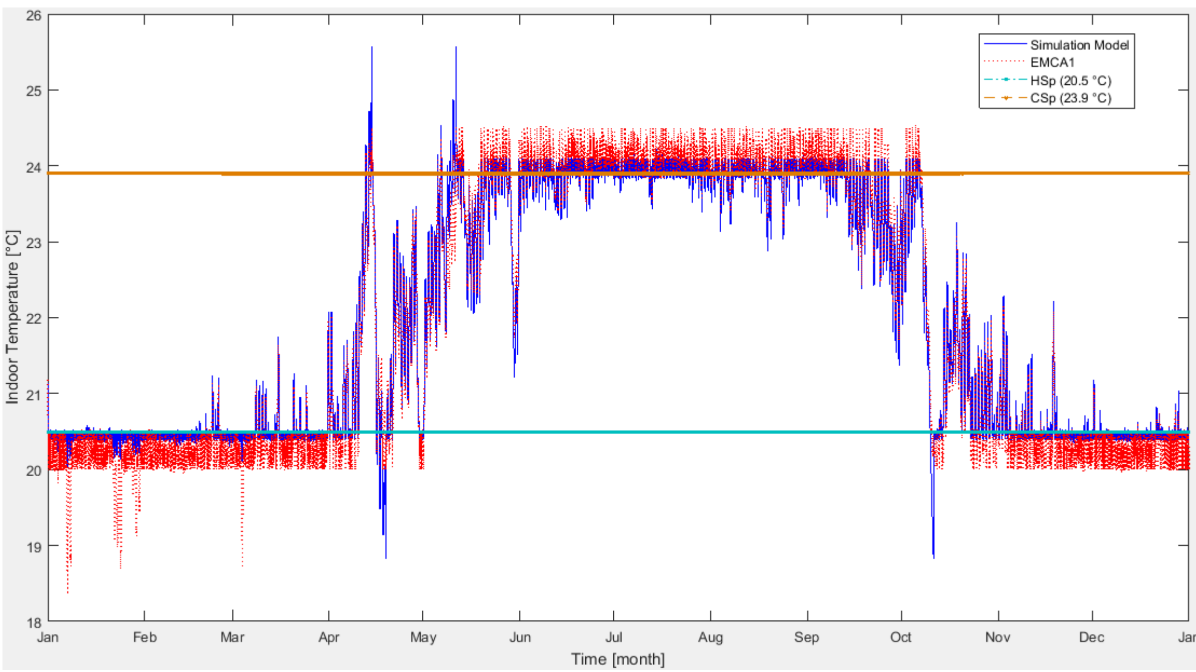

Figure 44. Residential EMCA1 – annual comparison of T_{ind} with the NZERTF original simulation model

The optimization solver is trying to minimize the objective function of residential EMCA1 given in Eq. (1.37) such that the forecasted T_{ind} given by Eq. (1.34) and Eq. (1.36) are maintained within the constraints of the problem. Figure 45 shows that the forecasted T_{ind} closely matches the original simulation values, albeit with minor deviations from the heating and cooling setpoints. In comparison, the temperature response of the simulation model to the forecasted control actions shows slightly larger deviations from heating and cooling setpoints.

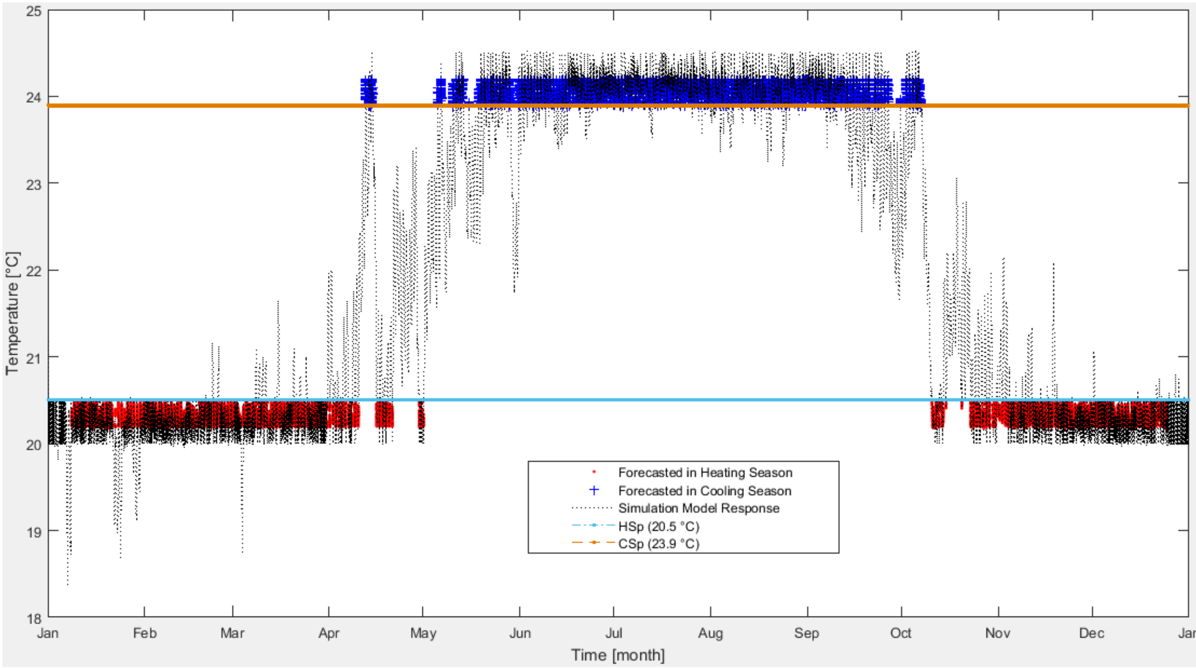

Figure 45. Residential EMCA1 - annual comparison between the forecasted and simulated T_{ind}

To better quantify the differences between the forecasted and simulated T_{ind} in residential EMCA1, Figure 46 shows the resulting % RMSE in both heating and cooling seasons. The behavior, limitation, and capability of the learning algorithm used for forecasting T_{ind} in residential EMCA1 was previously described in Sec. 3.

Over the course of one year, residential EMCA1 was expected to run 16 848 times based on its forecast horizon. As can be seen from Figure 46, only 44 % of the time, the optimization solver generated control actions and forecasted T_{ind}. This is because the on-time, off-time, upper, and lower bound constraints for residential EMCA1 are strict, which collectively increases the chance that the optimization solver cannot find a feasible solution to satisfy all constraints.

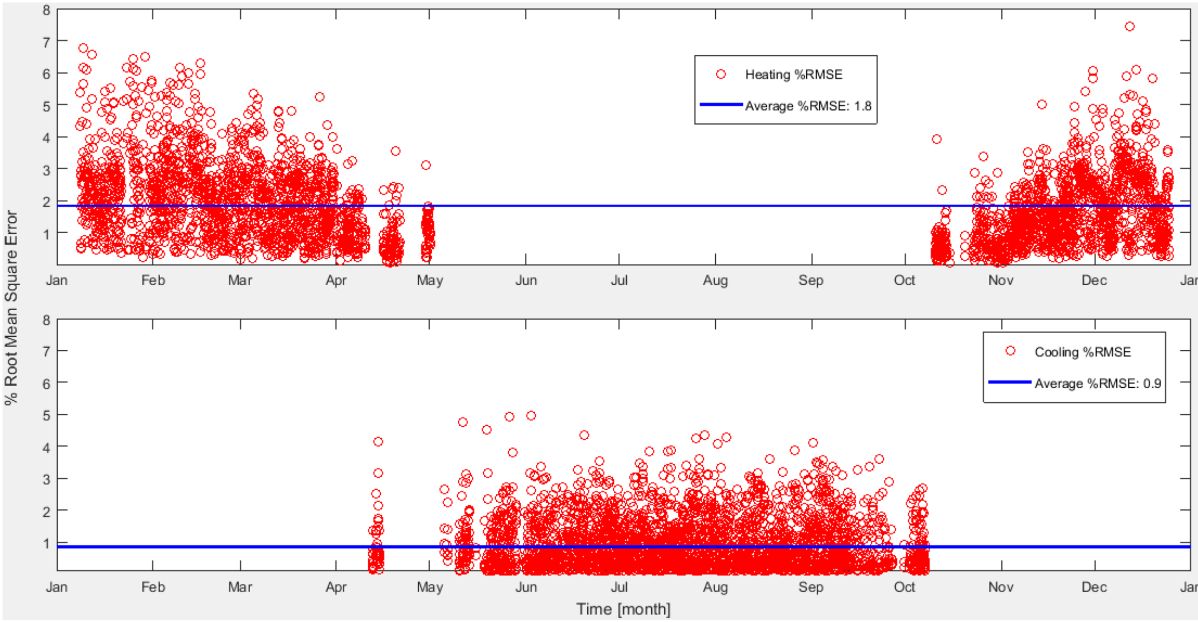

Figure 46. Residential EMCA1 - the % RMSE between forecasted and simulated T_{ind}

Furthermore, the thermal performance of residential EMCA1, as measured by PMV and PPD, was calculated. Figure 47 shows the annual comparisons of PMV between residential EMCA1 and the original simulation model of the NZERTF. The PMV corresponding to the original simulation model transitions between slightly warm and slightly cool temperature during the shoulder seasons, but it remains within the recommend thermal range of +0.5 and -0.5 in other times. In comparison, the PMV associated with residential EMCA1 remains within the recommended range during the shoulder season but oscillates around the upper recommended limit of + 0.5. In other words, the occupants are feeling slightly warmer than the original simulation model. In a few instances, the PMV index associated with residential EMCA1 is lower than the recommended comfort limit of -0.5, suggesting that the occupants feel slightly colder than the original simulation model. In general, it can be concluded that the occupants were comfortable throughout the simulation year except for 9 h (Table 18).

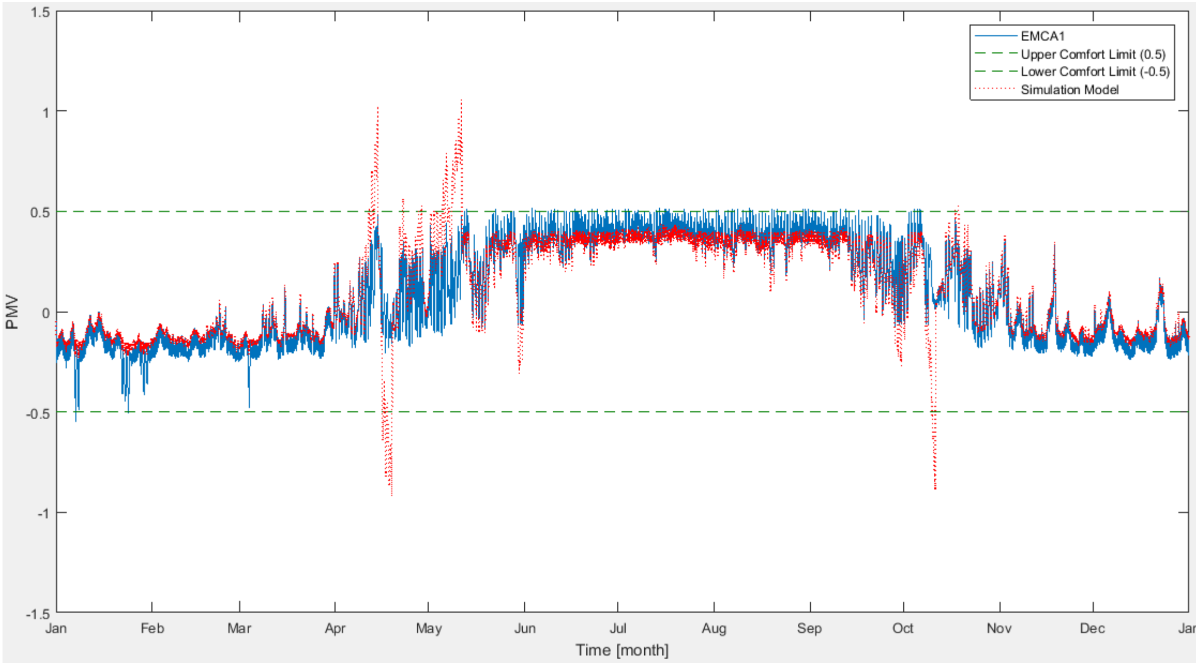

Figure 47. Residential EMCA1 – comparison of annual PMV with the NZERTF original simulation model

Similarly, Figure 48 shows the annual comparison of PPD between residential EMCA1 and the original simulation model. According to ANSI/ASHRAE Standard 55, PPD of less than 10 % are considered comfortable conditions. The PPD corresponding to the original simulation model suggest that a large percentage of the occupants were uncomfortable during the shoulder seasons, but for a shorter time. In comparison, the PPD corresponding to the residential EMCA1 suggest that fewer occupants were uncomfortable in the cooling season but for a longer time. Thermal comfort is mainly impacted in the cooling season. The occupants are generally comfortable in the heating season. Note that the lowest value of PPD is 5 %, suggesting that five percent of the occupants will always feel uncomfortable regardless.

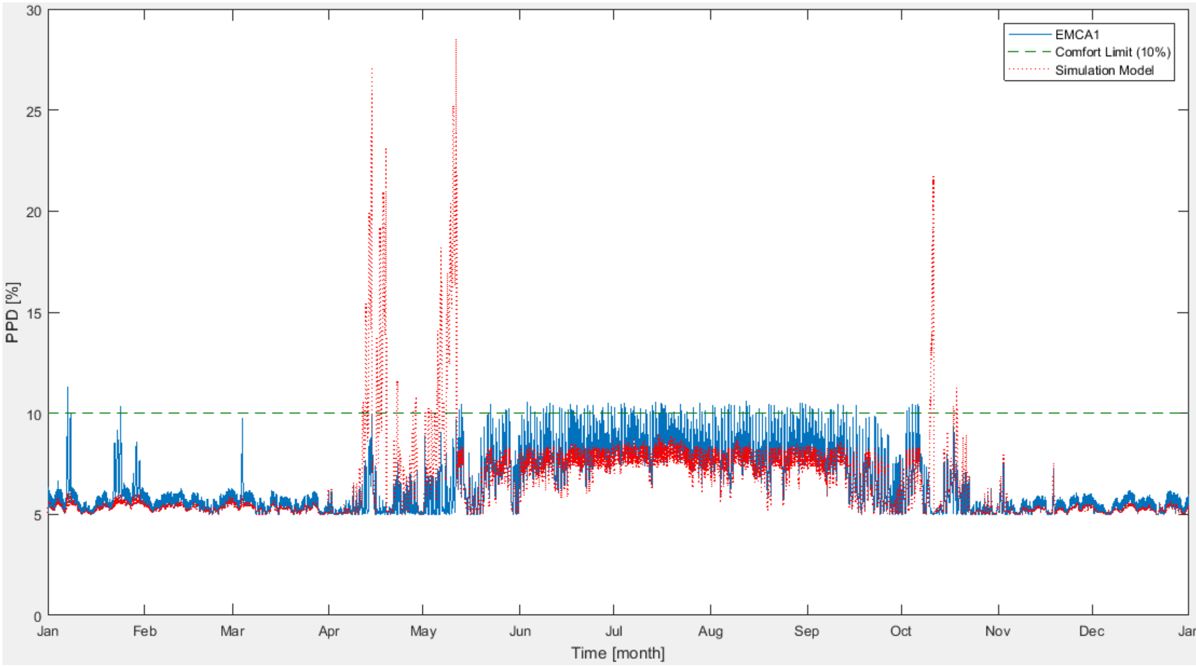

Figure 48. Residential EMCA1 - comparison of annual PPD with the NZERTF original simulation model

Appendix C

Residential EMCA2

The mathematical description of the residential EMCA2 for minimizing the cost of operating the heat pump was presented in Section 4.2.1.3.2. A forecast horizon of one day was chosen for this algorithm to take advantage of the full range of variability in the structure of the RTP tariff. Since the optimization problem is defined over one day, it is computationally difficult for the optimization solver to forecast heat pump control actions for each simulation time step in a reasonable amount of time. Therefore, the forecast horizon was divided into 60 bins, each bin holding 24 min of data. Average values of all forecasted variables in each bin was computed and used as a representative sample. This effectively reduced the forecast horizon to 60 min, which is computationally less time consuming. Since the new forecast horizon is 60 min, the output of the optimization solver is also a vector of length sixty. Each element of the vector represents 24 forecasted control actions. For example, if the 2^{nd} Stage is given as the first element of the output vector, then the heat pump is operated in the 2^{nd} Stage for the next 24 min.

Thermal Performance

The annual comparison of T_{ind} profiles of residential EMCA2 and the original simulation model is shown in Figure 49. In both heating and cooling seasons, T_{ind} is tightly controlled by the original simulation model based on the deadbands of the differential controllers given in Table 6. There are minor deviations from the setpoints in both heating and cooling seasons, but larger variations during the shoulder seasons. The indoor temperature fluctuations during the shoulder seasons are due to the deadbands of the differential controllers as it switches between heating and cooling seasons. Residential EMCA2 shows slightly larger deviations in T_{ind} from the setpoints because it uses wider deadbands. Also, the variation in indoor temperature is affected by repeating the same control action for 24 consecutive simulation steps.

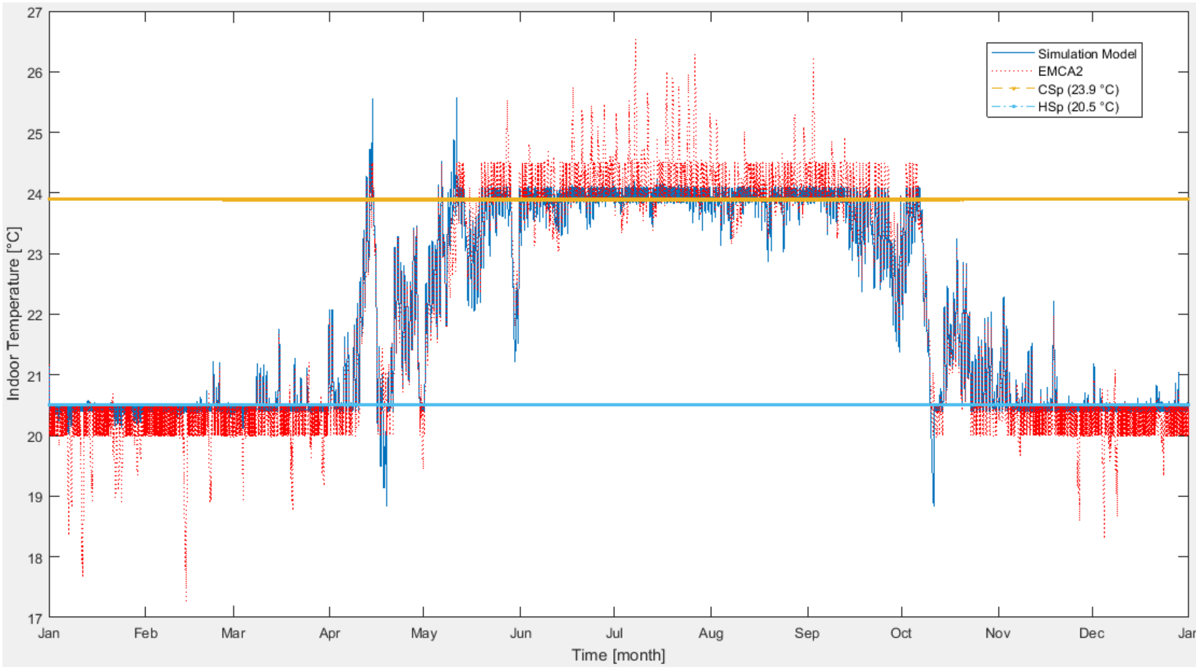

Figure 49. Residential EMCA2 - annual comparison of T_{ind} with the NZERTF original simulation model

The optimization solver is trying to minimize the objective function of residential EMCA2 given in Eq. (1.42) such that the forecasted T_{ind} given by Eq. (1.34) and Eq. (1.36) are maintained within the constraints of the problem. Figure 50 shows that the forecasted T_{ind} closely matches the original simulation values, albeit with minor deviations from the heating and cooling setpoints. In comparison, the temperature response of the simulation model to the forecasted control actions shows more frequent and larger deviations from heating and cooling setpoints.

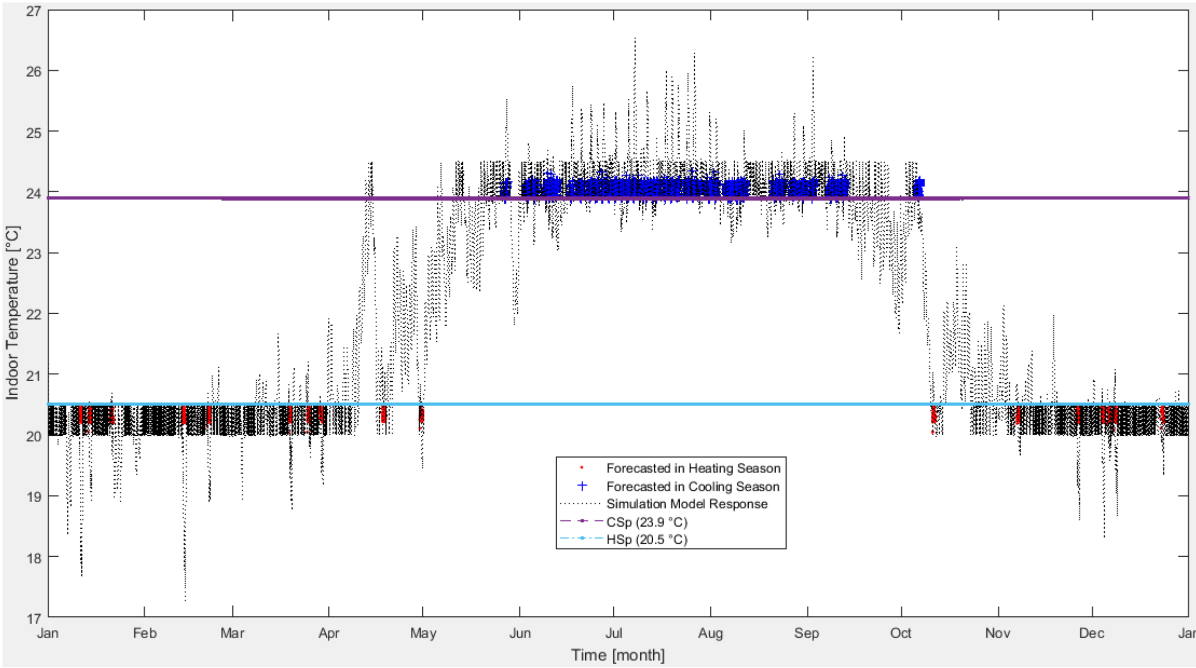

Figure 50. Residential EMCA2 - annual comparison between the forecasted and simulated T_{ind}

To better quantify the differences between the forecasted and simulated T_{ind} in residential EMCA2, Figure 51 shows the resulting % RMSE in both heating and cooling seasons. The behavior, limitation, and capability of the learning algorithm used for forecasting T_{ind} in residential EMCA2 was previously described in Sec. 3.

Over the course of one year, residential EMCA2 was expected to run 351 times based on its forecast horizon. As can be seen from Figure 51, only 17 % of the time, the optimization solver generated control actions and forecasted T_{ind}. This is because the forecast horizon for residential EMCA2 is 1440 min and the upper and lower bound constraints are stringent. Having a long forecast horizon introduces extended delays in providing feedback to the optimization solver. Due to this delay, residual errors in forecasting are accumulated over time, amounting to much larger deviations in the simulated T_{ind} and fewer solutions that can satisfy all constraints.

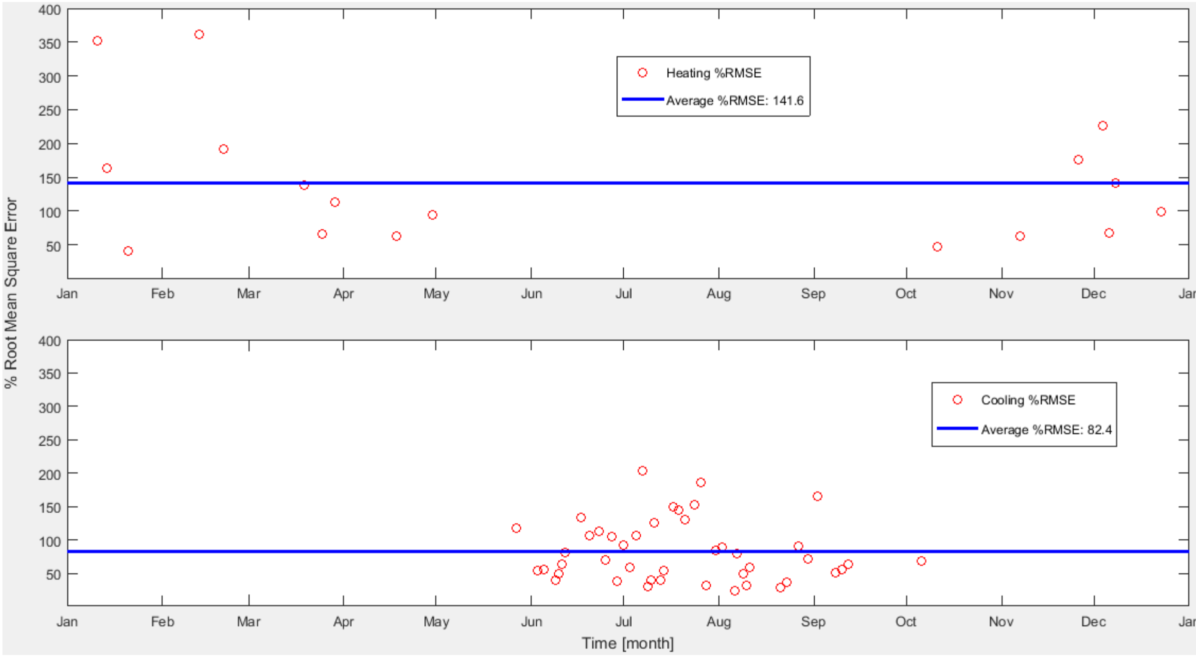

Figure 51. Residential EMCA2 - the % RMSE between forecasted and simulated T_{ind}

Furthermore, the thermal performance of residential EMCA2, as measured by PMV and PPD, was calculated. Figure 52 shows an annual comparison of PMV between residential EMCA2 and the original simulation model of the NZERTF. The PMV corresponding to the original simulation model transitions between slightly warm and slightly cool temperature during the shoulder seasons, but it remains within the recommend thermal range of +0.5 and -0.5 in other times. In comparison, the PMV associated with residential EMCA2 remains within the recommended range during the shoulder season but oscillates around the comfort limits, especially in the cooling season. In the cooling season, the occupants generally feel warmer and even uncomfortable in few instances compared to the original simulation model. In a few instances, the PMV index associated with residential EMCA2 is lower than the recommended comfort limit of -0.5, suggesting that the occupants feel slightly colder than the original simulation model. In general, it can be concluded that the occupants were comfortable throughout the simulation year except for 339 h (Table 18). This is a noteworthy increase in discomfort compared to residential EMCA1, suggesting that thermal comfort was sacrificed for more cost savings.

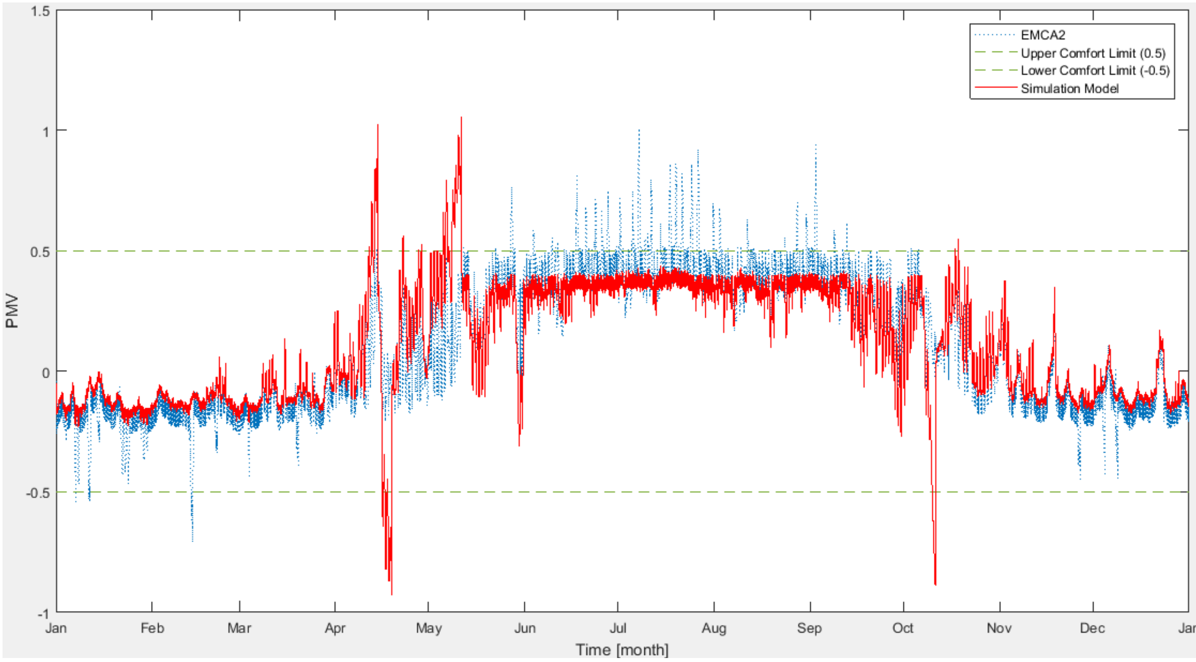

Figure 52. Residential EMCA2 - comparison of annual PMV with the NZERTF original simulation model

Similarly, Figure 53 shows the annual comparison of PPD between residential EMCA2 and the original simulation model. The PPD corresponding to the original simulation model suggest that a large percentage of the occupants were uncomfortable during the shoulder seasons but for a shorter period. In comparison, the PPD corresponding to the residential EMCA2 suggest that fewer occupants are uncomfortable in cooling season but for a longer period. Thermal comfort is mainly impacted in the cooling season. The occupants are generally comfortable in the heating season.

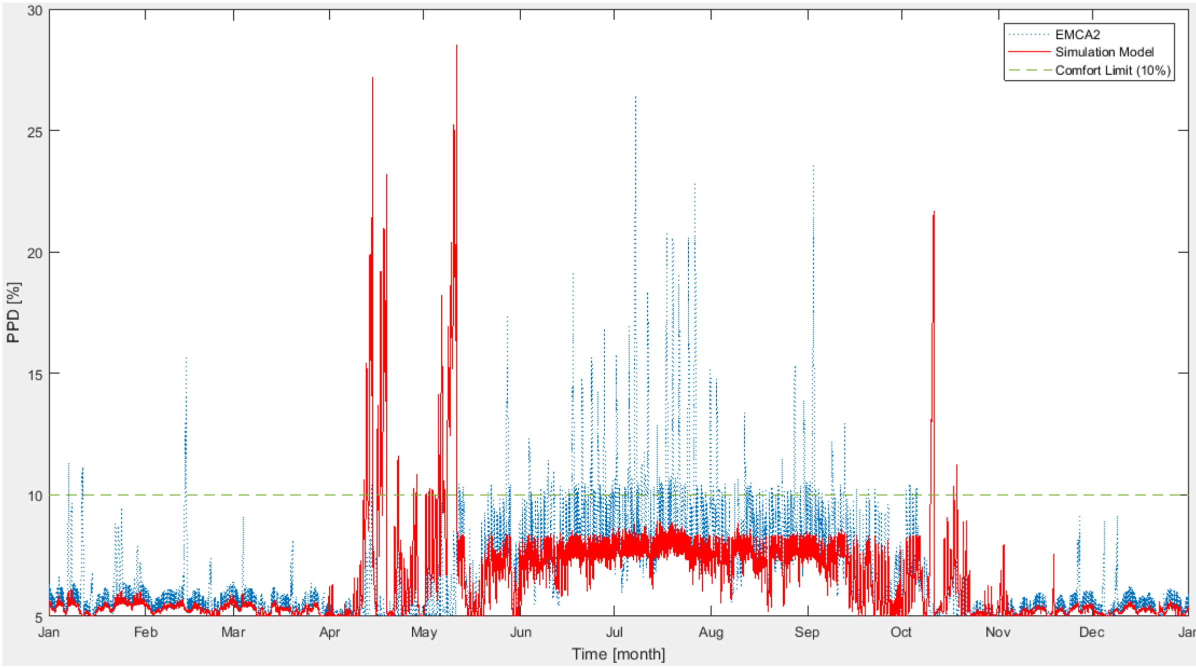

Figure 53. Residential EMCA2 - comparison of annual PPD with the NZERTF original simulation model

Minimizing Cost

As previously mentioned, the objective of residential EMCA2 is to minimize the cost of consuming energy. One way to accomplish this task is by shifting the operation of the heat pump from peak price of electricity to off-peak times, resulting in a lower cost. The following two examples highlight the behavior of residential EMCA2. Figure 54 shows a comparison between forecasted and simulated T_{ind} plotted with respect to the left axis, and heat pump power consumption and RTP tariff plotted with respect to right axis. The highest RTP peaks occurred in July (Figure 40) during the cooling season.

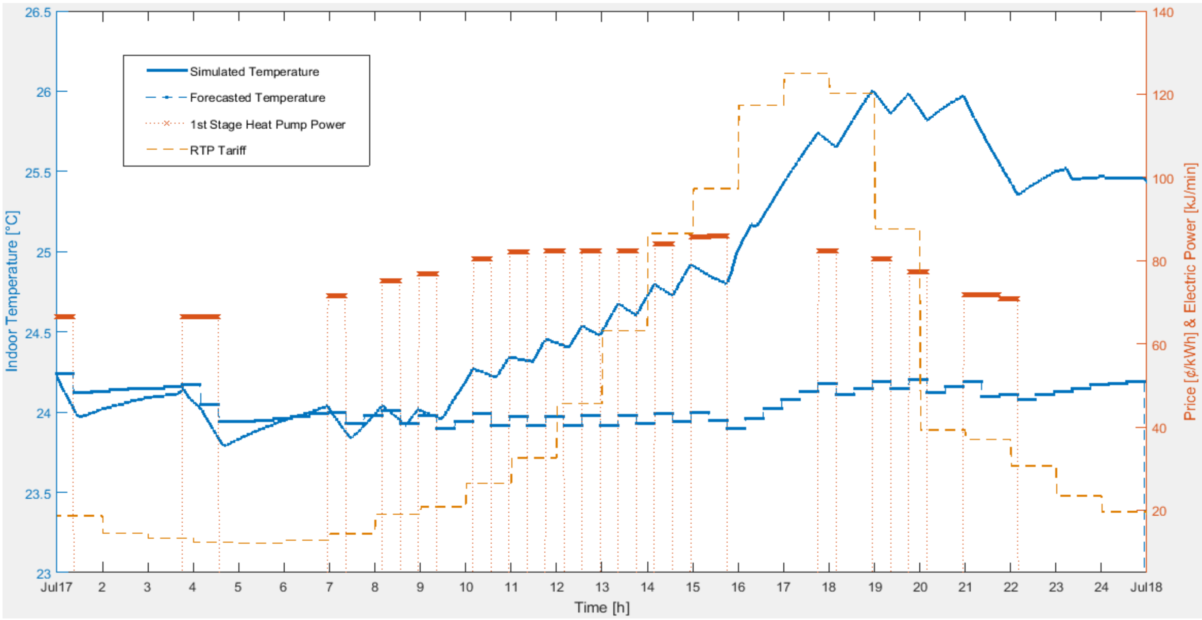

Figure 54. Residential EMCA2 - forecasted and simulated T_{ind} and heat pump power consumption during the highest RTP peaks (July 17th)

As can be seen from Figure 54, the forecasted T_{ind} is maintained within the constraints of residential EMCA2. However, the response of the simulation model to forecasted control actions shows large deviations in T_{ind}. The maximum temperature difference between the forecasted and simulated T_{ind} is 1.8 °C. The three highest RTP peaks, on this day, occur between 4:00 p.m. and 7:00 p.m. The optimization solver has shifted the operation of the heat pump away from these peak hours expect for 24 min when the 1st Stage is activated close to 6:00 p.m.

Likewise, Figure 55 shows a comparison between forecasted and simulated T_{ind} and heat pump power consumption with respect to the peak RTP tariff that occurred on the 19th of July.

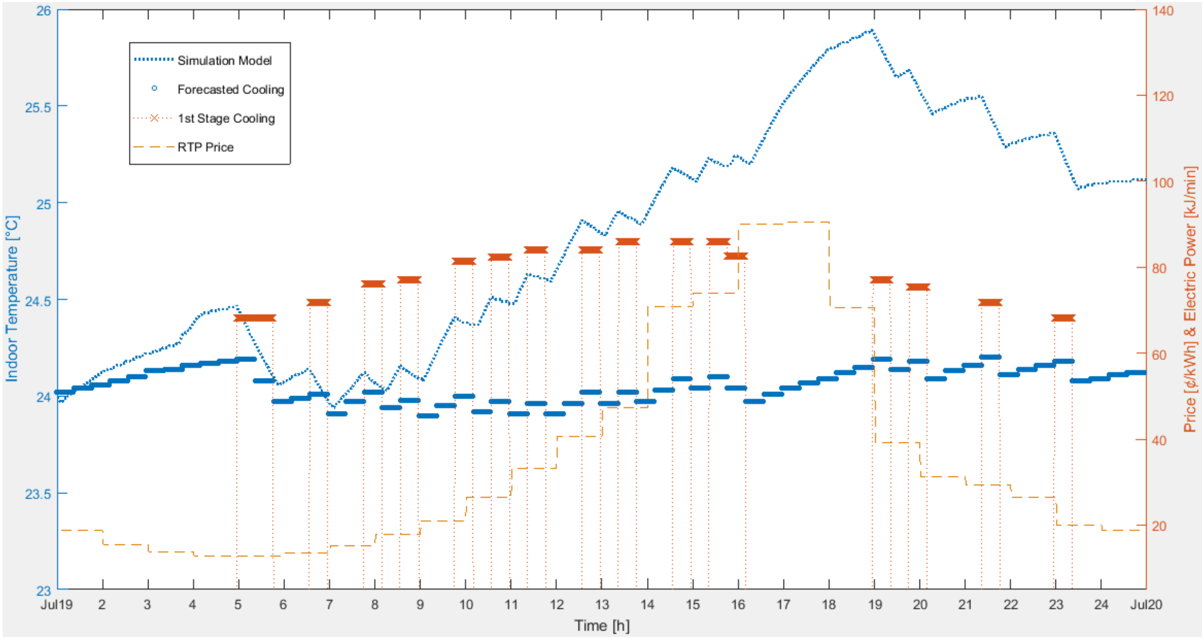

Figure 55. Residential EMCA2 - forecasted and simulated T_{ind} and heat pump power consumption during the second highest RTP peaks (July 19th)

As can be seen from Figure 55, the forecasted T_{ind} is maintained within the constraints of residential EMCA2. However, the response of the simulation model to forecasted control actions shows large deviations in T_{ind}. The maximum temperature difference between the forecasted and simulated T_{ind} is 1.7 °C. The two highest RTP peaks, on this day, occurred between 4:00 p.m. to 6:00 p.m. The optimization solver has shifted the operation of the heat pump away from these peak hours expect for 9 min when the 1st Stage remained activated past 4:00 p.m.

Appendix D

Residential EMCA3

The mathematical description of the residential EMCA3 for minimizing the cost of operating the heat pump while maintaining thermal comfort was presented in Sec.4.2.1.4.1. A forecast horizon of 4 h was chosen for this algorithm to take advantage of variability in the structure of the RTP tariff. Since the optimization problem is defined over 4 h, it is computationally difficult for the optimization solver to forecast heat pump control actions for each simulation time step in a reasonable amount of time. Therefore, the forecast horizon was divided into 60 bins, each bin holding 4 min of data. Average values of all forecasted variables in each bin was computed and used as a representative sample. This effectively reduced the forecast horizon to 60 min, which is computationally less time consuming. Since the new forecast horizon is 60 min, the output of the optimization solver is also a vector of length sixty. Each element of the vector represents 4 forecasted control actions. For example, if the 2nd Stage is given as the first element of the output vector, then the heat pump is operated in the 2nd Stage for the next 4 min.

Thermal Performance

The annual comparison of T_{ind} profiles of residential EMCA3 and the original simulation model is shown in Figure 56. In both heating and cooling seasons, T_{ind} is tightly controlled by the original simulation model based on the deadbands of the differential controllers given in Table 6. There are minor deviations from the setpoints in both heating and cooling seasons, but larger variations during the shoulder seasons. The indoor temperature fluctuations during the shoulder seasons are due to the deadbands of the differential controllers as it switches between heating and cooling seasons. Residential EMCA3 shows smaller variations during the shoulder seasons, but larger deviations in the heating and cooling seasons.

Residential EMCA3 exhibits large temperature deviations (Figure 56) because it is formulated in such a way that the optimization solver is required to maintain a balance between two different objectives, thermal comfort and cost. Depending on the choice of the dominance factor λ, the optimization solver can save more money or maintain a better thermal comfort. In residential EMCA3, the cost term is slightly dominant over the thermal comfort. In other words, the optimization solver is trying to minimize the cost of operating the heat pump by allowing the thermal comfort to fluctuate over a wider range.

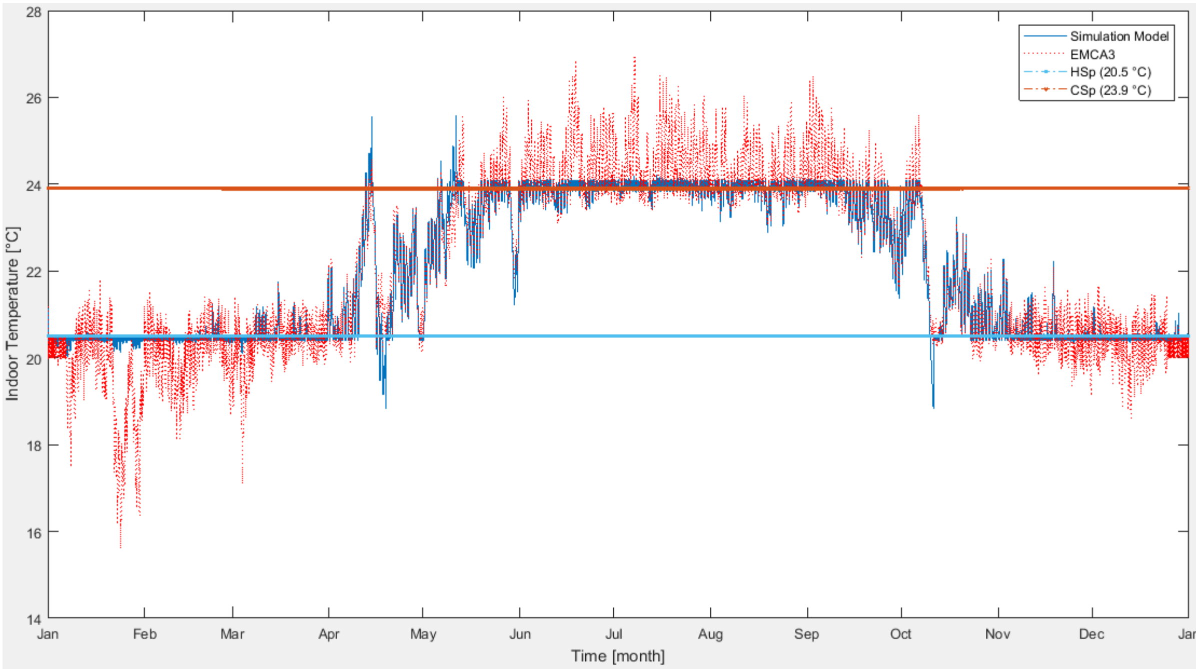

Figure 56. Residential EMCA3 – annual comparison of T_{ind} with the NZERTF original simulation model

The optimization problem solver is trying to minimize the objective function of residential EMCA3 given in Eq. (1.43) such that the forecasted T_{ind} given by Eq. (1.34) and Eq. (1.36) and the cost of consuming energy are maintained within the constraints of the problem. Figure 57 shows the annual comparison between the forecasted and simulated T_{ind}. Given the problem definition for residential EMCA3, the deviations of T_{ind} from the HS_p and CS_p are more frequent and larger compared to residential EMCA1 and residential EMCA2. Residential EMCA3 is not restricted by the upper and lower bound constraints; thus, it is more flexible in managing cost and thermal comfort.

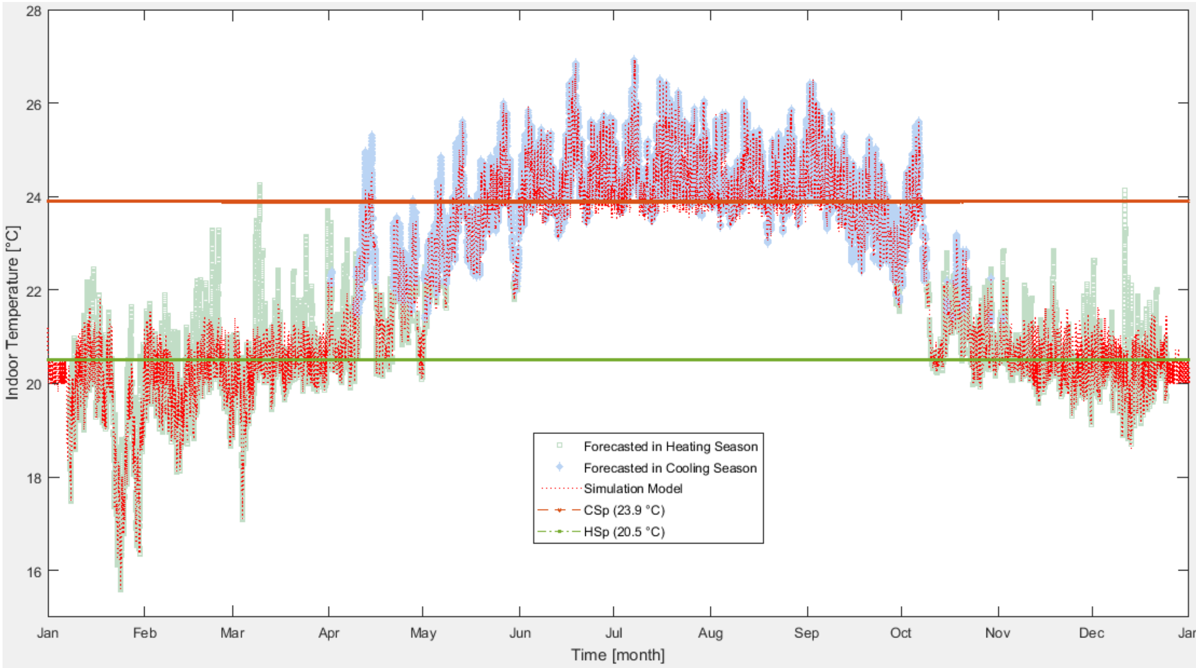

Figure 57. Residential EMCA3 - annual comparison between the forecasted and simulated T_{ind}

To better quantify the differences between the forecasted and simulated T_{ind} in residential EMCA3, Figure 58 shows the resulting % RMSE in both heating and cooling seasons. The behavior, limitation, and capability of the learning algorithm used for forecasting T_{ind} in residential EMCA3 was previously described in Sec. 3. In the heating season, Figure 58 shows that there are many instances in which residential EMCA3 overestimated the forecast of T_{ind} compared to the simulation model. In the cooling season, the forecasted and simulated T_{ind} are in good agreements.

Over the course of one year, residential EMCA3 was expected to run 2106 times based on its forecast horizon. As can be seen from Figure 58, the optimization solver generated control actions for all expected times. In other words, the optimization solver found a feasible solution every time that it was expected to run.

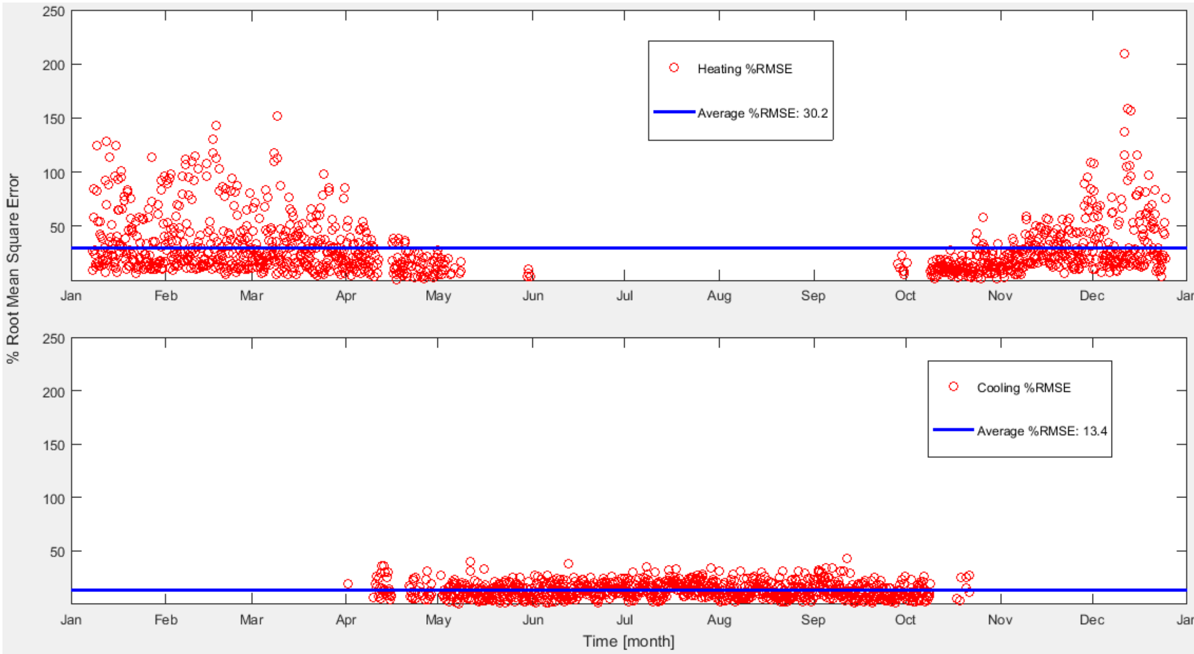

Figure 58. Residential EMCA3 - the % RMSE between forecasted and simulated T_{ind}

Furthermore, the thermal performance of residential EMCA3, as measured by PMV and PPD, was calculated. Figure 59 shows the annual comparison of PMV between residential EMCA3 and the original simulation model of the NZERTF. The PMV corresponding to the original simulation model transitions between slightly warm and slightly cool temperature during the shoulder seasons, but it remains within the recommend thermal range of +0.5 and -0.5 in other times. In comparison, the PMV associated with residential EMCA3 remains within the recommended range during the shoulder season but oscillates around the comfort limits, especially in the cooling season. In the cooling season, the occupants generally feel warmer compared to the original simulation model, and in some instances uncomfortable. In the heating season, the PMV values suggest that, on a few instances, the occupants feel uncomfortable compared to the original simulation model. In general, it can be concluded that the occupants were comfortable throughout the simulation year except for 1176 h (Table 18). This is a significant increase in discomfort compared to residential EMCA1 and residential EMCA2, suggesting that thermal comfort was sacrificed for more cost savings. The result was expected because λ was chosen such that the optimization solver would maximize cost savings while also not letting thermal comfort drift too far from the setpoints.

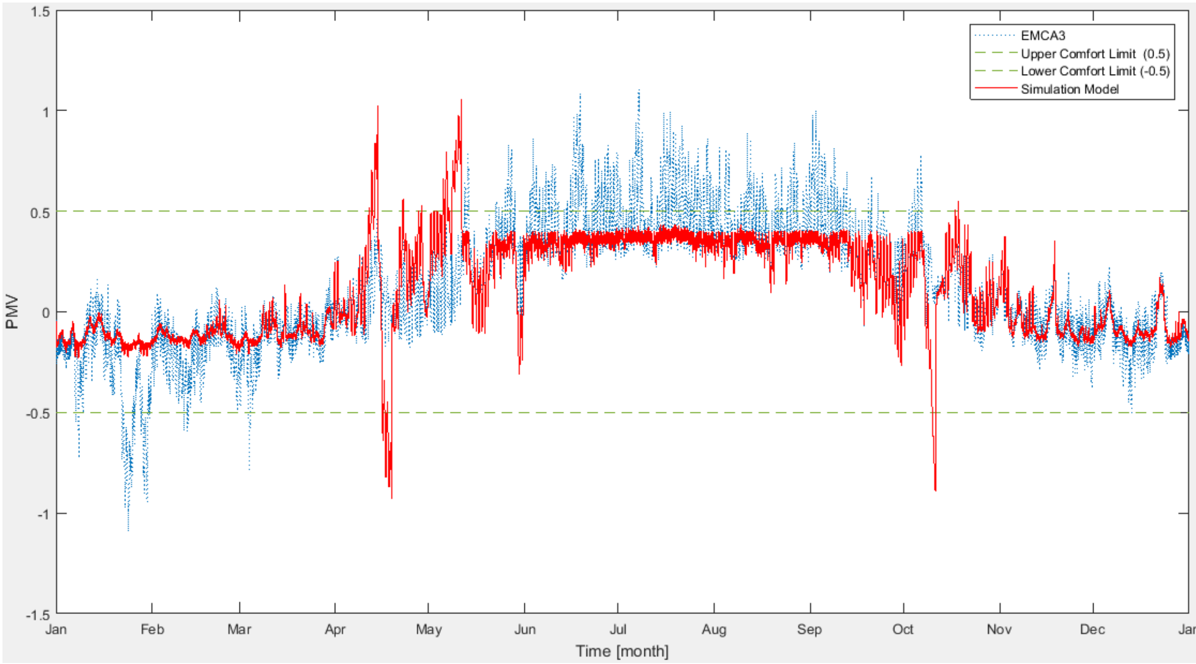

Figure 59. Residential EMCA3 – annual comparison of PMV with the NZERTF original simulation model

Similarly, Figure 60 shows the annual comparison of PPD between residential EMCA3 and the original simulation model. The PPD corresponding to the original simulation model suggest that a large percentage of the occupants were uncomfortable during the shoulder seasons but for a shorter period. In comparison, the PPD corresponding to the residential EMCA3 suggest that not only more occupants were uncomfortable, but they were also uncomfortable for a longer period. Thermal comfort is mainly impacted in the cooling season, but in the heating season some occupants were uncomfortable as well, albeit for a shorter period.

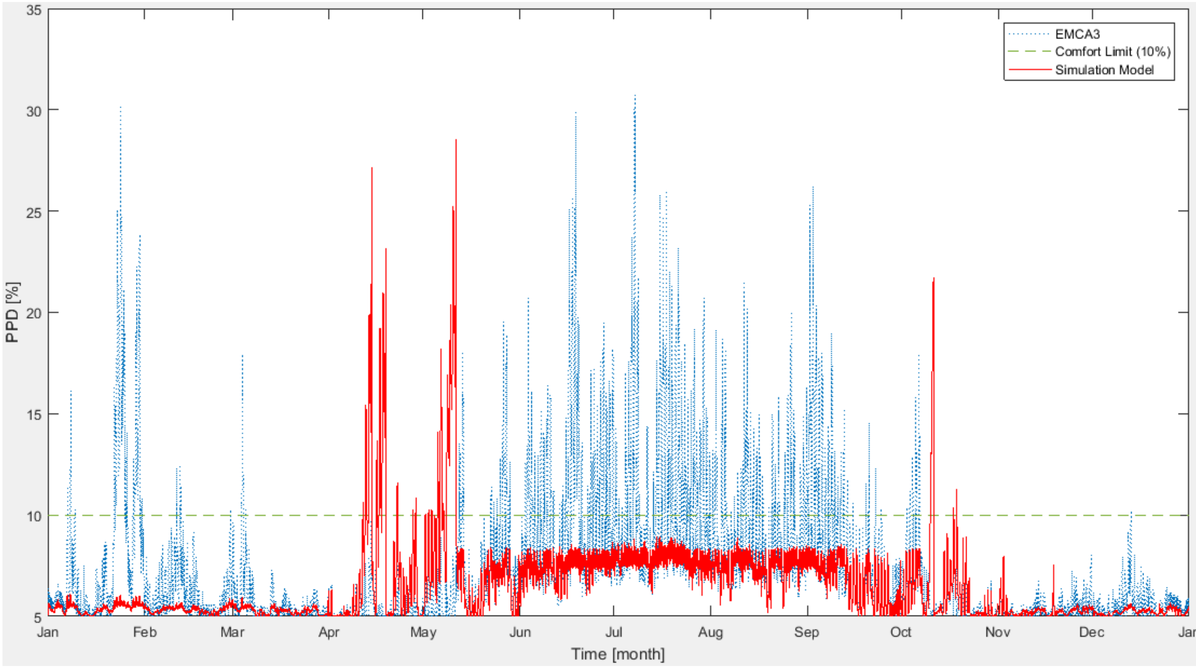

Figure 60. Residential EMCA3 – annual comparison of PPD with the NZERTF original simulation model

Minimizing Cost

As previously mentioned, the objective of residential EMCA3 is to minimize the cost of consuming energy while also maintaining thermal comfort. One way to accomplish this task is by shifting the operation of the heat pump from peak price of electricity to off-peak times, resulting in a lower cost. Figure 61 shows a comparison between forecasted and simulated T_{ind} plotted with respect to the left axis, and heat pump power consumption and RTP tariff plotted with respect to the right axis.

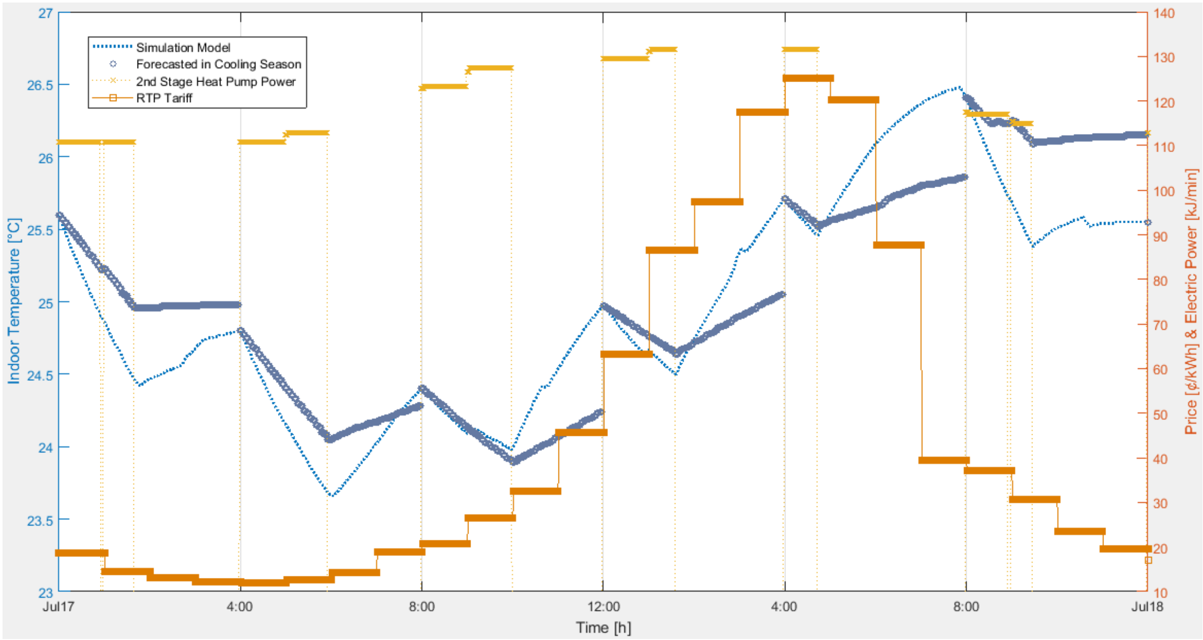

Figure 61. Residential EMCA3 - forecasted and simulated T_{ind} and heat pump power consumption during the highest RTP peaks (July 17th)

As can be seen from Figure 61, the forecasted T_{ind} is maintained within the constraints of residential EMCA3. However, the response of the simulation model to forecasted control actions shows large deviations in T_{ind}. The highest RTP peak (125.1 ¢/kWh) occurred between 4:00 p.m. and 5:00 p.m. Even though the highest peak occurred at the beginning of the forecast horizon at 4:00 p.m., the heat pump was activated immediately because the value of thermal comfort term in the objective function was dominating compared to the value of the cost term. It was dominating because the gap between the initial temperature and CS_p was significant. Hence, the heat pump operated for 45 min until the T_{ind} dropped below a threshold at which the value of the cost term started to dominate.

Appendix E

Residential EMCA4

The objective and mathematical description of residential EMCA4 is identical to the formulation of residential EMCA3, including all constraints, forecast horizon, and implementation described in Sec. 4.2.1.4.1 and Appendix D. The only difference is the value of the dominance factor $\lambda = 0.55$.

Thermal Performance

The annual comparison of T_{ind} profiles of residential EMCA4 and the original simulation model is shown in Figure 62. In both heating and cooling seasons, T_{ind} is tightly controlled by the original simulation model based on the deadbands of the differential controllers given in Table 6. There are minor deviations from the setpoints in both heating and cooling seasons, but larger variations during the shoulder seasons. The indoor temperature fluctuations during the shoulder seasons are due to the deadbands of the differential controllers as it switches between heating and cooling seasons. Residential EMCA4 shows smaller variations during the shoulder seasons, but larger deviations in the heating and cooling seasons.

Residential EMCA4 exhibits slightly different deviations (Figure 62) compared to residential EMCA3. In residential EMCA4, thermal comfort term is slightly dominant over the cost term. In other words, the optimization solver is trying to maintain better thermal comfort at a higher cost.

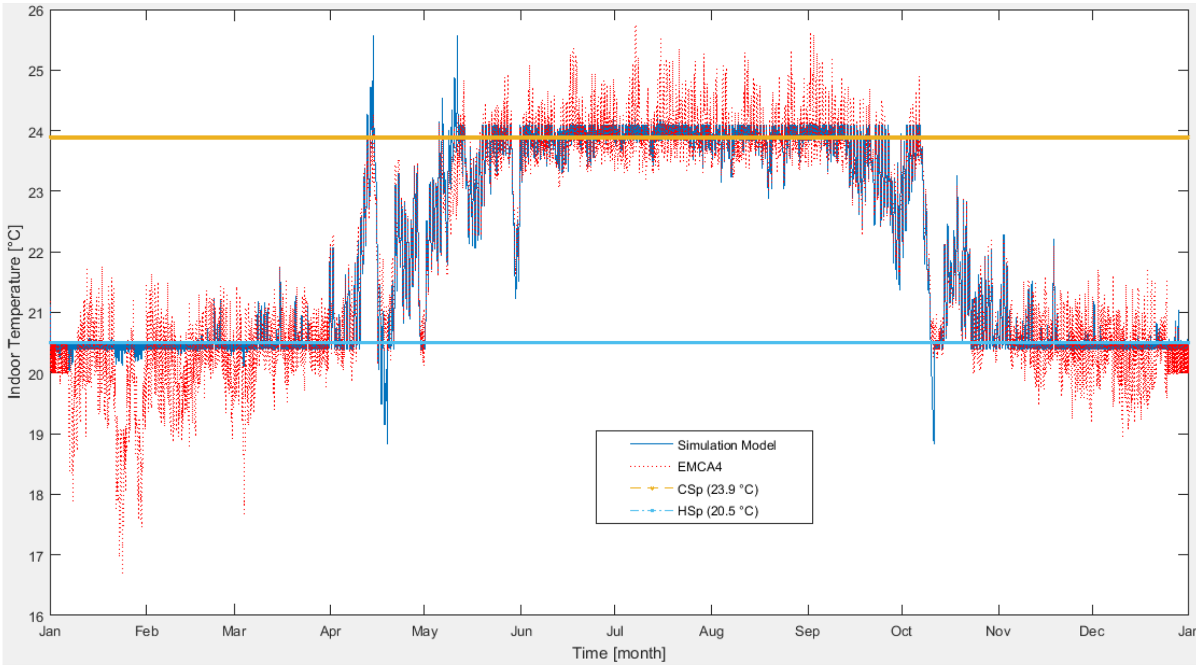

Figure 62. Residential EMCA4 – annual comparison of T_{ind} with the NZERTF original simulation model

Figure 63 shows the annual comparison between the forecasted and simulated T_{ind}. Given the problem definition for residential EMCA4, the deviations of T_{ind} from the HS_p and CS_p are more frequent and larger compared to residential EMCA1 and residential EMCA2 but slightly smaller compared to residential EMCA3, demonstrating the impact of choosing λ on the overall cost and thermal comfort. Like residential EMCA3, residential EMCA4 is flexible in managing cost and thermal comfort.

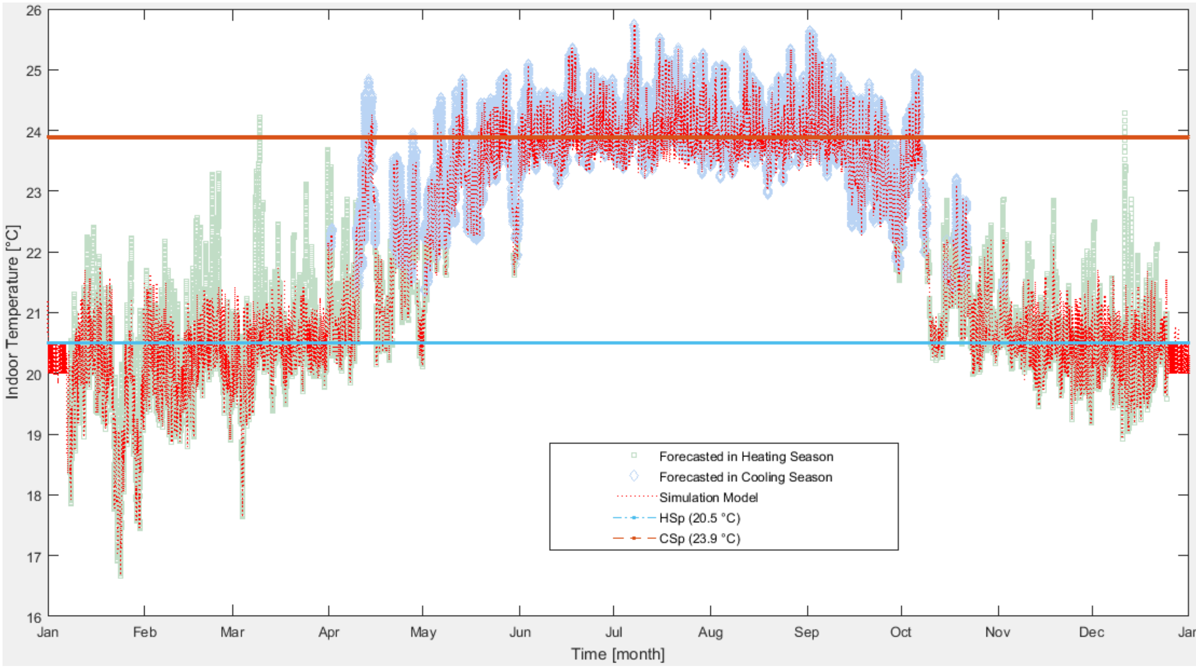

Figure 63. Residential EMCA4 – annual comparison between the forecasted and simulated T_{ind}

To better quantify the differences between the forecasted and simulated T_{ind} in residential EMCA4, Figure 64 shows the resulting % RMSE in both heating and cooling seasons. The behavior, limitation, and capability of the learning algorithm used for forecasting T_{ind} in residential EMCA3 was previously described in Sec. 3. In the heating season, Figure 64 shows that there are many instances in which residential EMCA4 overestimates the forecast of T_{ind} compared to the simulation model. In the cooling season, the forecasted and simulated T_{ind} are in good agreements.

Over the course of one year, residential EMCA4 was expected to run 2106 times based on its forecast horizon. As can be seen from Figure 64, the optimization solver generated control actions for all expected times. In other words, the optimization solver found a feasible solution every time that it was expected to run.

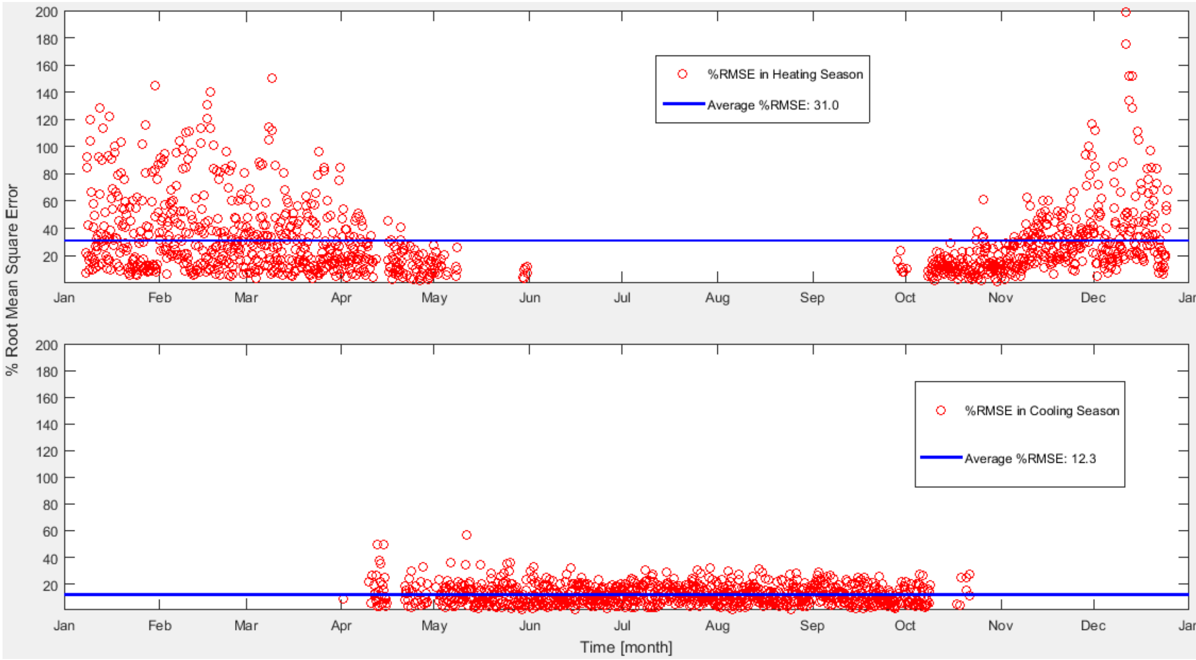

Figure 64. Residential EMCA4 - the % RMSE between forecasted and simulated T_{ind}

Furthermore, the thermal performance of residential EMCA4, as measured by PMV and PPD, was calculated. Figure 65 shows the annual comparison of PMV between residential EMCA4 and the original simulation model. The PMV corresponding to the original simulation model transitions between slightly warm and slightly cool temperature during the shoulder seasons, but it remains within the recommend thermal range of +0.5 and -0.5 in other times. In comparison, the PMV associated with residential EMCA4 remains within the recommended range during the shoulder seasons, but oscillates near the comfort limits, especially in the cooling season. In the cooling season, the occupants generally feel warmer compared to the original simulation model, and in some instances uncomfortable. In the heating season, the PMV values suggest that, on a few instances, the occupants feel uncomfortable compared to the original simulation model. In general, it can be concluded that the occupants were comfortable majority of the time during the simulation year except for 222 h (Table 18). This is a large increase in discomfort compared to residential EMCA1, but less than residential EMCA2 and residential EMCA3. This behavior is expected because the requirement for residential EMCA4 is to maintain thermal comfort first then reduce the cost.

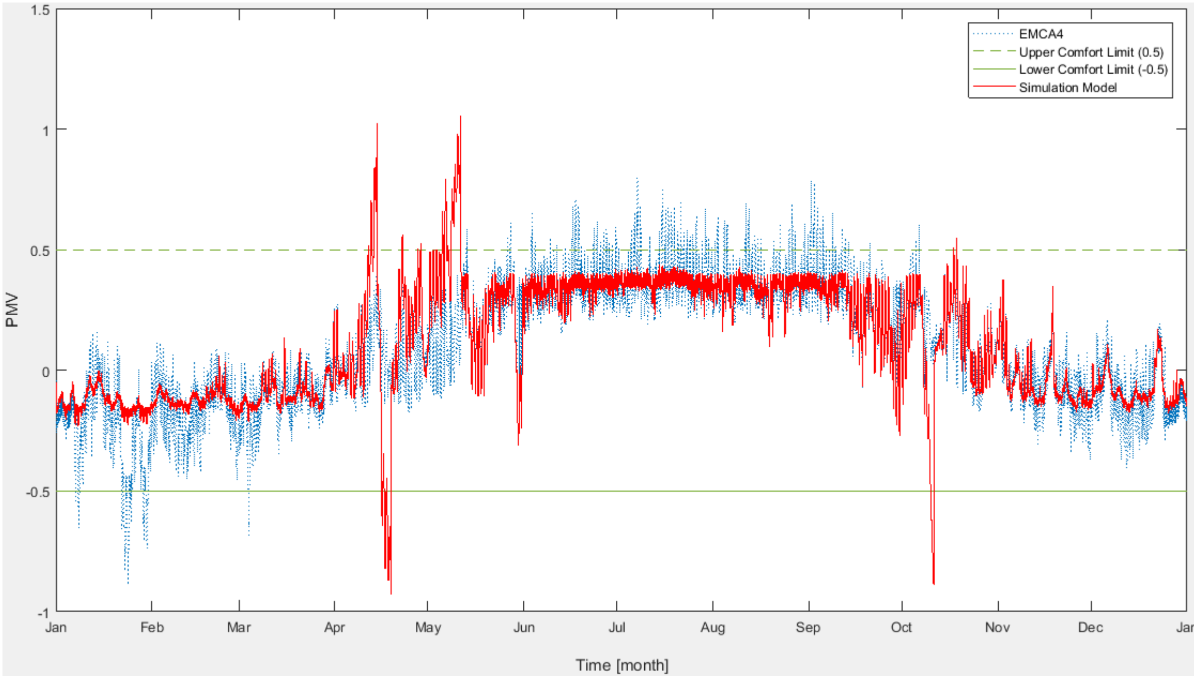

Figure 65. Residential EMCA4 – annual comparison of PMV with the NZERTF original simulation model

Similarly, Figure 66 shows the annual comparison of PPD between residential EMCA4 and the original simulation model. The PPD corresponding to the original simulation model suggest that a large percentage of the occupants were uncomfortable during the shoulder seasons but for a shorter period. In comparison, the PPD corresponding to the residential EMCA4 suggest that not only more occupants were uncomfortable, but they were uncomfortable for a longer period. Thermal comfort is mainly impacted in the cooling season, but in the heating season some occupants were uncomfortable as well, albeit for a shorter period.

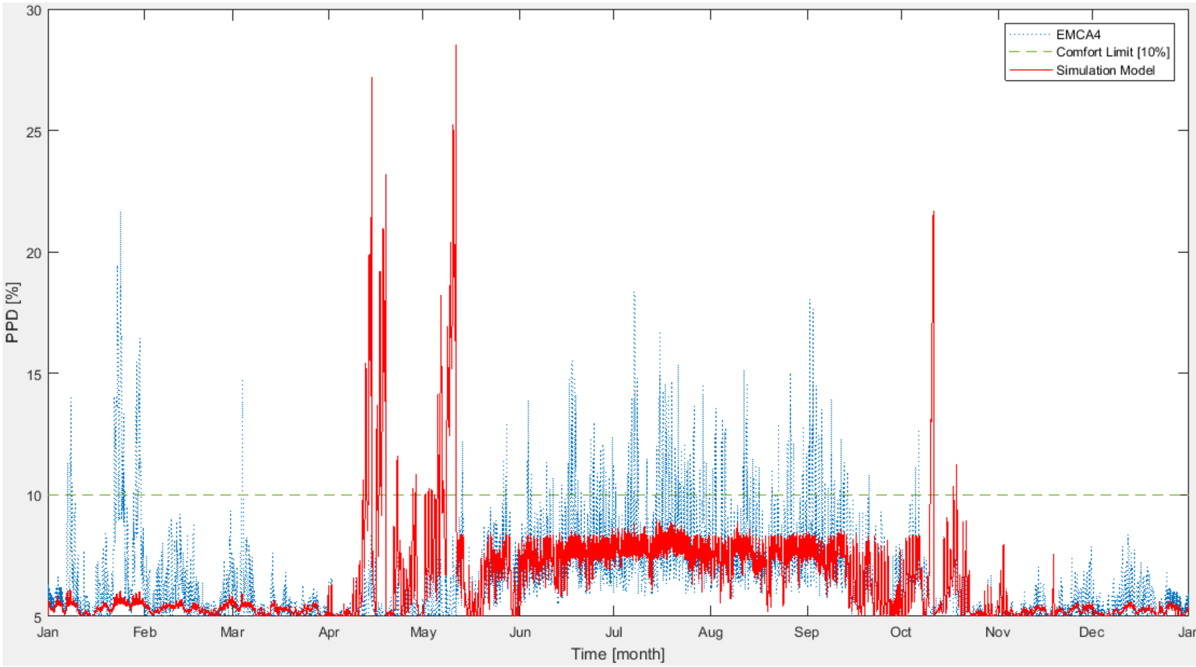

Figure 66. Residential EMCA4 – annual comparison of PPD with the original simulation model

Minimizing Cost

As previously mentioned, the objective of residential EMCA4 is to minimize the cost of consuming energy while also maintaining thermal comfort. One way to accomplish this task is by shifting the operation of the heat pump from peak price of electricity to off-peak times. This strategy may not be employed by residential EMCA4 because its task is to maintain thermal comfort first then reduce cost. Figure 67 shows a comparison between forecasted and simulated T_{ind} plotted with respect to the left axis, and heat pump power consumption and RTP tariff with respect to the right axis.

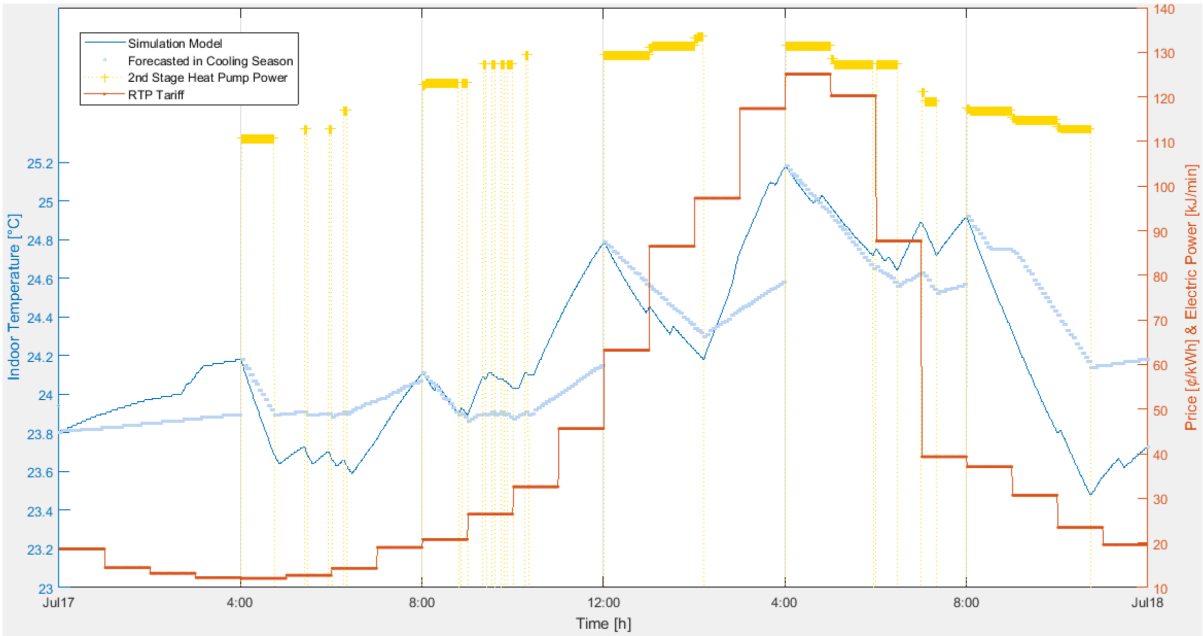

Figure 67. Residential EMCA4 - forecasted and simulated T_{ind} and heat pump power consumption during the highest RTP peaks (July 17th)

As can be seen from Figure 67, the forecasted T_{ind} is maintained within the constraints of residential EMCA4. However, the response of the simulation model to forecasted control actions shows large deviations in T_{ind}. The highest RTP peak (125.1 ¢/kWh) occurred between 4:00 p.m. and 5:00 p.m. Even though the highest peak occurred at the beginning of the forecast horizon at 4:00 p.m., the heat pump was activated immediately because the value of thermal comfort term in the objective function was dominating compared to the value of the cost term. It was dominating because the gap between the initial temperature and CS_p was significant. The heat pump operated continuously for 2 h, and after a brief downtime, reactivated again. This behavior is in contrast with residential EMCA3 where the heat pump only operated for 45 min until the T_{ind} dropped below a threshold where the balance was tipped over towards energy savings.

Appendix F

Residential EMCA5

Residential EMCA5 is the Default Controller described in Sec. 4.1. It was designed, as a best effort, to replicate the operation of the differential controllers used in the original simulation model of the NZERTF.

Thermal Performance

The annual comparison of T_{ind} profiles of residential EMCA5 and the original simulation model is shown in Figure 68.

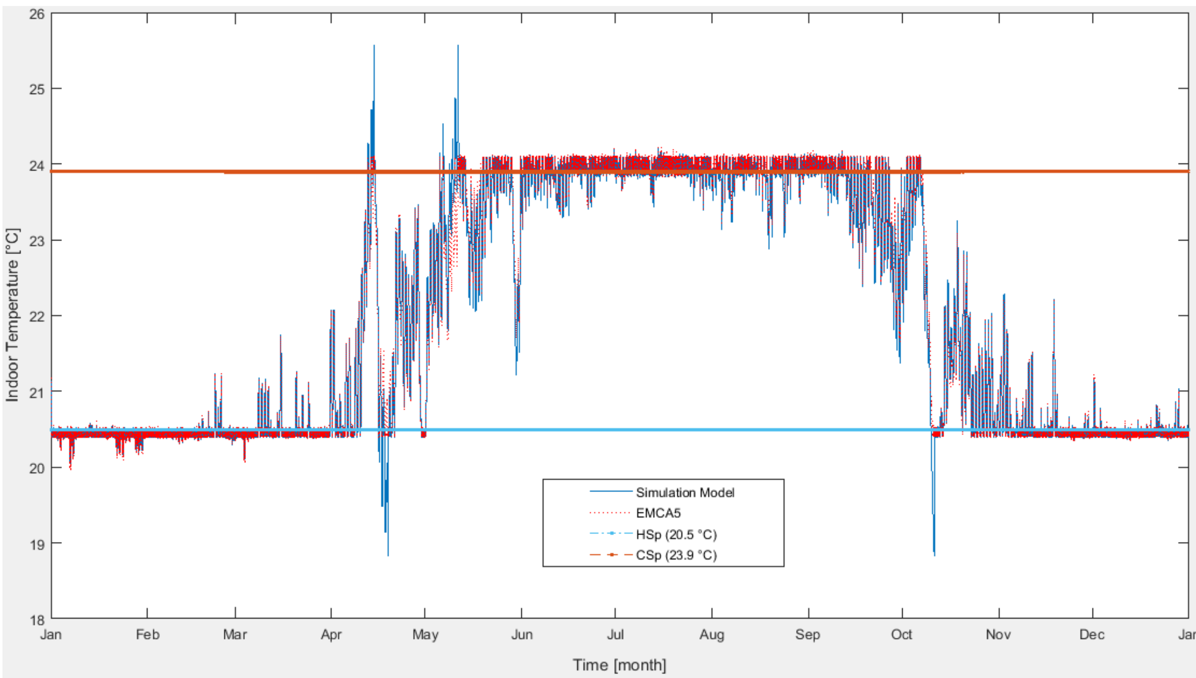

Figure 68. Residential EMCA5 - annual comparison of T_{ind} with the original simulation model

As can be seen from Figure 68, residential EMCA5 and the original simulation model have similar T_{ind} profiles. In both profiles, there are small variations from the heating and cooling setpoints. The original simulation model shows larger deviations in T_{ind} during the shoulder seasons, while these variations are smaller in residential EMCA5. To highlight their similarities and differences, two representative months for heating and cooling seasons are selected and shown in Figure 69 and Figure 70, respectively.

The top subplot in Figure 69 shows a comparison of T_{ind} between residential EMCA5 and the original simulation model in the month of January, while the bottom subplot shows three days with the lowest temperature drops.

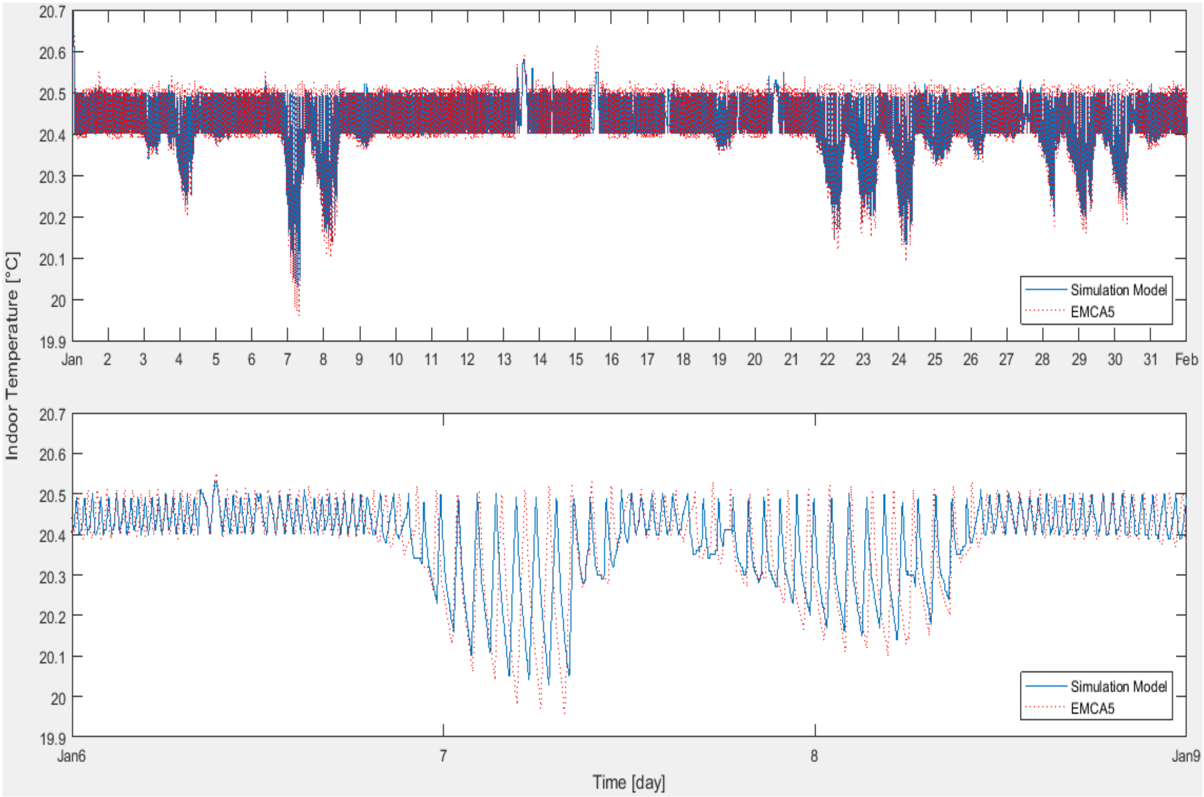

Figure 69. Residential EMCA5 – comparison of T_{ind} with the original simulation model

As can be seen from Figure 69, both temperature profiles are similar with minor differences in the magnitude of deviations from the HS_p. In both temperature profiles, the largest temperature decay from the HS_p occurred on the 7th of January. The maximum temperature decay of the original simulation model is 0.2 °C, where the maximum temperature decay of residential EMCA5 is 0.54 °C.

Similarly, the top subplot of Figure 70 shows a comparison of T_{ind} between residential EMCA5 and the original simulation model in the month of July, while the bottom subplot captures a few days with larger variations in the indoor temperature.

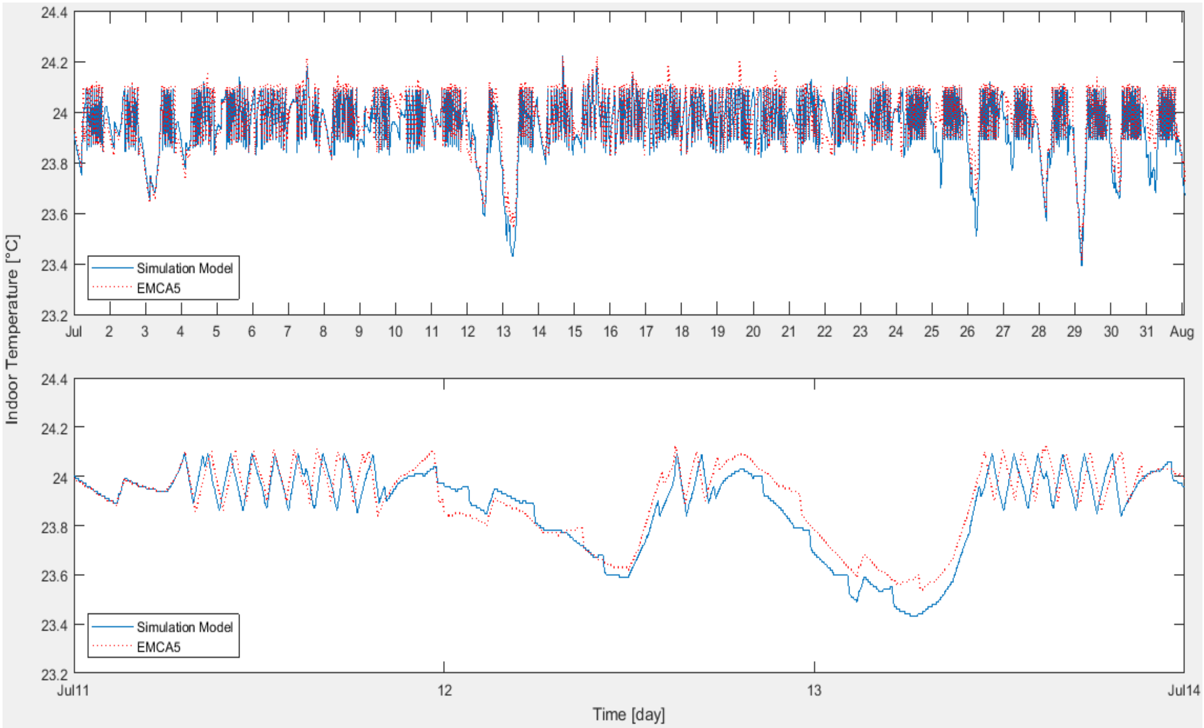

Figure 70. Residential EMCA5 - a comparison of T_{ind} with the original simulation model

As can be seen from Figure 70, both temperature profiles are similar. The largest temperature difference is 0.16 °C between the two profiles in the bottom subplot.

Furthermore, the thermal performance of residential EMCA5, as measured by PMV and PPD, was calculated. Figure 71 shows the annual comparison of PMV between residential EMCA5 and the original simulation model. The PMV corresponding to the original simulation model transitions between slightly warm and slightly cool temperatures during the shoulder seasons, but it remains within the recommend thermal range of +0.5 and -0.5 in all other seasons. In comparison, the PMV associated with residential EMCA5 remains within the recommended range in all seasons, including the shoulder seasons. According to the information in Table 18, the discomfort index for residential EMCA5 is 0 h, suggesting that the occupants have been comfortable throughout the simulation year. The impact of residential EMCA5 on thermal discomfort was expected to be minimal because it was designed to maintain thermal comfort regardless of energy consumption.

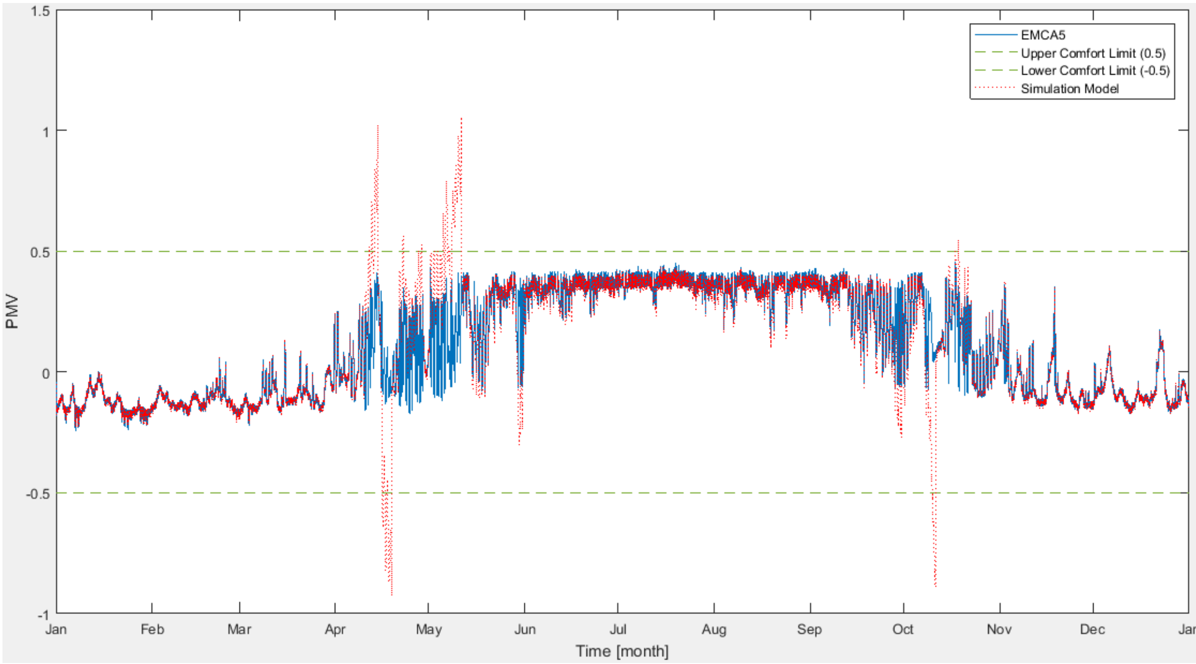

Figure 71. Residential EMCA5 - comparison of annual PMV with the original simulation model

Likewise, Figure 72 shows the annual comparison of PPD between residential EMCA5 and the original simulation model. The PPD values corresponding to the original simulation model suggest that a large percentage of the occupants were uncomfortable during the shoulder seasons, but for a shorter period. The PPD values corresponding to the residential EMCA5 confirms that the occupants were comfortable throughout the year and the maximum value of PPD is well within the 10 % of the thermal comfort limit.

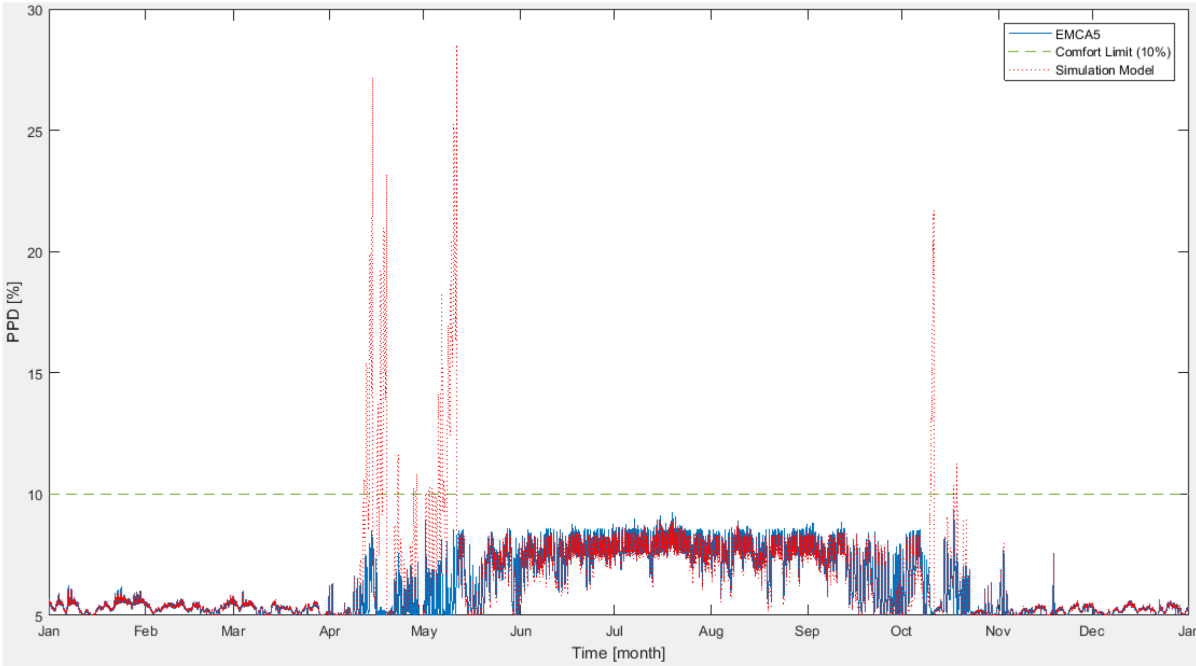

Figure 72. Residential EMCA5 - comparison of annual PPD with the original simulation model

Appendix G

Residential EMCA6

Residential EMCA6 is identical to residential EMCA5; it only uses wider deadbands (Table 5) for controlling different stages of the heat pump.

Thermal Performance

The annual comparison of T_{ind} profiles of residential EMCA6 and the original simulation model is shown in Figure 73.

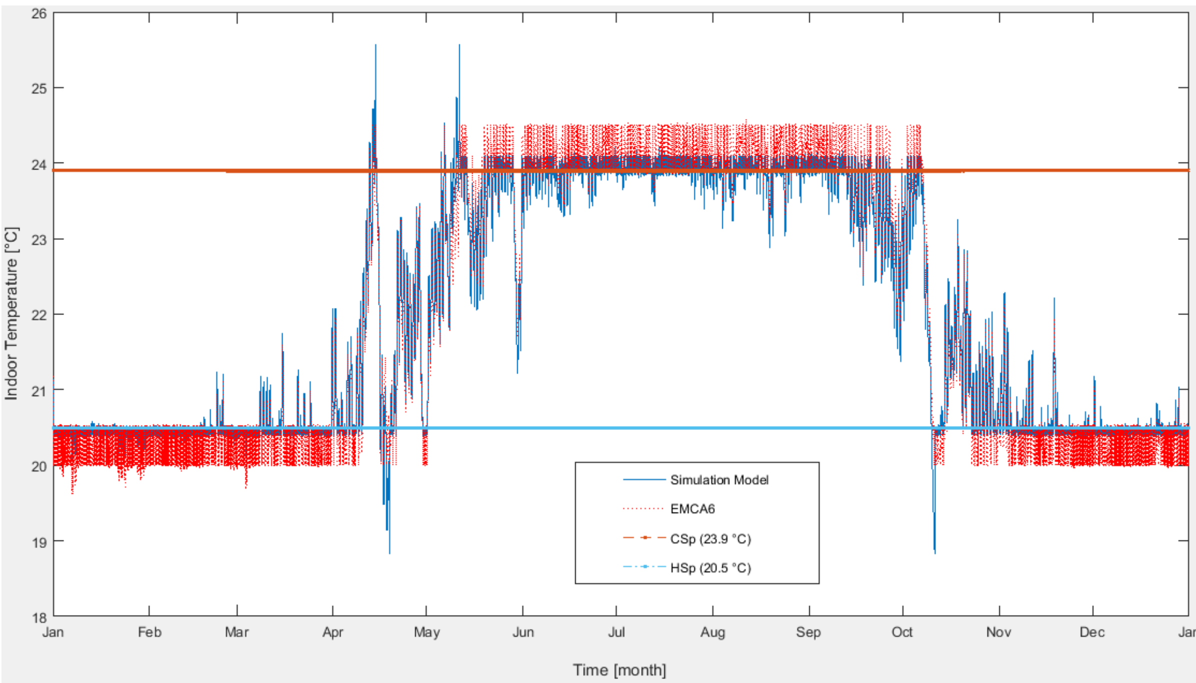

Figure 73. Residential EMCA6 - annual comparison of T_{ind} with the original simulation model

As can be seen from Figure 73, residential EMCA6 and the original simulation model do not have similar T_{ind} profiles because the deadbands for residential EMCA6 were relaxed. In both profiles, there are small variations from the heating and cooling setpoints. The original simulation model shows larger deviations in T_{ind} during the shoulder seasons, while these temperature variations are smaller in residential EMCA6. To highlight their similarities and differences, two representative months for heating and cooling seasons are selected and shown in Figure 74 and Figure 75, respectively.

The top subplot in Figure 74 shows a comparison of T_{ind} between residential EMCA6 and the simulation model in January, while the bottom subplot shows three days with the lowest temperature drops.

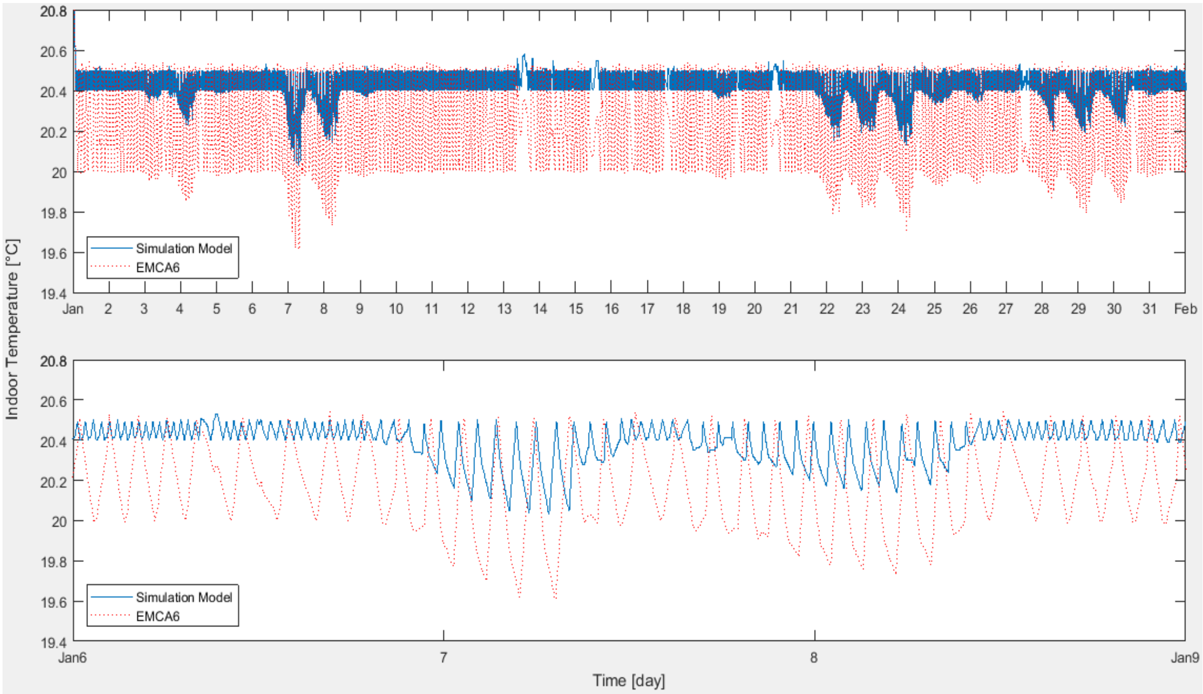

Figure 74. Residential EMCA6 - a comparison of T_{ind} with the original simulation model

As can be seen from Figure 74, both temperature profiles fluctuate within their respective deadbands from the HS_p. In both temperature profiles, the largest temperature decay from the HS_p occurred on the 7th of January. The maximum temperature decay of the original simulation model is 0.2 °C, where the maximum temperature decay of residential EMCA6 is 0.89 °C.

Similarly, the top subplot of Figure 75 shows a comparison of T_{ind} between residential EMCA6 and the original simulation model in the month of July, while the bottom subplot captures a few days with larger variations in the indoor temperature

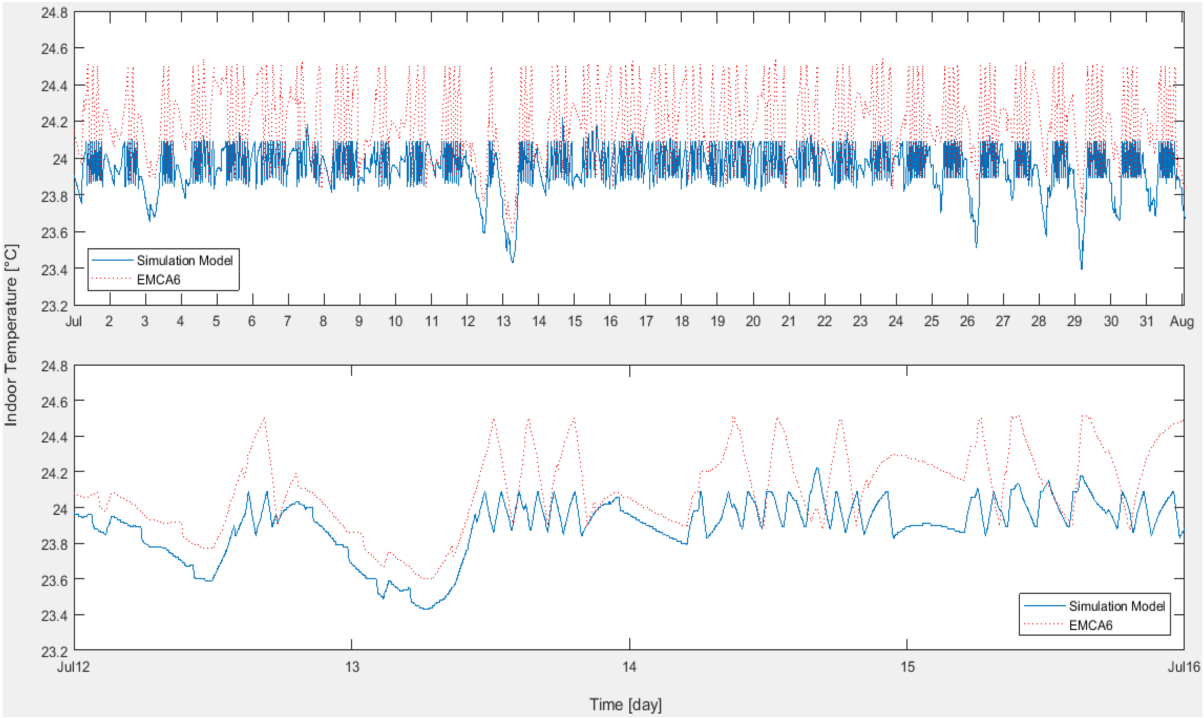

Figure 75. Residential EMCA6 - a comparison of T_{ind} with the original simulation model

As can be seen from Figure 75, both temperature profiles fluctuate within their respective deadbands from the CS_p. The largest temperature increase of for both profiles occurred on the 14th of July. The largest temperature increase of for the original simulation model was 0.33 °C, while the maximum temperature increase for residential EMCA6 was 0.62 °C.

Furthermore, the thermal performance of residential EMCA6, as measured by PMV and PPD, was calculated. Figure 76 shows the annual comparison of PMV between residential EMCA6 and the original simulation model. The PMV corresponding to the original simulation model transitions between slightly warm and slightly cool temperature during the shoulder seasons, but it remains within the recommend thermal range of +0.5 and -0.5 in all other seasons. In comparison, the PMV associated with residential EMCA6 generally within the recommended range in the heating and shoulder seasons. In the cooling season, the PMV associated with residential EMCA6 oscillates around the upper recommended limit of + 0.5. In other words, the occupants are feeling slightly warmer than the original simulation model. In general, it can be concluded that the occupants were comfortable throughout of the simulation year except for 37 h (Table 18).

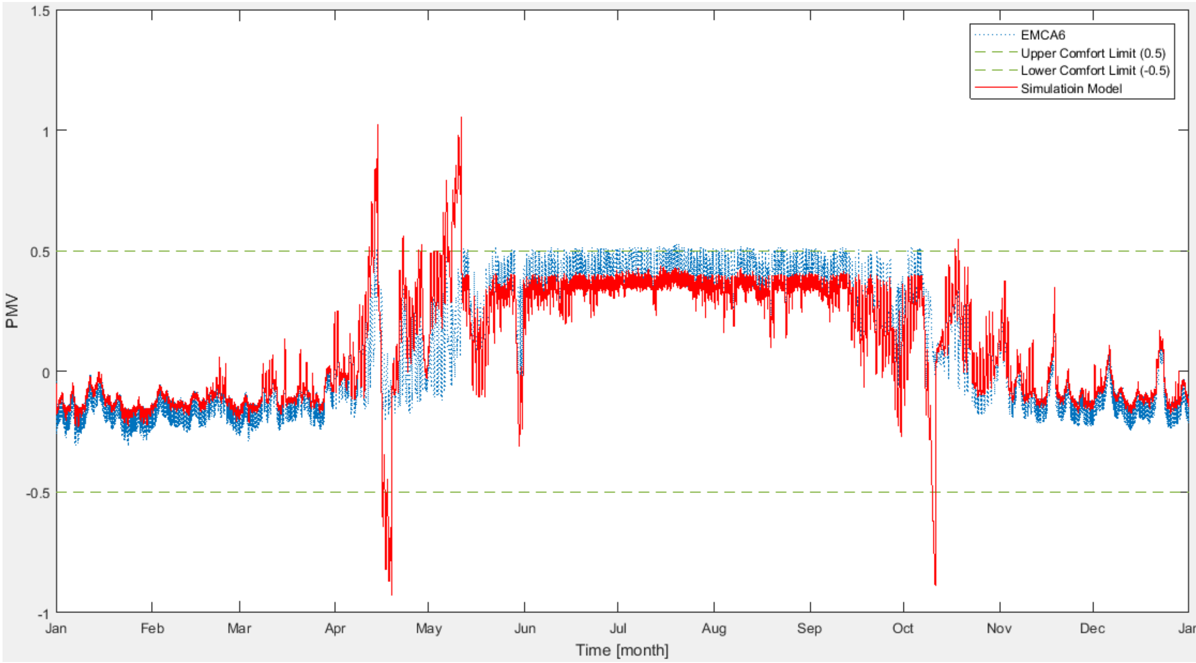

Figure 76. Residential EMCA6 - comparison of annual PMV with the original simulation model

Similarly, Figure 77 shows the annual comparison of PPD between residential EMCA6 and the original simulation model. The PPD values corresponding to the original simulation model suggest that a large percentage of the occupants were uncomfortable during the shoulder seasons, but for a shorter period. The PPD values corresponding to the residential EMCA6 suggest that not only more occupants were uncomfortable, but they were uncomfortable for a longer period. In general, the maximum value of PPD is well within the 10 % thermal comfort limit.

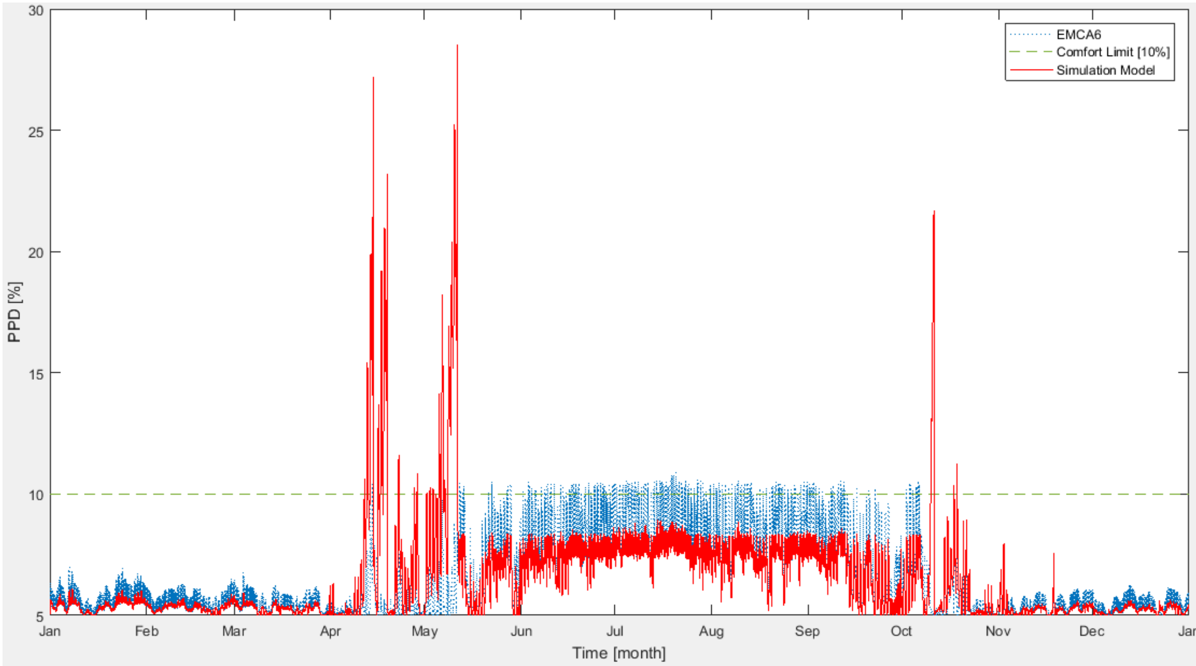

Figure 77. Residential EMCA6 - comparison of annual PPD with the original simulation model

Nomenclature

AE	assessment engine
AEUI	AE user interface
AHP	Analytical Hierarchy Process
ANSI	American National Standards Institute
ASHRAE	American Society of Heating, Refrigerating and Air-Conditioning Engineers
ASTM	American Society for Testing and Materials
CCD	cooling control decisions
cHSD	cooling 2nd Stage deadband
CI	consistency index
cLSD	cooling 1st Stage deadband
cLSTO	cooling 1st Stage time-out
coolToHeat	cool to heating season deadband
CR	consistency ratio
C_{scale}	comparison scale
CS_p	cooling temperature setpoint
DBM	division by maximum
DBS	division by sum
DCTBE	default control timer before the end
DCTS	default control timer at the start
Diff	difference
DR	demand response
E_{c1}	1st Stage heat pump thermal capacity for cooling
E_{c2}	2nd Stage heat pump thermal capacity for cooling
E_{h1}	1st Stage heat pump thermal capacity for heating
E_{h2}	2nd Stage heat pump thermal capacity for heating
E_{h3}	3rd Stage capacity for heating
EISA	Energy Independence and Security Act
EMCA	energy management control algorithm
FDD	fault detection and diagnostics
hASD	3rd Stage heating deadband
HCD	heating control decisions
heatToCool	heat to cooling season deadband
hHSD	2nd Stage heating deadband
hHSTO	2nd Stage heating time-out
hLSD	1st Stage heating deadband
hLSTO	1st Stage heating time-out
HS_p	heating setpoint
HVAC	heating, ventilating, and air-conditioning
IEEE	Institute of Electrical and Electronics Engineers
ISO	International Organization for Standardization
ITFM	indoor temperature forecast model
kWh	kilowatt hour
MATLAB	Matrix Laboratory
M_C	mapping cost
MCDM	multi-criteria decision-making

M_{DC}	mapping discomfort
M_E	mapping energy consumption
MPC	matrix of pairwise comparisons
NIST	National Institute of Standards and Technology
NZERTF	Net-Zero Energy Residential Test Facility
P_{c1}	1st Stage electrical power for Cooling
P_{c2}	2nd Stage electrical power for Cooling
P_{h1}	1st Stage electrical power for heating
P_{h2}	2nd Stage electrical power for Heating
P_{h3}	3rd Stage electrical power for Heating
PJM	Pennsylvania-New Jersey-Maryland Interconnection
PMV	predicted mean vote
PPD	predicted percentage of dissatisfied
PPD_{wc}	PPD-Weighted criterion
q_{hp}	rate of heat generated inside a residence by the heat pump;
q_l	rate of heat generated inside a residence by the internal loads
q_{sol}	total solar heat gain added to a residence
R_C	cost ratio
R_{DC}	discomfort ratio
R_E	energy ratio
RI	random index
RTP	real-time pricing
S_{CF}	cost scale factor
S_{DF}	discomfort scale factor
S_{EF}	energy scale factor
T_∞	outside ambient dry-bulb temperature
T_i	initial indoor temperature
T_{ind}	first floor dry-bulb indoor temperature
TMY	typical meteorological year
TRNSYS	Transient System Simulation Tool
UA	overall heat transfer coefficient
YALMIP	Yet Another Linear Matrix Inequalities Parser
λ	the dominance factor
τ	building time constant

List of Publications

1. F. Omar and S. T. Bushby, “A Self-Learning Algorithm for Temperature Prediction in a Single Family Residence,” *NIST Tech. Note 1891*, 2015.
2. F. Omar, S. T. Bushby, and R. D. Williams, “A self-learning algorithm for estimating solar heat gain and temperature changes in a single-Family residence,” *Energy Build.*, vol. 150, 2017.
3. F. Omar, S. T. Bushby, and R. D. Williams, “Assessing the Performance of Residential Energy Management Control Algorithms: Muti-Criteria Decision Making Using the Analytical Hierarchy Process,” *NIST Tech. Note 2017,* 2018.
4. Under review in Energy and Buildings:
    a. F. Omar, S. T. Bushby, and R. D. Williams, “Assessing the Performance of Residential Energy Management Control Algorithms: Muti-Criteria Decision Making Using the Analytical Hierarchy Process,”.
5. Planned, F. Omar, S. T. Bushby, and R. D. Williams, “Energy Management Control Algorithms for the Net Zero Residential Test Facility,” *NIST Tech. Note xxxx*, 2018.

References

[1] EIA, “Monthly Energy Review,” *Table 7.6 Electricity End Use, U.S. Energy Information Administration*, 2018. [Online]. Available: https://www.eia.gov/totalenergy/data/monthly/pdf/sec7_19.pdf. [Accessed: 13-Mar-2018].

[2] EIA, “Annual Energy Outlook 2018 with projections to 2050,” *Table 4: Residential Sector Key Indicator and Consumption, U.S. Energy Information Administration*, 2018. [Online]. Available: https://www.eia.gov/outlooks/aeo/pdf/AEO2018.pdf. [Accessed: 13-Mar-2018].

[3] “Energy Independence and Security Act of 2007,” United States, Public Law 110-140, 2007.

[4] NIST, “NIST Framework and Roadmap for Smart Grid Interoperability Standards, Release 3.0,” *NIST Spec. Publ. 1108R3*, 2014.

[5] “Demand Response | Department of Energy.” [Online]. Available: http://energy.gov/oe/technology-development/smart-grid/demand-response. [Accessed: 16-Oct-2015].

[6] U.S. Department of Energy, “Benefits of Demand Response in Electricity Markets and Recommendations for Achieving Them,” 2006.

[7] J. S. Vardakas, N. Zorba, and C. V. Verikoukis, “A Survey on Demand Response Programs in Smart Grids: Pricing Methods and Optimization Algorithms,” *IEEE Commun. Surv. Tutorials*, vol. 17, no. c, pp. 1–1, 2014.

[8] R. Deng, Z. Yang, M.-Y. Chow, and J. Chen, “A Survey on Demand Response in Smart Grids: Mathematical Models and Approaches,” *IEEE Trans. Ind. Informatics*, vol. 11, no. 3, pp. 1–1, 2015.

[9] P. Siano, “Demand response and smart grids—A survey,” *Renew. Sustain. Energy Rev.*, vol. 30, pp. 461–478, 2014.

[10] E. Balke, G. Nellis, S. Klein, H. Skye, V. Payne, and T. Ullah, “Detailed energy model of the National Institute of Standards and Technology Net-Zero Energy Residential Test Facility: Development, modification, and validation,” *Sci. Technol. Built Environ.*, vol. 0, no. 0, pp. 1–14, 2017.

[11] S. A. Klein et al, “TRNSYS 17: A Transient System Simulation program, Solar Energy Laboratory, University of Wisconsin, Madison, USA,” *Trnsys*, 2010.

[12] Google product, “Google Code Archive - Long-term storage for Google Code Project Hosting.,” 2013. [Online]. Available: https://code.google.com/archive/p/matlabcontrol/. [Accessed: 17-Sep-2014].

[13] H. Fanney, V. Payne, T. Ullah, N. Lisa, M. Boyd, F. Omar, M. Davis, H. Skye, B. Dougherty, B. Polidoro, W. Healy, J. Kneifel, and B. Pettit, “Net-zero and Beyond! Design and Performance of NIST’s Net-zero Energy Residential Test Facility,” *Energy Build. 101*, pp. 95–109, 2015.

[14] F. Omar and S. T. Bushby, “Simulating Occupancy in The NIST Net-Zero Energy Residential Test Facility,” *NIST Tech. Note 1817*, 2013.

[15] T. Fast, T. Wall, and L. Chen, "Java Native Access," 2007. [Online]. Available: https://github.com/java-native-access/jna. [Accessed: 22-Aug-2016].

[16] Google, "Protocol Buffers | Google Developers," 2008. [Online]. Available: https://developers.google.com/protocol-buffers/. [Accessed: 10-Sep-2014].

[17] IBPSA-USA, "Best Directory | Building Energy Software Tools." [Online]. Available: http://www.buildingenergysoftwaretools.com/. [Accessed: 15-Aug-2015].

[18] F. Incropera and D. DeWitt, "Introduction to Heat Transfer," 4th ed., Wiley, 2002, pp. 240–249.

[19] M. Davis, W. Heally, M. Boyd, L. Ng, V. Payne, H. Skye, and T. Ullah, "Monitoring Techniques for the Net-Zero Energy Residential Test Facility," NIST Technical Note 1854, 2014.

[20] "Chapter 15. Fenestration," in *ASHRAE Handbook: Fundamentals,* ASHRAE, 2013, p. 13.

[21] "Chapter 15. Fenestration," in *ASHRAE Handbook: Fundamentals,* ASHRAE, 2013, p. 17.

[22] J. A. Duffie and W. A. Beckman, "Solar Radiation," in *Solar Engineering of Thermal Processes,* 3rd ed., Wiley, 2006, pp. 3–17.

[23] M. Rubin, "Solar optical properties of windows," *Energy Res.,* vol. 6, pp. 123–133, 1982.

[24] P. Lei, "A Linear Programming Method for Synthesizing Origin-Destination (O-D) Trip Tables from Traffic Counts for Inconsistent Systems," Virginia Polytechnic Institute and State University, 1998.

[25] J. S. Armstrong, Ed., "Principle of Forecasting: A Handbook for Researchers and Practitioners," in *Appendix,* Kluwer Academic Publishers, 2001, p. 470.

[26] F. Omar and S. T. Bushby, "A Self-Learning Algorithm for Temperature Prediction in a Single Family Residence," *NIST Tech. Note 1891*, 2015.

[27] F. Omar, S. T. Bushby, and R. D. Williams, "A self-learning algorithm for estimating solar heat gain and temperature changes in a single-Family residence," *Energy Build.,* vol. 150, 2017.

[28] J. Lofberg, "YALMIP : a toolbox for modeling and optimization in MATLAB," in *2004 IEEE International Conference on Robotics and Automation (IEEE Cat. No.04CH37508),* 2004, pp. 284–289.

[29] The MathWorks, "Optimization Toolbox User's Guide R2017a," 2017.

[30] W. V. Payne, "NZERTF's Heat Pump Capacity Outputs," Private Communications, National Institute of Standards and Technology, MD, 2013.

[31] C. Chen, S. Kishore, and L. V. Snyder, "An innovative RTP-based residential power scheduling scheme for smart grids," *ICASSP, IEEE Int. Conf. Acoust. Speech Signal Process. - Proc.,* pp. 5956–5959, 2011.

[32] A. H. Mohsenian-Rad and A. Leon-Garcia, "Optimal residential load control with price prediction in real-time electricity pricing environments," *IEEE Trans. Smart*

Grid, vol. 1, no. 2, pp. 120–133, 2010.

[33] M. Avci, M. Erkoc, A. Rahmani, and S. Asfour, "Model predictive HVAC load control in Buildings using real-time electricity pricing," *Energy Build.*, vol. 60, pp. 199–209, 2013.

[34] A. Afram, F. Janabi-sharifi, A. S. Fung, and K. Raahemifar, "Artificial neural network (ANN) based model predictive control (MPC) and optimization of HVAC systems : A state of the art review and case study of a residential HVAC system," *Energy Build.*, vol. 141, pp. 96–113, 2017.

[35] J. H. Yoon, R. Baldick, and A. Novoselac, "Demand response control of residential HVAC loads based on dynamic electricity prices and economic analysis," *Sci. Technol. Built Environ.*, vol. 22, no. 6, pp. 705–719, 2016.

[36] T. Cui, S. Chen, Y. Wang, Q. Zhu, S. Nazarian, and M. Pedram, "Optimal co-scheduling of HVAC control and battery management for energy-efficient buildings considering state-of-health degradation," *Proc. Asia South Pacific Des. Autom. Conf. ASP-DAC*, vol. 25–28–Janu, pp. 775–780, 2016.

[37] F. Nägele, T. Kasper, and B. Girod, "Turning up the heat on obsolete thermostats: a simulation-based comparison of intelligent control approaches for residential heating systems," *Renew. Sustain. Energy Rev.*, vol. 75, pp. 1254–1268, 2017.

[38] J. Lu, T. Sookoor, V. Srinivasan, G. Gao, B. Holben, J. Stankovic, E. Field, and K. Whitehouse, "The Smart Thermostat: Using Occupancy Sensors to Save Energy in Homes," *Proc. ACM SenSys*, vol. 55, pp. 211–224, 2010.

[39] K. X. Perez, M. Baldea, and T. F. Edgar, "Integrated smart appliance scheduling and HVAC control for peak residential load management," *Proc. Am. Control Conf.*, vol. 2016–July, pp. 1458–1463, 2016.

[40] B. Urban and K. Roth, "A Data-Driven Framework for Comparing Residential Thermostat Energy Performance," Fraunhofer Center for Sustainable Energy Systems, Final Report | Co-Developed with NEST, 2014.

[41] J. Iwaro, a Mwasha, R. Williams, and R. Zico, "An Integrated Criteria Weighting Framework for the sustainable performance assessment and design of building envelope," *Renew. Sustain. Energy Rev.*, vol. 29, pp. 417–434, 2014.

[42] C. J. Hopfe, G. L. M. Augenbroe, and J. L. M. Hensen, "Multi-criteria decision making under uncertainty in building performance assessment," *Build. Environ.*, vol. 69, pp. 81–90, 2013.

[43] T. L. Saaty, *Multicriteria Decsion Making: The Analytic Hierarchy Process*. University of Pittsburgh, 1988.

[44] S. D. Pohekar and M. Ramachandran, "Application of multi-criteria decision making to sustainable energy planning - A review," *Renew. Sustain. Energy Rev.*, vol. 8, no. 4, pp. 365–381, 2004.

[45] G. A. Norris and H. E. Marshall, "Multiattribute decision analysis method for evaluating buildings and building systems.," *NIST Tech. Note 5663*, 1995.

[46] O. S. Vaidya and S. Kumar, "Analytic hierarchy process: An overview of

applications," *Eur. J. Oper. Res.*, vol. 169, no. 1, pp. 1–29, 2006.

[47] ASTM, "Standard Practice for Applying Analytical Hierarchy Process (AHP) to Multiattribute Decision Analysis of Investments Related to Buildings and Building Systems 1," 2016.

[48] S. Carlucci and L. Pagliano, "A review of indices for the long-term evaluation of the general thermal comfort conditions in buildings," *Energy Build.*, vol. 53, pp. 194–205, 2012.

[49] ISO 7730, "Erogonomics of the Thermal Environment - Analytical Determination and Interpretation of Thermal Comfort Using Calculation of the PMV and PPD Indices and Local Thermal Comfort Criteria," 2005.

[50] ASHRAE, "Standard 55-2010. Thermal Environmental Conditions for Human Occupancy.Atlanta: American Society of Heating Refrigerating and Air Conditioning Engineers," Atlanta, USA, 2010.

[51] N. Walikewitz, B. Jänicke, M. Langner, F. Meier, and W. Endlicher, "The difference between the mean radiant temperature and the air temperature within indoor environments: A case study during summer conditions," *Build. Environ.*, vol. 84, pp. 151–161, 2015.

[52] M. Langner, K. Scherber, and W. R. Endlicher, "Indoor heat stress: An assessment of human bioclimate using the UTCI in different buildings in Berlin," *DIE ERDE*, vol. 144, no. 3–4, pp. 260–273, 2013.

[53] L. Ng, "A Software Program for Calculating PMV and PPD." Private Communications, National Institute of Standards and Technology, MD, 2017.

[54] A. Persily and L. de Jonge, "Carbon dioxide generation rates for building occupants," *Indoor Air*, vol. 27, no. 5, pp. 868–879, 2017.

[55] A. Ishizaka and M. Lusti, "How to derive priorities in AHP: A comparative study," in *Central European Journal of Operations Research*, 2006, vol. 14, no. 4, pp. 387–400.

[56] R. D. F. S. M. Russo and R. Camanho, "Criteria in AHP: A systematic review of literature," *Procedia Comput. Sci.*, vol. 55, no. Itqm, pp. 1123–1132, 2015.